Fall 11-29-2011

Spectroscopic Studies of Carbocyanine and 2,4,6-Trisubstituted Pyridine Dyes for Bioanalytical and pH Indicating Applications

Gala M. Chapman
Georgia State University, gchapman2@student.gsu.edu

SPECTROSCOPIC STUDIES OF CARBOCYANINE AND 2,4,6-TRISUBSTITUTED PYRIDINE DYES FOR BIOANALYTICAL AND pH INDICATING APPLICATIONS

by

GALA CHAPMAN

Under the Direction of Dr. Gabor Patonay

ABSTRACT

In part A, the effect of varying short-chain alkyl substitution on the spectroscopic properties of cyanine dyes was examined. Molar absorptivities and quantum yields were determined for groups of pentamethine and heptamethine dyes for which the substitution of the indole nitrogen was varied. For both sets of dyes, increasing alkyl chain length did not significantly change quantum yield or molar absorptivity. These results may be useful in designing new cyanine dyes.

In part B, the effect of structure on the suitability of 2,4,6-trisubstituted pyridines as color pH indicators was studied by determining spectral effects of protonation, molar absorptivities, pK_a values, and the structural origin of the spectral behavior. Good color indicating properties result from aniline substitution at the 4 position of pyridine and electron donating substitution at the 2 and 6 positions of pyridine, which provide a strong red shift in the spectra and greater red shifted peak absorptivity, respectively.

INDEX WORDS: Cyanine dyes, 2,4,6-Trisubstituted pyridines, Spectroscopy, Quantum yield, Molar absorptivity, Substitution effects

SPECTROSCOPIC STUDIES OF CARBOCYANINE AND 2,4,6-TRISUBSTITUTED PYRIDINE DYES FOR BIOANALYTICAL AND pH INDICATING APPLICATIONS

by

GALA CHAPMAN

A Thesis Submitted in Partial Fulfillment of the Requirements for the Degree of

Master of Science

in the College of Arts and Sciences

Georgia State University

2011

SPECTROSCOPIC STUDIES OF CARBOCYANINE AND 2,4,6-TRISUBSTITUTED PYRIDINE DYES FOR BIOANALYTICAL AND pH INDICATING APPLICATIONS

by

GALA CHAPMAN

Committee Chair: Dr. Gabor Patonay

Committee: Dr. Gabor Patonay

Dr. Maged Henary

Dr. Gangli Wang

Electronic Version Approved:

Office of Graduate Studies

College of Arts and Sciences

Georgia State University

December 2011

DEDICATION

I would like to dedicate this thesis in loving memory of my mother, Leslie Uhl. Thank you for bringing me into this world, for nurturing my love of nature, science, reading, and art, and for helping to make my education financially possible. I miss you and I love you more than the sky!

ACKNOWLEDGMENTS

This work would not have been possible without the tremendous amount of support I received from all of the wonderful people in my life.

Dr. Patonay, thank you for giving me the space to grow and become independent as a scientist while still being there to answer my questions and to challenge me. Dr. Henary, thank you for your financial support and for encouraging me to work harder and smarter. Thank you Drs. Shahab Shamsi, Zhen Huang, Gangli Wang, and all of the chemistry faculty and staff at GSU for everything you've done for me over the years. Garfield, thank you for always being there to lend a helping hand and a good laugh, I've really enjoyed working with you. Alison, Jamilah, Eric, Andy, Eduardo, Rita, Lakshminarayana, Toral, Jennifer, and everyone else past and present in the Patonay and Henary labs, thank you for being my partners in crime and shoulders to lean on.

To my parental units (Dad, Sarah, and John): thank you for your encouragement, financial assistance, and for helping to make me the person I am today. Max, thank you for your patience, understanding, and helpful attitude, and for all of the big and little things you've done to help me along this long and arduous path. To "Da Boss" Terri Moss, thank you for introducing me to the joy that is boxing; I would not have stayed sane through grad school without it. To Tom and Vickie Perkins, thank you for providing a spiritual home for me, may the blessings you give to others come back to you multiplied many times. Last but certainly not least, a big thank you to all of my other fantastic friends from outside the chemistry department (you know who you are), whose amazing accomplishments inspire me and whose unwavering belief in me has helped me do more than I ever thought possible. You all have made me a happier, healthier, humbler, less stressed and more confident human being. I love you guys!

TABLE OF CONTENTS

TABLE OF CONTENTS

TABLE OF CONTENTS

TABLE OF CONTENTS

LIST OF TABLES

LIST OF FIGURES

LIST OF FIGURES

LIST OF FIGURES

LIST OF ABBREVIATIONS

AA	Acetic acid
ACN	Acetonitrile
AT	Acquisition time
d_1	Delay
DMSO	Dimethyl sulfoxide $(CH_3)_2SO$
DMSO-*d*6	Deuterated dimethyl sulfoxide $(CD_3)_2SO$
ε (M^{-1} cm^{-1})	Molar absorptivity
ε (C V^{-1} m^{-1})	Dielectric constant or relative permittivity
EtOH	Ethanol
ϕ	Quantum Yield
ICG	Indocyanine green
ICT	Intramolecular charge transfer
λ_{EXC}	Wavelength of fluorescence excitation
λ_{MAX}^{AB}	Wavelength of maximum absorption
λ_{MAX}^{AB}	Wavelength of maximum fluorescence emission
MeOH	Methanol
MS (ESI+)	Electrospray (ionization) mass spectrometry
NIR	Near infrared
NMR	Nuclear magnetic resonance (spectroscopy)
pK_a	Aqueous acid dissociation constant
p_sK_a	Acid dissociation constant in solvent or solvent-water mixture
PL1	Pulse power level
PTSA	*p*-Toluenesulfonic acid
PW	Pulse width
PW90	90° Pulse width
R800	Rhodamine 800
Std. Dev.	Standard deviation
S/N	Signal-to-noise ratio
T_1	Spin lattice relaxation time
THAM	Tris(hydroxymethyl)aminomethane
%RSD	Percent relative standard deviation

PART A: CYANINE DYE STUDY

A.1 The Effect of Varying Short-Chain Alkyl Substitution on the Molar Absorptivity and Quantum Yield of Cyanine Dyes

Chapter A.1 is identical to "Chapman, G., Henary, M., Patonay, G. The Effect of Varying Short-Chain Alkyl Substitution on the Molar Absorptivity and Quantum Yield of Cyanine Dyes. *Anal. Chem. Insights* **2011**, *6*, 29-36." The synthesis and ^{1}H NMR characterization of dyes MHI-85 and MHI-71 was carried out by Dr. Maged Henary, ESI-MS was carried out by Dr. Lifang Wang, and I was responsible all of the other experimental work discussed herein.

A.1.1 Introduction

Cyanine dyes are a class of conjugated, fluorescent molecules with polymethine chromophores composed of an odd number of carbon atoms. These dyes exhibit unusually long-wavelength absorbance and fluorescence relative to the size of their chromophores, typically absorbing light in the visible to near infrared (NIR) region.[1] These compounds were originally utilized as sensitizing additives to photographic emulsions, but their unique structural and photophysical characteristics have since proven useful for a wide variety of other applications requiring photosensitive materials, such as optical recording media and solar cells.[2-4] Additionally, cyanine dyes can be used as fluorescent labels of both proteins and DNA, thereby greatly enhancing the sensitivity of fluorescence detection for these types of biomolecules.[5-7] NIR-absorbing cyanine dyes are particularly well-suited for use as fluorescent labels of proteins and nucleic acids, as

there is no interfering autofluorescence from biomolecules at these long wavelengths, and have been applied to both *in vitro* analytical studies and *in vivo* biomedical imaging.[5-9] Due to the tremendous utility and versatility of this class of compounds, significant research efforts are being directed at developing new cyanine dyes functionalized for specific applications and optimizing the properties of these dyes.

In the process of developing new dyes, it is important to determine how varying the heteroaromatic ring nitrogen substituents influences spectroscopic behavior. Cyanine dye structures are commonly modified at these positions to enhance binding interactions, make the dyes pH sensitive, or improve their solubility in various solvents. Understanding how these modifications may influence the absorption characteristics and quantum efficiency is important for designing new compounds with specific functional and spectroscopic characteristics. Cyanine dyes in the excited singlet state can decay back to the ground state through four major pathways: fluorescence, intersystem crossing, internal conversion, and photoisomerization. Of the radiationless decay processes, it has been suggested that photoisomerization is the most significant, followed by internal conversion.[10,11] The extent of photoisomerization has been shown to be dependent on dye rigidity,[12] which may be influenced by both backbone structure and side chain substitution. By introducing rigidifying structures or rotation-hindering bulky substituents, photoisomerization would be expected to decrease with a corresponding increase in quantum yield.[13,14]

The purpose of this study was to investigate the effect of varying alkyl group length substitution of the indole ring nitrogen on the molar absorptivities and quantum yields of cyanine dyes. Molar absorptivities (ε) of each dye were calculated as per the

Beer-Lambert law, and fluorescence quantum yields (ϕ) were determined by a relative method. Two classes of cyanine dyes were studied: pentamethine cyanine dyes and ring-stabilized heptamethine cyanine dyes. These two different dye "backbones," which differ in terms of the substitution and length of the polymethine chain as well as the heterocyclic moieties at either end of the polymethine chain, were chosen as models to ensure that the observed results are widely applicable to a range of cyanine dyes, rather than peculiar to one subgroup of dyes. The pentamethine cyanine dyes studied all had a 4,5:4',5'-Dibenzo-3,3,3',3'-tetramethylindadicarbocyanine backbone, the structure of which is shown in Figure A.1.1.

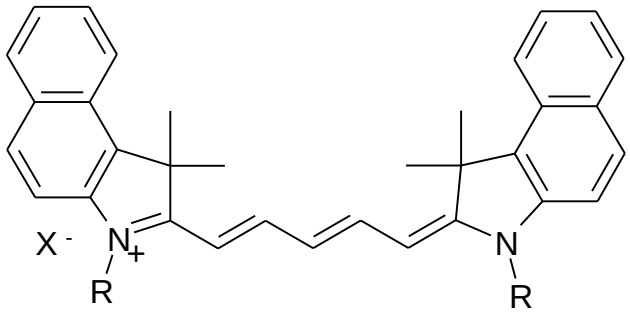

MHI-85	R = $(CH_2)_4SO_3^-$ Na^+	
666	R = *n*-Butyl	X = PF_6
829	R = Isopentyl	X = PF_6
IR-676	R = Methyl	X = I

Figure A.1.1. Structure of pentamethine cyanine backbone and substituents in dyes studied

The heptamethine cyanine dyes studied all had a 2-[2-[2-Chloro-3-[(1,3-dihydro-3,3-dimethyl-1-propyl-2*H*-indol-2-ylidene)ethylidene]-1-cyclohexen-1-yl]ethenyl]-3,3-dimethyllindolium backbone, the structure of which is shown in Figure A.1.2.

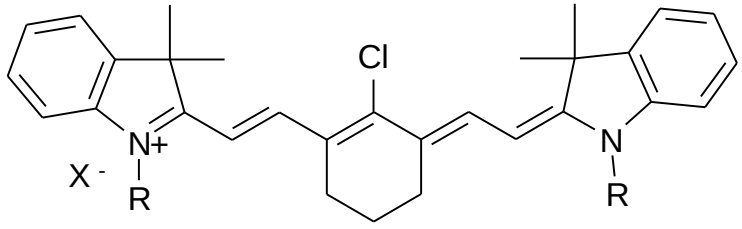

MHI-71	R = *n*-Butyl	X = I
IR-780	R = *n*-Propyl	X = I
IR-786	R = Methyl	X = ClO_4

Figure A.1.2. Structure of heptamethine cyanine backbone and substituents in dyes studied

A.1.2 Experimental

A.1.2.1 Instrumentation

Absorbance spectra were measured using a Perkin-Elmer Lambda 20 UV-Visible Spectrophotometer (Perkin-Elmer Incorporated, Waltham, MA) interfaced to a PC, with a spectral bandwidth of 2 nm. Fluorescence spectra for the pentamethine cyanine dyes were obtained using a Shimadzu RF-1501 Spectrofluorophotometer (Shimadzu Scientific Instruments, Columbia, MD) interfaced to a PC, with the spectral bandwidths for both excitation and emission set to 10 nm and the sensitivity set to "high." Fluorescence spectra for the heptamethine cyanine

dyes were obtained using a ISS K2 Multifrequency Phase Fluorometer (ISS Inc., Champaign, IL) interfaced to a PC, with the spectral bandwidths set to 10 nm. The excitation source used for the ISS K2 Fluorometer was an external 690 nm class IIIB laser (≤100 mW, S/N 901290, Lasermax Inc., Rochester, NY). Disposable absorbance cuvettes and quartz fluorescence cuvettes with pathlengths of 1.00 cm were used for absorbance and fluorescence measurements, respectively. All calculations were carried out using Microsoft Excel (Microsoft Corporation, Redmond, WA).

A.1.2.2 Chemicals and reagents

Pentamethine dyes 666 (≥98.0%) and 829 (≥99.5%) were obtained from Organica Feinchemie GmbH (Wolfen, Germany). IR-676 iodide (97%) was obtained from Spectrum Info Limited (Kiev, Ukraine). Rhodamine 800 chloride (R800) (Fluorescence Reference Standard, Sigma-Aldrich, St. Louis, MO) was also obtained for use as a reference standard in the determination of the quantum yield of the pentamethine dyes. Heptamethine dyes IR-780 iodide (99%) and IR-786 perchlorate (98%) were obtained from Aldrich Chemical Co. (Milwaukee, WI) and Sigma-Aldrich, respectively. Indocyanine green (ICG) (lot GG01, 82.0% purity, TCI America, Portland, OR) was obtained for use as a standard in the determination of the quantum yield of the heptamethine dyes. The purchased dyes were used without further purification.

Pentamethine dye MHI-85 and heptamethine dye MHI-71 were synthesized in our lab following near infrared dye syntheses described in the literature.[15]

A.1.2.3 Dye synthesis

MHI-85 was synthesized as illustrated in Equation 1. The pentacarbocyanine dye MHI-85 was obtained by the condensation reaction between benz[e]indolium salt and malonaldehyde bis(phenylimine) monohydrochloride under basic conditions.

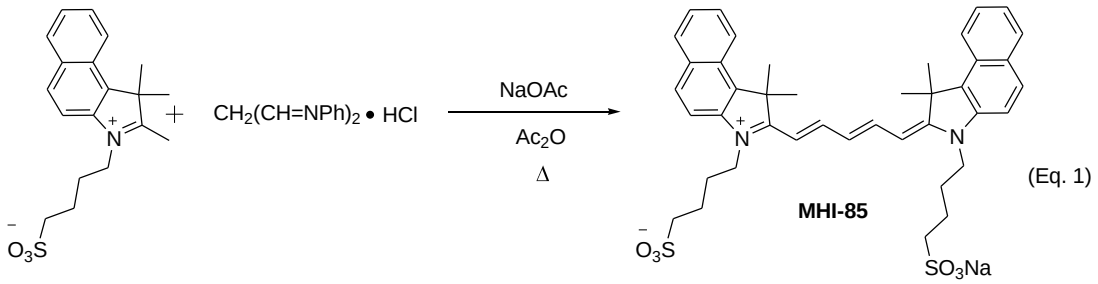

The purified product consisted of dark purple-blue crystals, mp 244-246 °C, yield 85%; ^{1}HNMR (300 MHz, DMSO-*d6*): **δ**= 8.46 (t, *J* = 12.0 Hz, 2H), 8.25 (d, *J* = 8.4 Hz, 2H), 8.08 (d, *J* = 3.6 Hz, 2H), 8.05 (d, *J* = 3.6 Hz, 2H), 7.78 (d, *J* = 8.4 Hz, 2H), 7.68 (t, *J* = 7.5 Hz, 2H), 7.51 (t, *J* = 7.5 Hz, 2H), 6.67 (t, *J* = 12.0 Hz, 1H), 6.43 (d, *J* = 13.8 Hz, 2H), 4.25 (s, 4H), 2.60-2.50 (m, 4H), 1.97 (s, 12H), 1.85-1.75 (m, 8H). MS (ESI+): calcd. for $C_{41}H_{45}N_2S_2O_6^+$ $[M - Na]^+$ 725.2719; found 725.2688.

MHI-71 was synthesized as illustrated in Equation 2. The heptacarbocyanine dye MHI-71 containing cyclohexene in the middle was synthesized by condensing the salt of Fischer base with Vilsmeier-Haack reagent under basic conditions to produce the dye.

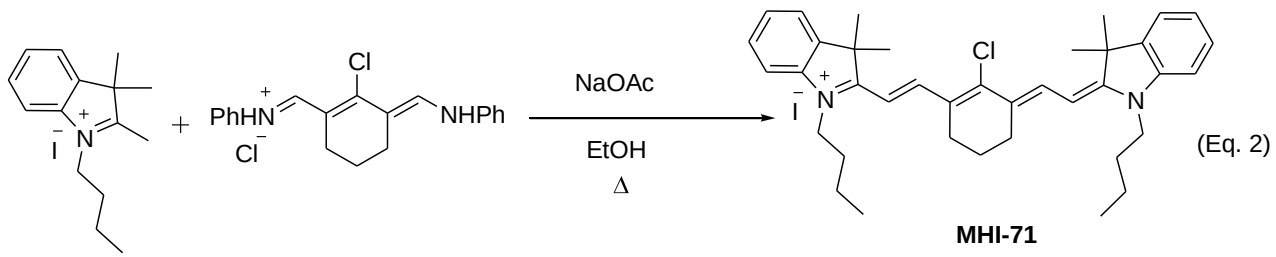

MHI-71 (Eq. 2)

The purified product consisted of iridescent golden-green crystals, mp 219-221 ℃, yield 80%; ^{1}H NMR (300 MHz, $CDCl_3$): **δ**= 8.37 (d, *J* = 13.0 Hz, 2H), 7.45-7.37 (m, 4H), 7.30-7.20 (m, 4H), 6.24 (d, *J* = 13.0, 2H), 4.22 (t, *J* = 6.0 Hz, 4H), 2.75 (t, *J* = 6.0 Hz, 4H), 2.08-1.98 (m, 2H), 1.90-1.80 (m, 4H), 1.74 (s, 12H), 1.56-1.46 (m, 4H), 1.04 (t, *J* = 6 Hz, 6H). MS (ESI+): calcd. for $C_{38}H_{48}N_2Cl^+$ $[M - I]^+$ 567.3521; found 567.3506.

A.1.2.4 Stock solutions

Stock solutions of the dyes were prepared by weighing the solid on a 5-digit analytical balance directly into a brown glass vial and adding methanol (MeOH) (LC-MS Chromasolv Grade, Sigma-Aldrich, St. Louis, MO) via a class A volumetric pipette (Kimble/Kontes, Vineland, NJ.). The contents of the vial were vortexed for 20 seconds, then sonicated for 5 minutes to ensure complete dissolution. The stock solutions were protected from light and stored in the freezer when not in use.

A.1.2.5 Method of determining molar absorptivity

Stock solutions were used to prepare five to six samples in methanol with concentrations ranging from 0.25-10 μM. Samples were prepared in 5.00(±0.02) and 10.00(±0.02) mL volumetric flasks using a 5-50 μL Micropipette 821 and a 200-1000 μL Pipetman (P1000) micropipette (Gilson, Inc., Middleton, WI.). The absorbance spectrum of each sample was measured using the Perkin

Elmer Lambda 20 Spectrophotometer, and the absorbance at the wavelength of maximum absorbance (λ_{MAX}^{AB}) was determined. The absorbance values (A) of each sample at λ_{MAX}^{AB} were plotted as a function of dye concentration (C), and the linear regression equation was computed.

A.1.2.6 Method of determining quantum yield

Standards were chosen with wavelengths of maximum emission within 10 nm of those of the unknowns to prevent errors resulting from wavelength dependent variation in fluorimeter response. Samples of the dyes and their respective standards were prepared from stock solutions such that their absorbance at λ_{MAX}^{AB} was less than 0.1 (to prevent the inner filter effect in fluorescence measurements). The absorbance and fluorescence spectra of each sample were obtained concurrently to minimize experimental error from photobleaching and potential solubility issues, and for all scans, the standard was run both prior to and following the unknowns (to ensure no change in instrumental response over the course of the runs). For both the pentamethine and heptamethine dyes, duplicate absorbance scans were obtained and the absorbance values at both the λ_{MAX}^{AB} and λ_{EXC} were averaged. The emission spectra of the pentamethine dyes were measured in triplicate using the RF-1501 fluorimeter with the excitation wavelength set to 620 nm. The emission spectra of the heptamethine dyes were measured in triplicate using the ISS-K2 fluorimeter with a 690 nm excitation wavelength. For both sets of dyes, the area under each fluorescence curve was calculated and corrected for the Rayleigh peak area (if necessary). The average fluorescence peak areas were then calculated for each sample.

A.1.3 Results and discussion

Molar absorptivities of each dye (in methanol) were computed from the slope of the linear regression plots of absorbance versus concentration. Absorbance values greater than or equal to 2.0 were excluded from these data sets. The molar absorptivities (ε) were then calculated at λ_{MAX}^{AB} from the least squares slopes of the respective data sets, as per Beer's law.

Provided in Table A.1.1 is a summary of the found λ_{MAX}^{AB} values and average calculated molar absorptivities (ε) for the pentamethine cyanine dyes and R800 as a reference sample. Also included in Table 1 are the standard deviations and percent relative standard deviations of the calculated molar absorptivities. The similarities in the λ_{MAX}^{AB} values of the cyanine dyes indicate the similarity in substitution. For dyes 666, 829, and IR-676, the substituents are all electron-donating alkyl groups. MHI-85 exhibits virtually no shift in absorbance maximum relative to those found for the alkyl-substituted dyes 666 and 829, indicating that the sulfonate moiety is far enough removed from the chromophore that its electron-withdrawing effects have insignificant influence. The molar absorptivities of the dyes at λ_{MAX}^{AB} do not vary greatly amongst themselves and do not follow any apparent trend based on substitution. Butyl-substituted dye 666 exhibited the greatest molar absorptivity, followed by methyl-substituted IR-676, followed by isopentyl-substituted dye 829. Butylsulfonato-substituted MHI-85 had the lowest observed molar absorptivity. The differences between dyes 666, 829, and IR-676 are not statistically significant, as the molar absorptivities of these dyes fall within the outer limits of each others ranges of standard deviation. However, the differences in molar absorptivity between MHI-85 and both dyes 666 and IR-676 are statistically significant, if relatively small.

The lower molar absorptivity of butylsulfonato-substituted MHI-85 relative to the other dyes may be due to substituent chain length, effects of the sulfonate moiety, or the presence of minor impurities. The molar absorptivity values showed good precision, with reasonably low percent relative standard deviations (1.7% - 7.4%) for all of the dyes.

Table A.1.1. Summary of wavelengths of maximum absorbance (λ_{MAX}) and averages, standard deviations, and percent relative standard deviations of calculated molar absorptivities (ε) at λ_{MAX} for the pentamethine cyanine dyes and the standard (R800)

Dye	λ_{MAX} (nm)	Avg. ε (λ_{MAX}) (L mol^{-1} cm^{-1})	Std. Dev. ε (λ_{MAX}) (L mol^{-1} cm^{-1})	% RSD ε (λ_{MAX})
MHI-85	680	1.7E+05	2.6E+04	14.81
666	680	2.2E+05	1.2E+04	5.37
829	680	2.0E+05	1.5E+04	7.41
IR-676	675	2.08E+05	3.5E+03	1.66
R800	679	7.1E+04	4.3E+03	6.14

Provided in Table A.1.2 is a summary of the found λ_{MAX}^{AB} values and average calculated ε values at the λ_{MAX}^{AB} for the heptamethine cyanine dyes and ICG as a reference sample. Also included in Table 2 are the standard deviations and percent relative standard deviations of the calculated molar absorptivities. The similarities in the λ_{MAX}^{AB} values amongst the cyanine dyes indicate the similarity in substitution; all are substituted with electron-donating alkyl groups. As with the pentamethine dyes, the molar absorptivities of the heptamethine dyes at λ_{MAX}^{AB} do not vary greatly amongst themselves and do not follow any apparent trend based on substitution. Propyl-substituted IR-780 exhibited the greatest molar absorptivity, followed by methyl-substituted IR-786, followed by butyl-substituted MHI-71. Only the differences in molar

absorptivity between MHI-71 and IR-786 and between MHI-71 and IR-780 are statistically significant (the ranges of molar absorptivity specified by the standard deviations are mutually exclusive). The molar absorptivity values showed good precision, with reasonably low percent relative standard deviations (0.88% - 8.45%) for all of the dyes.

Table A.1.2. Summary of wavelengths of maximum absorbance (λ_{MAX}) and averages, standard deviations, and percent relative standard deviations of calculated molar absorptivities (ε) at λ_{MAX} for the heptamethine cyanine dyes and the standard (ICG)

Dye	λ_{MAX} (nm)	Avg. ε (λ_{MAX}) (L mol^{-1} cm^{-1})	Std. Dev. ε (λ_{MAX}) (L mol^{-1} cm^{-1})	% RSD ε (λ_{MAX})
IR-786	774	2.6E+05	2.2E+04	8.45
IR-780	779	2.74E+05	2.4E+03	0.88
MHI-71	779	1.64E+05	6.6E+03	4.01
ICG	783	1.25E+05	1.2E+03	0.98

Provided in Figures A.1.3 and A.1.4 are representative comparisons of the absorbance and emission spectra of the pentamethine and heptamethine dyes, respectively. For both sets of dyes, the fluorescence and absorbance spectra are reasonably good mirror images of one another (with the exception of the Soret peak visible at lower wavelengths in the absorbance spectrum), and the Stokes' shifts provided in Tables A.1.3 and A.1.4 are relatively small, ranging from 20-23 nm (321-348 cm^{-1}). This indicates minor structural changes between the ground and excited singlet states of these dyes.

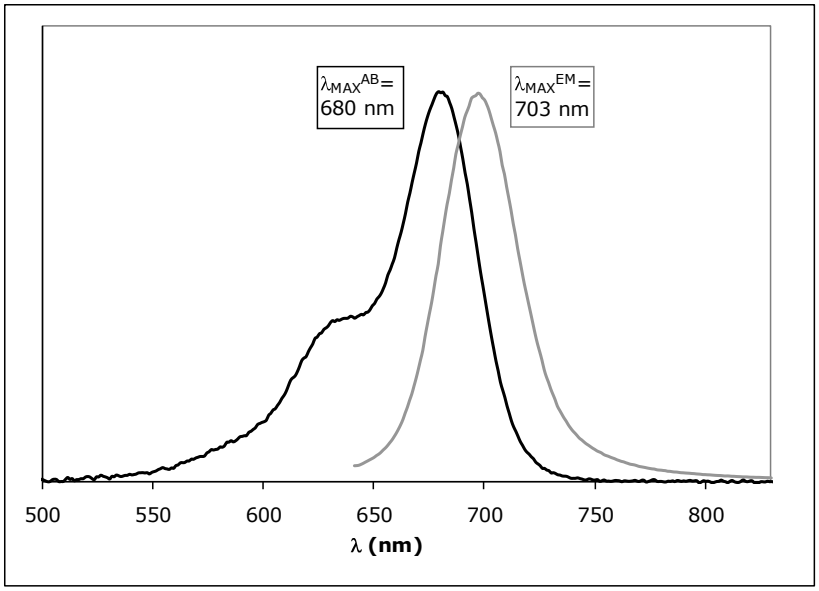

Figure A.1.3. Comparison of relative absorption and emission spectra of MHI-85 in methanol, with labeled wavelengths of maximum absorbance (λ_{MAX}^{AB}) and emission (λ_{MAX}^{EM})

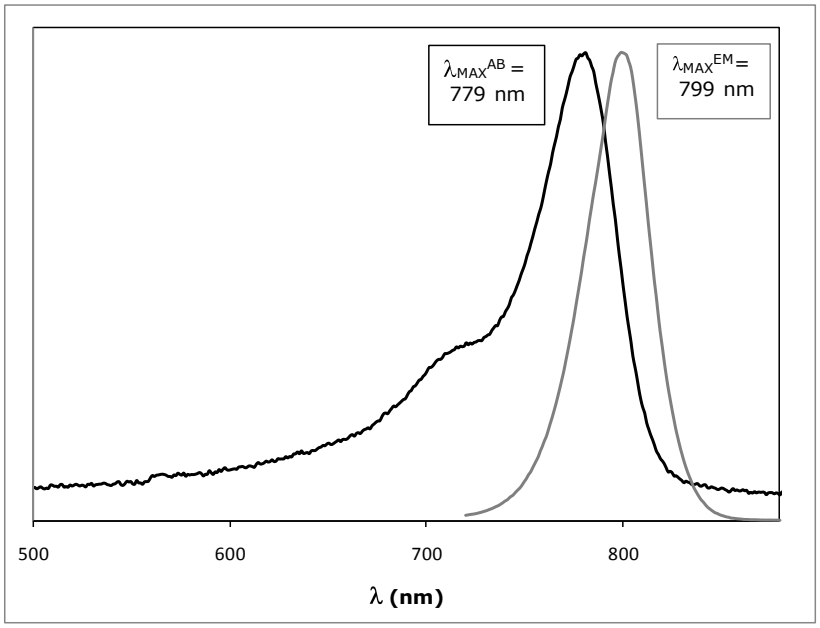

Figure A.1.4. Comparison of relative absorption and emission spectra of MHI-71 in methanol, with labeled wavelengths of maximum absorbance (λ_{MAX}^{AB}) and emission (λ_{MAX}^{EM})

Table A.1.3. Average wavelengths of maximum absorbance (λ_{MAX}^{AB}) and emission (λ_{MAX}^{EM}) and Stokes' shifts of pentamethine cyanine dyes

Dye	λ_{MAX}^{AB} (nm)	λ_{MAX}^{EM} (nm)	Stokes' Shift (cm^{-1})
IR-676	675	698	488
666	680	703	481
829	680	702	461
MHI-85	680	703	481

Table A.1.4. Average wavelengths of maximum absorbance (λ_{MAX}^{AB}) and emission (λ_{MAX}^{EM}) and Stokes' shifts of heptamethine cyanine dyes

Dye	λ_{MAX}^{AB} (nm)	λ_{MAX}^{EM} (nm)	Stokes' Shift (cm^{-1})
IR-786	774	796	357
IR-780	779	799	321
MHI-71	779	799	321

The fluorescence quantum yields of each of the cyanine dyes were calculated relative to the standard from their respective average fluorescence peak areas (F), average absorbances at λ_{EXC} (A), and the published quantum yield of the standard (ϕ_S), as per the following equation. In this equation, the indices S and U refer to the standards and the unknowns, respectively.

$$\phi_U = \phi_S * F_U / F_S * A_S / A_U$$

Methanol was used as the solvent for both the standards and the unknowns; therefore no correction for solvent refractive index was necessary in this equation. This calculation assumes negligible variation in instrument response within the range of emission wavelengths exhibited by the unknowns with respect to the standard emission wavelengths.

Provided in Table A.1.5 are the average quantum yields of the pentamethine dyes calculated relative to R800 as determined from multiple studies, along with their standard deviations and percent relative standard deviations. Reproducibility of results following duplicate determinations of quantum yield was good for dyes MHI-85 and IR-676, with percent relative standard deviations of 5.6 and 5.1 percent, respectively; accordingly no further determinations were made. However, reproducibility was poor for dyes 666 and 829, accordingly the quantum yield of dye 666 was determined two additional times, and the quantum yield of dye 829 was determined one additional time in an attempt to improve reproducibility. Following these further studies, a significant improvement in reproducibility was observed for dye 666 but not dye 829. Nonetheless, even taking into account the high percent relative standard deviations, the average quantum yields of the pentamethine dyes did not vary significantly with increasing alkyl *N*-substitution. Additionally, it appears that the addition of solubility-enhancing anionic sulfonate groups to these alkyl *N*-substituents has no significant effect on the quantum yield.

Provided in Table A.1.6 are the average quantum yields of the heptamethine dyes calculated relative to ICG as determined from duplicate studies, along with their standard deviations and percent relative standard deviations. Reproducibility of results following duplicate determinations of quantum yield was good for all of the dyes, with IR-786, IR-780, and MHI-71 having percent relative standard deviations of 2.8, 4.5, and 6.8 percent, respectively; accordingly no further determinations of quantum yield were made. Overall, the quantum yields of the heptamethine dyes were much lower than those of the pentamethine dyes, as expected,[16] and as with the pentamethine dyes, the average quantum yields of the heptamethine dyes did not vary significantly with increasing alkyl *N*-substitution.

Table A.1.5. Average quantum yields (ϕ) calculated for pentamethine dyes and their standard deviations and percent relative standard deviations

Dye	Average ϕ	Std. Dev. ϕ	%RSD ϕ
MHI-85	0.175	0.0098	5.6
666	0.19	0.0260	13.9
829	0.17	0.0405	23.7
IR-676	0.164	0.0084	5.1

Table A.1.6. Average quantum yields (ϕ) calculated for heptamethine dyes and their standard deviations and percent relative standard deviations

Dye	Average ϕ	Std. Dev. ϕ	%RSD ϕ
IR-786	0.076	0.0022	2.8
IR-780	0.076	0.0035	4.5
MHI-71	0.077	0.0053	6.8

A.1.4 Conclusions

Based on these results, it can be generalized that increasing the chain length of short-chain alkyl substituents on the heterocyclic indole nitrogens has little to no effect on the quantum yields and molar absorptivities of cyanine dyes, and the addition of sulfonate groups to the ends of these alkyl *N*-substituents also does not change the quantum yield. The lack of effect on quantum yield may be attributable to the fact that the *N*-substituents are not directly conjugated to the chromophore and therefore have little to no effect on internal conversion-type energy loss, and that additionally, these short chain substituents do not provide adequate steric hindrance to interfere sufficiently with photoisomerization to *cis*-cyanine. The implications of these results are significant to the design and synthesis of new cyanine dyes. As previously mentioned, cyanine dyes are frequently modified at these heterocyclic nitrogen positions to enhance binding interactions, make the dyes pH sensitive, or improve solubility. Accordingly, provided the

functional group is not directly attached to the chromophore, but instead “bridged” by a short alkyl substituent, introducing this group should have little effect on the quantum yield of the dye relative to a structurally similar dye lacking this functionality. For example, if one wished to modify a dye with desirable spectroscopic properties to be more water soluble or to bind more strongly with DNA or protein by adding a charged or polar functionality, this modification could be carried out without concern for loss or change of the desired spectral characteristics. Additionally, these results suggest that quantum yields of new cyanine dyes can be roughly predicted prior to their synthesis and characterization based on quantum yields of structurally similar preexisting dyes, provided that such data exists.

PART B: SPECTROSCOPIC BEHAVIOR OF 2,4,6-TRISUBSTITUTED PYRIDINES: PROTONATION BEHAVIOR, AGGREGATION PROPERTIES, AND MOLAR ABSORPTIVITIES OF POTENTIAL pH INDICATORS

The research in this portion of the thesis investigates the potential suitability of a series of 2,4,6-trisubstituted pyridine dyes for use as nonaqueous pH indicators by studying the spectral effects of protonation with different acids in different solvents, the molar absorptivities of protonated and unprotonated forms of the dyes, the pK_a values of the dyes (chapter B.1) and the structural origin of the spectral behavior observed in these dyes (chapter B.2).

B.1 Protonation Studies, Molar Absorptivities, and pK_a Determination of 2,4,6-Trisubstituted Pyridines Using Absorption Spectroscopy

B.1.1 Introduction

B.1.1.1 Pyridine and pyridine derivatives: natural occurrence and applications

Pyridine and its derivatives are a group of biologically and chemically important compounds with a myriad of applications. Pyridine derivatives occur in biological systems in nicotinamide adenine dinucleotide (NAD^+ and NADH), an important cofactor for the catalysis of biological redox reactions.[17] Pyridine also occurs naturally as a structural element of the B-vitamins niacin and pyridoxal, as well as a number of alkaloids produced by plants, including nicotine.[18] Pyridine itself is a commonly used polar aprotic solvent, and its derivatives find applications in agriculture, medicine, and other industries.[18,19]

One particularly important subclass of pyridine derivatives are the 2,4,6-trisubstituted pyridines. Some of these compounds have shown promise as anticancer drugs that work by inhibiting topoisomerases I and II.[20] However, the majority of applications of 2,4,6-trisubstituted pyridines are more directly related to their photophysical properties. These compounds have found applications in thermal recording materials,[21] photographic acid mediated imaging media,[22] and photocurable compositions for stereolithography. Additionally, 2,4,6-triaryl pyridines can act as dye lasers in appropriate solvents.[23]As a result of the larger distribution of excited state energy levels in solution, these and other dye lasers can be used for a much broader range of wavelengths than gas or solid state lasers, making them particularly well suited to applications in tunable and pulsed lasers.

Additionally, 2,4,6-trisubstituted pyridines can be used as pH indicators and ion probes. For example, a compound possessing a terpyridine moiety (two 2-pyridyl substituents at the 2' and 6' positions) and a 4'-aminomethylphenyl substituent linked to a heptamethine cyanine dye has been applied successfully as a NIR-fluorescing pH probe for *in vivo* applications. The terpyridine moiety acts as the proton receptor, while the cyanine functionality provides the NIR fluorescence. As this compound was found to have a pK_a near physiological pH and a linear fluorescence response in the physiological pH range, it proved useful for *in vivo* fluorescence measurement of intracellular pH, as evidenced by confocal microscopy studies of liver cells stained with the dye.[24]

Accordingly, although these compounds are structurally unrelated to cyanine dyes, they share several similarities in terms of their applications based on photophysical properties, and additionally, the two families can be combined to create pH-sensitive fluorophores for *in vivo* pH sensing applications. Additionally, it is important to note that linking a 2,4,6-trisubstituted

pyridine moiety to a cyanine dye (or other group) strongly modulates the pK_a of the pyridine moiety; 2,2':6',2" terpyridine alone possesses a pK_{a1} value of 4.16,[25] whereas the pK_{a1} of the cyanine-terpyridine compound was found to be 7.1.[24]

In a study carried out by Garcia-Acosta et al., a series of 2,6-diphenylpyridine compounds with variously substituted *p*-anilino substituents at the 4 position were found to be useful as ion probes.[25] Pyridines functionalized at the 2,4, and 6 positions with electron-donating groups have a donor-acceptor structure as shown in Figure B.1.1.

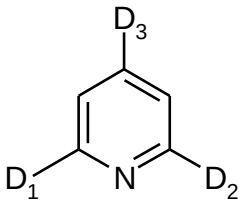

Figure B.1.1. Donor-acceptor structure of 2,4,6-trisubstituted pyridines

When one of the donor groups is also a nucleophile (such as a *p*-anilino group), binding of cations can either occur at the donor group or the acceptor pyridine group. Compounds with *p*-anilino substituents at the 4-position (D_3) were found to respond nonselectively to a variety of metal cations, with complexation occurring at either the aminophenyl donor group or the pyridine acceptor group. Complexation with metals at the pyridine group was attributed to a bathochromic shift in the absorption spectrum, whereas complexation with metals at the anilino group was attributed to a slight hypsochromic shift in the absorption spectrum. Addition of certain anions to these metal complexes resulted in either a decrease or an increase the intensity of absorption, which was attributed to the formation of ion pairs or anion-mediated relocation of the metal ion from the anilino donor binding site to the pyridine acceptor binding site,

respectively. Accordingly, metal complexes of these compounds may be applied for differential anion sensing purposes by observing the spectrophotometric response of ensembles containing different metal complexes of these compounds to different anions and looking for a "fingerprint" recognition pattern.[26]

For certain 2,4,6-trisubstituted pyridines (such as those with a *p*-anilino substituent), protonation results in a pronounced color change corresponding to the appearance of a new peak in the absorption spectrum with a significant (~100 nm) bathochromic shift, which increases to a maximum as increasing concentrations of acid are added. Addition of greater concentrations of acid beyond that corresponding to this maximum results in a decrease in absorption intensity of this bathochromic peak and a hypsochromic shift in the spectrum. These two distinct sets of spectral changes (which each display separate, clearly defined isosbestic behavior) can be correlated to the presence of two protonation equilibria.[26] The first equilibrium is presumably related to the conversion of nonprotonated dye to the singly protonated form of the dye, whereas the second equilibrium is associated with the conversion of the singly protonated form of the dye to the doubly protonated form. These equilibria and their acid dissociation equilibrium constants are generalized in Equation 3, where "B" is the basic form of any of the dyes studied and HB^+ and H_2B^{2+} are the singly and doubly protonated forms of the dyes, respectively.

$$\underset{\text{red shift}}{B} \overset{K_{a2}}{\rightleftharpoons} HB^+ \overset{K_{a1}}{\rightleftharpoons} \underset{\text{blue shift}}{H_2B^{2+}} \qquad \text{(Eq 3)}$$

This pH-dependent color change makes these compounds potentially useful as pH indicators, and may be studied readily using absorption spectroscopy.

B.1.1.2 Solvent considerations

To study the protonation characteristics of 2,4,6-trisubstituted pyridines in nonaqueous solutions, the choice of solvent is extremely important. The most obvious consideration is the solubility of the compound in the solvent. Additionally, the solvent must also have a high dielectric constant (relative permittivity, ε) for ionic dissociation to occur; at the very least it needs to be greater than 10.[27] Accordingly, the best solvent choices for these purposes are polar aprotic solvents with $\varepsilon > 10$, which are capable of readily dissolving 2,4,6-trisubstituted pyridines while simultaneously permitting dissociation of acids and protonation. Dimethylformamide, acetonitrile (ACN), and dimethylsulfoxide (DMSO) seem to be the best candidates for these purposes, possessing relatively high dielectric constants, however, dimethylformamide is hydrolyzed in the presence of strong acids and is therefore incompatible.[28] Accordingly, either DMSO or ACN would be appropriate solvents for studying protonation of these compounds.

One other consideration when choosing a nonaqueous solvent to is the donor number of the solvent, which is a measure of its strength as a Lewis base (the larger the donor number, the more basic the solvent).[29] Solvents with high donor numbers promote the dissociation of an acid by acting as a base, and similarly, diminish the strength of a base dissolved in the same solvent. Donor numbers and dielectric constants of water, ACN, and DMSO are summarized in Table B.1.1.

Table B.1.1. Dielectric constants[30] and donor numbers[31] of water, acetonitrile, and DMSO

Solvent	Dielectric constant ε ($C \cdot V^{-1} \cdot m^{-1}$)	Donor number DN (kcal/mol)
H_2O	78	18
ACN	37	14
DMSO	47	30

Acetonitrile has a lower dielectric constant than water and accordingly, dissociation of acids occurs to a lesser extent than in aqueous solutions. Additionally, it has a lower donor number than water, and is therefore a weaker base. Accordingly, an increase in the acid dissociation constant (pK_a) is observed for almost all compounds dissolved in acetonitrile; bases become significantly stronger and acids become significantly weaker.[32] DMSO also has a lower dielectric constant than water, but it has a significantly larger donor number, reflecting its ability to act as a Lewis base. As discussed in the previous paragraph, basic solvents tend to promote the dissociation of acids while diminishing the strength of bases dissolved in the same solvent. This behavior is best illustrated in Table B.1.2 via a comparison of some pK_a values of acidic and basic compounds determined in water, acetonitrile, and DMSO.

Table B.1.2. Comparison of acid dissociation constants (pK_a) of some acidic and basic compounds in water,[33] DMSO,[34] and ACN[35-38] at 25° C

Compound	pK_a in H_2O	pK_a in ACN	pK_a in DMSO
Acetic Acid	4.80	23.51	12.6
Phenol	9.99	29.14	18
p-Toluenesulfonic acid (PTSA)	-2.8	8.45	0.9
HCl	-7	8.9	1.8
Aniline	9.4	10.62	3.6
Pyridine	5.2	12.53	3.4

The pK_a values of acids and bases provided in Table B.1.2 show the effects of each solvent on acid and base strength. From the above data, it can be generalized that among the three solvents, acids tend to be strongest in water, less strong in DMSO, and least strong in ACN. The observation of greater acid strength in water than in DMSO demonstrates the importance of dielectric constant with respect to the dissociation of acids, and the massive differences in acid

strength between DMSO and ACN can be attributed to both the higher dielectric constant and donor number possessed by DMSO. It can also be generalized that among the three solvents, bases tend to be strongest in acetonitrile, followed by water, with the weakest base strength observed in DMSO. The weak base strength in DMSO is a reflection of its high basicity (donor number). The increase in pK_a observed in ACN relative to water is due to both the lower donor number and lower dielectric constant of ACN. These effects on acid and base strength must be taken into consideration in this study, as all of the experiments (except determination of pK_a) will be conducted exclusively in nonaqueous solvents or solvents containing small concentrations of water.

B.1.1.3 Determination of acid dissociation constants

There are a variety of different options for determining acid dissociation constants (pK_a) of compounds, including amperometric titrations, nuclear magnetic resonance (NMR) spectroscopy, fluorescence spectroscopy, and UV-visible absorption spectroscopy. However, the unique absorption behavior and the appearance of an absorption peak corresponding only to the singly protonated form of the dye makes absorption spectroscopy a logical choice for pK_a determination of 2,4,6-trisubstituted pyridine dyes. Additionally, UV-visible spectrophotometric determination of pK_a allows the use of lower concentrations of analyte (micromolar range) than required for amperometric or NMR methods.

Special considerations must be taken into account to determine the aqueous pK_a values of water-insoluble compounds. Most approaches involve determining acid dissociation constants (p_sK_a) in organic solvent-water mixtures of varying composition and extrapolating the p_sK_a to zero percent water to determine the aqueous pK_a. Such methods typically yield linear

relationships provided that the dielectric constants of the solvent-water mixtures are greater than 47 (to avoid Bjerrum-type ion association).[39] One commonly used method is the Yasuda-Shedlovsky extrapolation, in which the sum of the experimentally determined p_sK_a values and the logarithm of the molarity of water in the solvent-water mixture in which it was determined ($p_sK_a + \log[H_2O]$) are plotted as a function of the inverse of the dielectric constant of the solvent-water mixture ($1/\varepsilon$).[40] The aqueous pK_a is then determined by solving for $p_sK_a + \log[H_2O]$ when $1/\varepsilon = 1/\varepsilon_{H2O}$ and subtracting the logarithm of the molarity of pure water. A similar, somewhat simpler approach is to plot the p_sK_a as a function of percentage organic solvent and solve for the y-intercept.[41] When this methodology is used, it has been determined that in some solvent-water mixtures, the slope of p_sK_a versus percent organic solvent is relatively constant, regardless of the analyte. For example, in ethanol-water mixtures, the slope of this line has been reported as remaining relatively constant at around 0.03665.[42] Therefore, a quick (albeit less accurate) determination of aqueous pK_a can be made by titration in a single solvent-water mixture and extrapolation to zero can be accomplished by subtracting the product of the reported slope of the line and percent ethanol from the p_sK_a determined in the solvent-water mixture.

B.1.1.4 Goals of this study

The aim of this study is to relate the potential suitability of 2,4,6-trisubstituted pyridine dyes as nonaqueous pH indicators to their structures by studying the absorption spectra and molar absorptivities, particularly of the singly protonated and unprotonated forms of the dyes. For these absorption studies, acetonitrile was initially chosen over dimethylsulfoxide for ease of handling, and fortuitously, the use of ACN facilitated the study of both protonation equilibria using relatively low concentrations of acid, whereas much higher concentrations were found to be

necessary when DMSO was employed (as discussed in detail in section B.2). Protonation with a number of different strong and weak acids was tested, including hydrochloric acid, perchloric acid, *para*-toluenesulfonic acid, acetic acid, and phenol. The effects of solvent composition (percent water) and ionic strength on protonation with hydrochloric acid was tested in semi-aqueous solutions of acetonitrile. Molar absorptivities of the basic and singly protonated forms of eight of the dyes were determined as per the Beer-Lambert law. Molar absorptivities could not be reliably determined for two of the dyes, which demonstrated unstable absorption characteristics most likely due to aggregation, as evidenced by separate aggregation studies. The acid dissociation constants p_sK_{a1} and p_sK_{a2} of two of the dyes were determined spectroscopically in a solvent composed of 50% water and 50% ethanol with a constant ionic strength of 0.1 M and constant concentration of dye; in these experiments the pH was adjusted using $HClO_4$. Calculated p_sK_a values were extrapolated to zero percent ethanol and corrected for ionic strength to determine the aqueous pK_a. Both the spectroscopic characteristics and pK_a values of the dyes were then related to their structures.

B.1.2 Experimental

B.1.2.1 Materials and instrumentation

All 2,4,6-trisubstituted pyridine dyes were obtained from Dr. Maged Henary and used without further purification. Purities were verified by ^{1}H NMR as a routine task when the dyes were synthesized and further confirmed by determination of melting point ranges. Structures of the dyes are provided in Figure B.1.2. In this figure, terpyridine dye F has been grouped with terpyridine dyes I and J to emphasize structural similarity between these compounds. Perchloric

acid ($HClO_4$; 69.5%, Lot No. 02829ER) and *para*-toluenesulfonic acid monohydrate (PTSA; 98.5%) were obtained from Aldrich Chemical Co. (Milwaukee, WI). Hydrochloric acid (HCl; 12.309 M), glacial acetic acid (AA; 99.5%), and phenol ($\geq$99.9%, Lot No. 36596HMV) were obtained from Sigma-Aldrich (St. Louis, MO). Sodium chloride (NaCl; 99+%) and acetonitrile (ACN; 99.9%, 0.03% H_2O) were obtained from Fisher Scientific (Fairlawn, NJ). Acetonitrile was stored over freshly dried 4Å molecular sieves. Type 1 ultrapure water (18.2 MΩ cm) was obtained from a Barnstead Nanopure Water System (Thermo Fisher Scientific, Waltham, MA). Koptec ethanol (EtOH; 200 proof; 99.5% min) and BDH reference standard buffers (pH 4.00 $\pm$ 0.01, pH 7.00 $\pm$ 0.01, pH 10.00 $\pm$ 0.02) for calibrating the electrode were obtained from VWR (Radnor, PA). Tris(hydroxymethyl)aminomethane (THAM; 99.9+% ultrapure grade) was obtained from Aldrich Chemical Co. (Milwaukee, WI) for use in standardizing perchloric acid solutions used in the pK_a titrations.

Absorption spectra were measured using either a Perkin-Elmer Lambda 20 UV-Vis-NIR Spectrophotometer (Perkin-Elmer Incorporated, Waltham, MA) or a Cary 3G UV-Vis Spectrophotometer (Agilent Technologies Incorporated, Santa Clara, CA). Disposable Fisherbrand polystyrene cuvettes (Fisher Scientific) with pathlengths of 1.00 cm were used for absorption measurements of solutions in acetonitrile and in ethanol-water mixtures. A ROSS® pH electrode (operational pH range: 0-14; Orion Research, Inc., Beverly, MA) was used for pH measurements and calibrated using a three point calibration method with pH 4.00, pH 7.00, and pH 10.00 reference standard buffer solutions. All calculations were carried out using Microsoft Excel (Microsoft Corporation, Redmond, WA).

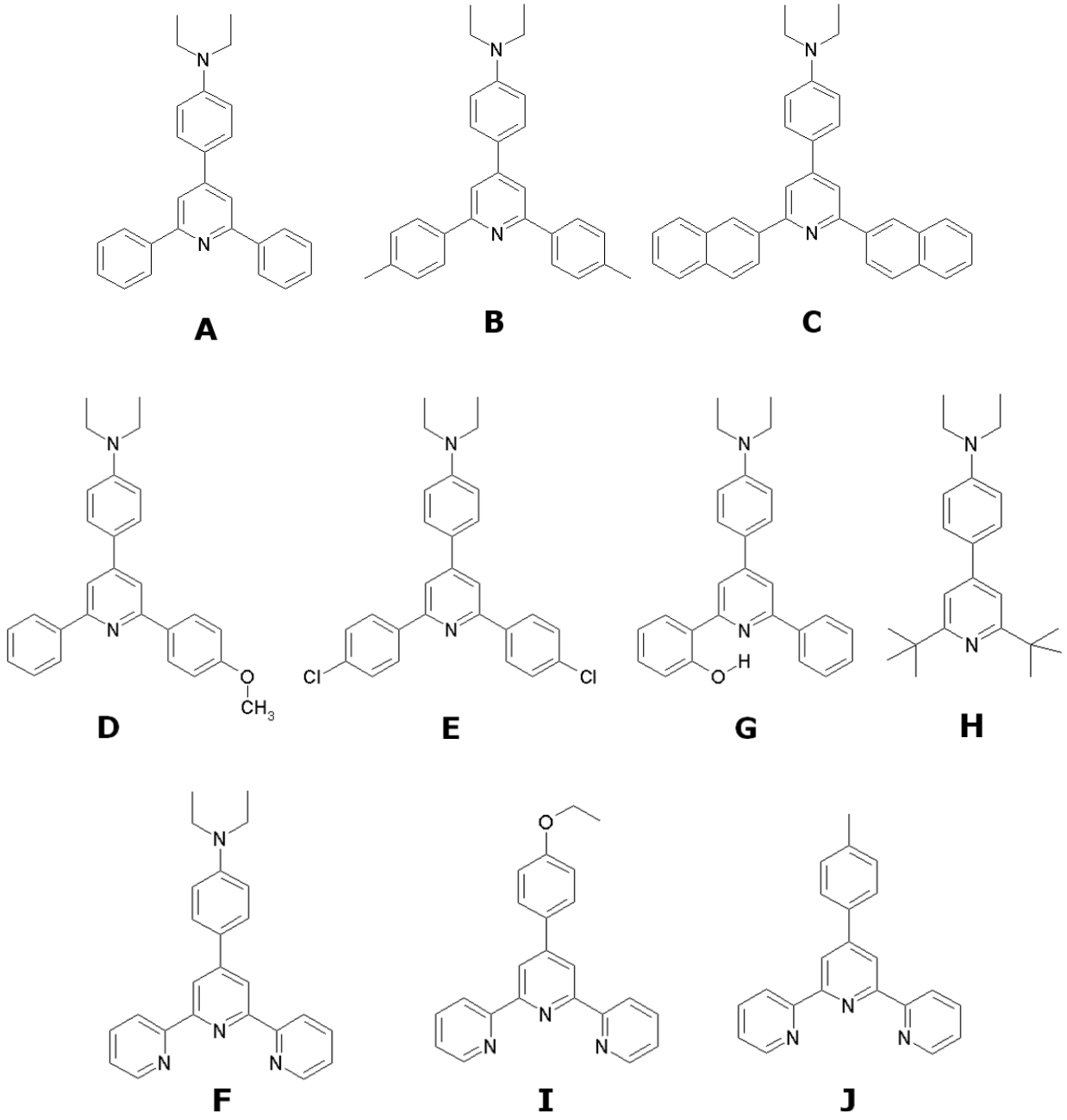

Figure B.1.2 Structures of 2,4,6-trisubstituted pyridines studied

B.1.2.2 Preparation of stock solutions

Stock solutions of the compounds were prepared by weighing the solid on a 5-digit analytical balance directly into a glass vial and adding ACN via a class A volumetric pipette

(Kimble/Kontes, Vineland, NJ.) and/or an adjustable volume micropipette (Gilson, Inc., Middleton, WI.) such that the final solution had a concentration of 1 mM. The contents of the vial were vortexed for 20 seconds, then sonicated for 10 minutes to ensure complete solvation. The stock solutions were protected from light and stored in the freezer when not in use. Secondary 0.1 mM stock solutions of dyes were prepared to make up working solutions just prior to absorption studies by a 1:10 dilution of the dye with ACN in a class A volumetric flask.

A parent stock solution of 1 M hydrochloric acid was prepared by dilution of 12.3 M HCl in ultrapure H_2O using class A volumetric pipettes. A secondary 0.1 M HCl solution was prepared by 1:10 dilution of this parent solution with ultrapure H_2O. Preparation of 1, 2, 3, 4, 5, and 10 mM "daughter" stock solutions of HCl in H_2O was carried out by serial dilutions of the secondary solution in volumetric flasks. These solutions were used for the initial protonation studies in HCl.

For the ionic strength studies, a parent stock solution of sodium chloride was prepared by weighing out an appropriate amount of NaCl on a five digit analytical balance to obtain 100 mL of 0.1 M NaCl, quantitatively transferring the salt to a 100.00 mL class A volumetric flask, and filling to the mark with ultrapure H_2O. Constant ionic strength HCl stock solutions (I = 5 mM) were prepared by pipetting appropriate amounts of the secondary 0.1 M HCl solution into volumetric flasks to make the final solutions 1 mM, 2 mM, 3 mM, and 4 mM HCl, then pipetting appropriate amounts of NaCl into these solutions to make the ionic strength 5 mM overall. For example, the 1 mM HCl solution contained 4 mM NaCl, the 2 mM HCl solution contained 3 mM NaCl, and so on. Additionally, three extra solutions were made to study the effect of increasing the ionic strength when the concentration of acid is held constant. To this end, solutions that were 3 mM HCl with ionic strengths of 10 mM, 50 mM, and 100 mM were prepared by addition

of appropriate amounts of 0.1 M NaCl solution. Note that the I = 5 mM solutions had final ionic strengths of 100 µM when diluted in their working solutions, and the I = 10, 50, and 100 mM solutions had final ionic strengths of 200, 1000, and 2000 µM, respectively, when diluted in their working solutions.

Initial studies of the dyes were carried out using HCl (prepared in H_2O), but studies on the effect of $\%H_2O$ in the solution indicated that the solvent composition has an effect on the protonation characteristics. Accordingly, all other acid solutions were prepared directly in acetonitrile; when the solutions were prepared in this manner the final working solutions contained a maximum of less than 0.1% added H_2O from the acid, thereby making this variable negligible. A parent stock solution of 1 M acetic acid was prepared in acetonitrile using class A volumetric pipettes, from which a secondary stock solution of 1 mM acetic acid in acetonitrile was prepared by serial dilutions of the parent stock (1:100 and 1:10) into volumetric flasks using class A volumetric pipettes. A 0.1 M parent stock solution of perchloric acid was prepared by diluting 69.5% $HClO_4$ in acetonitrile. Parent stock solutions of 0.1 M *para*-toluenesulfonic acid and phenol were prepared by weighing out appropriate amounts of the solids on an analytical balance, quantitatively transferring the solid to a class A 50.0 mL volumetric flask and filling to the mark with ACN. A 1:100 dilution of each of the $HClO_4$, PTSA, and phenol parent solutions using class A volumetric pipettes and volumetric flasks produced 1 mM daughter solutions in acetonitrile.

For the molar absorptivity studies of the dyes, a parent stock solution of 1 M hydrochloric acid was prepared by dilution of 12.3 M HCl in acetonitrile using class A volumetric pipettes A secondary 0.1 M HCl solution was prepared by 1:10 dilution of this parent solution with

acetonitrile. A tertiary 1 mM daughter stock solution of HCl in ACN was carried out by a 1:100 dilution of the secondary solution.

For the pK_a studies of the dyes, 1 L of a solution containing 50% EtOH and 50% H_2O (v/v) was prepared, and a 2 M solution of NaCl was prepared in triply deionized water. A 1 M perchloric acid solution was prepared by dilution of 69.5% $HClO_4$ with the 50% EtOH/H_2O solution, with addition of 30.5% water from the 69.5% $HClO_4$ solution accounted for by adding an appropriate amount of additional EtOH to maintain a final solvent composition of 50% EtOH/H_2O. Secondary $HClO_4$ solutions with concentrations of 0.1 M, and 0.01 M were prepared from the 1 M solution by dilution such that the final solvent compositions of each secondary solution was also 50% EtOH in H2O (v/v). The ionic strength of the 0.01 M $HClO_4$ solution was adjusted to 0.1 M using the NaCl solution; the addition of excess water from the NaCl solution was compensated for by adding an equal volume of ethanol to maintain a solvent composition of 50% EtOH/H_2O. All solutions were prepared in volumetric flasks and promptly transferred to airtight containers, which were purged with N_2 and sealed with parafilm after preparation and after each use. Stock solutions of dyes B and E were prepared by weighing out the dye, adding an appropriate amount of ethanol to make a stock solution that was at least 1 mM in concentration, and sonicating to dissolve the solution.

B.1.2.3 Initial protonation studies in HCl (dyes B, C, and H)

Initial protonation studies were carried out to determine the effect of varying concentrations of HCl, solvent composition (percent water), and ionic strength on the spectroscopic behavior of the dyes. Solutions for the protonation studies of dyes using HCl were prepared by adding 0.100 mL of one of the daughter acid stock solutions (1-5 mM) and 1.00 mL of a secondary (0.1 mM) dye

solution to one of five 5 mL class A volumetric flasks, which were then filled to the mark with ACN. The five resulting working solutions were 20 µM dye, 2% H_2O, and 20, 40, 60, 80, and 100 µM HCl. In some cases a sixth working solution containing 200 µM HCl was prepared by the same method as the others but using the 10 mM HCl daughter stock. Absorption spectra were then collected and analyzed. These studies were carried out for dyes B, C, and H.

It was of interest to determine whether the changing ionic strength in the previously described protonation studies had any effect on the protonation behavior, whether increasing the ionic strength to higher concentrations affects this behavior, and also to determine how the percentage of water affects this behavior. To this end, protonation studies identical to those described in the previous paragraph were carried out using HCl solutions of varying concentrations at constant ionic strength. These constant ionic strength protonation studies were compared to protonation studies of the dyes with varying concentrations of HCl (with no correction for ionic strengths) to ensure that the observed spectral behavior was due to the changing concentration of acid alone. Additionally, protonation studies were carried out to test the effect of increasing the ionic strength when the concentration of acid is held constant by making working solutions in a manner identical to that described in the previous paragraph using the HCl stock solutions that were 3 mM HCl and I = 5 mM, 10 mM, 50 mM, and 100 mM. Finally, studies of the effect of percent water on the spectral characteristics of the protonated dyes were carried out. Working solutions were prepared by pipetting 0.1 mL of the 3 mM HCl and 0, 0.1, or 0.3 mL ultrapure H_2O into each 5 mL volumetric flask, along with 1 mL of 0.1 mM secondary dye stock solution, resulting in solutions that contained 2%, 4%, or 8% H_2O (by volume), respectively. Constant and varied ionic strength studies and studies of the effect of

percent water were carried out for dyes B and C, and the results were assumed to be representative of all of the dyes.

B.1.2.4 Protonation studies using acetic acid, phenol, PTSA, and $HClO_4$

The weak acids phenol and acetic acid and the strong acids PTSA and $HClO_4$ were considered as possible protonating agents for the dyes. Solutions for the protonation studies of dyes using these other acids were prepared by adding 0.100 – 0.500 mL of the 1 mM acid stock solutions (prepared in acetonitrile) and 1.00 mL of a secondary (0.1 mM) dye solution to one of five 5 mL class A volumetric flasks, which were then filled to the mark with ACN. The five resulting working solutions were essentially anhydrous (<0.1% H_2O), containing 20 µM dye and 20, 40, 60, 80, or 100 µM acid. In some cases a sixth working solution containing 200 µM acid was prepared by the same method as the others by pipetting 1.000 mL of the 1 mM acid stock solution into the working solution. Protonation studies using phenol and acetic acid were carried out for dye C but were not pursued beyond this as no protonation occurred. Protonation studies using PTSA were carried out for dyes C and H, and protonation studies using $HClO_4$ were carried out for all of the dyes. Perchloric acid was ultimately chosen as the best acid for these studies as it is the only one of these acids known to be fully dissociated in acetonitrile;[32] hence the cessation of protonation studies using PTSA after testing two dyes despite the fact that protonation by this acid was observed.

B.1.2.5 Method of determining molar absorptivities

The absorption spectra of working solutions of varying dye concentrations were measured, and the absorbance at the wavelength of maximum absorbance (λ_{MAX}^{AB}) was determined. The

absorption (A) of each sample at λ_{MAX}^{AB} were plotted as a function of concentration (C), the linear regression equation was computed, and the molar absorptivity (ε) was taken as the slope, as per Beer's law,

$$A = \varepsilon bC$$

where b is the pathlength of the cell (1.000 cm). Absorptivities were determined in duplicate and averages and percent relative standard deviations were calculated. Molar absorptivities for the basic forms of the dyes were determined in acetonitrile. Absorptivities for the protonated forms of most of the dyes were determined by adding a constant amount of hydrochloric acid in acetonitrile (<0.1% H_2O) to the dye solutions and taking the absorption at the bathochromic peak λ_{MAX} (where present) thought to correspond to the singly protonated form of the dye. Preliminary protonation studies in which HCl concentration was varied and dye concentration was held constant were carried out; the concentration of HCl resulting in the greatest observed bathochromic peak absorptivity was chosen as the concentration used to determine the protonated form molar absorptivity. However, for dye F (terpyridine dye with 4' diethylamino substituent) the concentration of HCl was varied with the dye concentration to maintain the singly protonated form, as this dye showed a stronger dependence of extent of protonation on acid concentration than the others. Additionally, molar absorptivities of the protonated and basic forms of terpyridine dyes I and J could not be determined as these dyes exhibited aggregation behavior that strongly changed the absorptivities over time.

Although perchloric acid was found to be ideal for the protonation studies, unfortunately it could not be used in the molar absorptivity studies. As $HClO_4$ is a strong acid even in

acetonitrile, when dye concentrations were decreased while the concentration of $HClO_4$ was held constant, the extent of protonation of almost all of the dyes changed significantly as the equilibrium shifted, as per Le Châtelier's principle. When a weaker acid such as HCl was used, this shift in equilibrium was far less apparent and stable absorptivities (for all dyes except F) were obtained even without changing the acid concentration relative to the dye concentration.

B.1.2.6 Aggregation studies of dyes F, I, and J

Attempts at determining molar absorptivities of terpyridine dyes I and J resulted in nonlinear results, and additionally, measuring the absorption of a single solution of dye I over time yielded massively different absorption values. This strange behavior prompted time-dependent aggregation studies of terpyridine dyes I and J, in which the absorption of single solutions of the singly protonated and non-protonated forms of each dye were measured multiple times over the course of an hour. An analogous aggregation study was carried out for terpyridine dye F as a control. For dye F, absorption was determined at two different wavelengths and plotted as a function of time. Additionally, the ratio of absorbances at the two wavelengths was plotted as a function of time. No other dyes were studied as the unstable absorption behavior observed in dyes I and J was not observed in other dyes.

B.1.2.7 Standardization of $HClO_4$ solutions for pK_a determination

Perchloric acid solutions were standardized indirectly by a 1:100 dilution of the 1 M $HClO_4$ solution in 50% EtOH / 50% H_2O with deionized water to a total volume of 200 mL (such that the final percentage of ethanol was 0.5%); this dilution in water was carried out to ensure that the apparent endpoint of the titration was not perturbed by the high organic solvent content present

in the parent solution. This 0.01 M $HClO_4$ solution was used to titrate triplicate samples of THAM weighing between 0.02 and 0.03 g (weighed out to four significant figures on a five decimal place analytical balance). The THAM samples were dissolved fully in 20-30 mL triply deionized water prior to titration. Bromocresol green was used as an indicator, and the titration was carried out until the green endpoint was reached. The average molarity of this secondary solution was then calculated and used to calculate the molarities of the three perchloric acid solutions prepared in 50% EtOH / 50% H_2O.

B.1.2.8 Spectroscopic pK_a determination

Solutions for UV-visible spectroscopic pK_a determination were prepared by making up a solution that contained 20 µM dye and increasing concentrations of $HClO_4$ (by adding either 0.01 M, 0.1 M, or 1 M $HClO_4$) to vary the pH. Ionic strengths of each sample were adjusted to 0.1 M using 2 M NaCl, and appropriate volumes of EtOH and deionized H_2O were added such that the final solvent composition was 50% EtOH/H_2O. Samples were prepared to a final volume of 5 mL in a 10 mL test tube.

Each solution was thoroughly mixed and then part of the solution was transferred into a cuvette for measurement of the absorption spectrum. A pH electrode (calibrated by a 3-point calibration and equilibrated for at least 3 minutes in a solvent composition containing 50% EtOH/H_2O mixture) was inserted into the remaining solution and the pH was measured at the same time as the absorption spectrum.

UV-visible absorption spectroscopy can be used to determine the p_sK_a values of these compounds by preparing solutions of varying pH in a medium of constant solvent composition,

dye concentration, and ionic strength, and measuring the absorption at the red-shifted wavelength corresponding to HB^+. As the absorption at this wavelength is zero when no acid is present (all dye is in the basic form) and goes to zero when sufficiently high concentrations of acid are present (all dye is in the form H_2B^{2+}), any absorption at this wavelength ($A_{\lambda,\,HB+}$) is proportional to the concentration of HB^+ (C_{HB+}) as per Beer's law.

$$A_{\lambda,\,HB+} = \varepsilon b C_{HB+}$$

Since the two spectroscopic equilibria are clearly distinguished by two distinct sets of isosbestic points, it can be assumed that the two p_sK_a values are at least two units apart, and therefore it can be assumed that when $A_{\lambda,\,HB+}$ reaches a maximum, essentially all of the dye present is in the singly protonated form (HB^+); in other words, the concentration of HB^+ is equal to the formal concentration F of the dye:

$$F = [B]_0 = [B] + [HB^+] + [H_2B^{2+}] = [HB^+] \qquad \text{when } A_{\lambda,\,HB+} \text{ is at a maximum}$$

By definition, when $pH = p_sK_{a1}$, $[H_2B^{2+}] = [HB^+]$ and because the p_sK_{a1} values are at least two units apart, $[B] \approx 0$. Accordingly, when $pH = p_sK_{a1}$, half of the dye present is in the singly protonated form.

$$F = [B]_0 = [B] + [HB^+] + [H_2B^{2+}] = 2[HB^+];$$

$$[HB^+] = \tfrac{1}{2}\,F \qquad (\text{when } pH = p_sK_{a1})$$

Because absorption is linearly proportional to concentration, and the absorption at λ_{HB+} is zero when all B is converted to H_2B^{2+}, when pH = p_sK_{a1}, the absorption of the red shifted peak is half the maximum absorption at this wavelength.

$A_{\lambda, HB+} = ½\ A_{\lambda, HB+\ MAX}$ (when pH = p_sK_{a1})

The same relationship holds when pH = pK_{a2}; by definition, at pH = pK_{a2}, [B] = [HB^+] and because the p_sK_a values are at least two units apart, [H_2B^{2+}] ≈ 0, so at this pH, [HB^+] = ½ F. Because absorption is linearly proportional to concentration, and the absorption at λ_{HB+} is zero when the dye is in its deprotonated form B, when pH = p_sK_{a2}, the absorption of the red shifted peak is half the maximum absorption at this wavelength.

$A_{\lambda, HB+} = ½\ A_{\lambda, HB+\ MAX}$ (when pH = p_sK_{a2})

Accordingly, both p_sK_a values were determined by plotting absorption at λ_{HB+} as a function of pH, which resulted in a Gaussian shaped curve, determining $A_{\lambda, HB+\ MAX}$, and solving for pH for $A_{\lambda, HB+} = ½\ A_{\lambda, HB+\ MAX}$ from the function defining the linear side regions of the curve both at pH lower than the pH corresponding to $A_{\lambda, HB+\ MAX}$ (to determine p_sK_{a1}) and at pH higher than the pH corresponding to $A_{\lambda, HB+\ MAX}$ (to determine p_sK_{a2}).

The acid dissociation constants determined in the solvent water mixture (p_sK_a) were then used to calculate the aqueous acid dissociation constants (pK_a) by assuming that the slope of p_sK_a versus percent EtOH is 0.03665 and extrapolating to zero percent EtOH. The effect of ionic

strength on the aqueous pK_a was accounted for by subtracting 0.04 from the calculated aqueous pK_a (as I = 0.100 M in these experiments).[43]

B.1.3 Results and discussion

B.1.3.1 Protonation studies in HCl (dyes B, C, and H)

Protonation studies of dyes B, C and H were carried out using HCl. As mentioned previously, HCl stock solutions were prepared in ultrapure water, accordingly the working solutions were 2% H_2O. Absorption spectra from the protonation studies of dyes B, C, and H are provided in Figures B.1.3, B.1.4, and B.1.5, respectively.

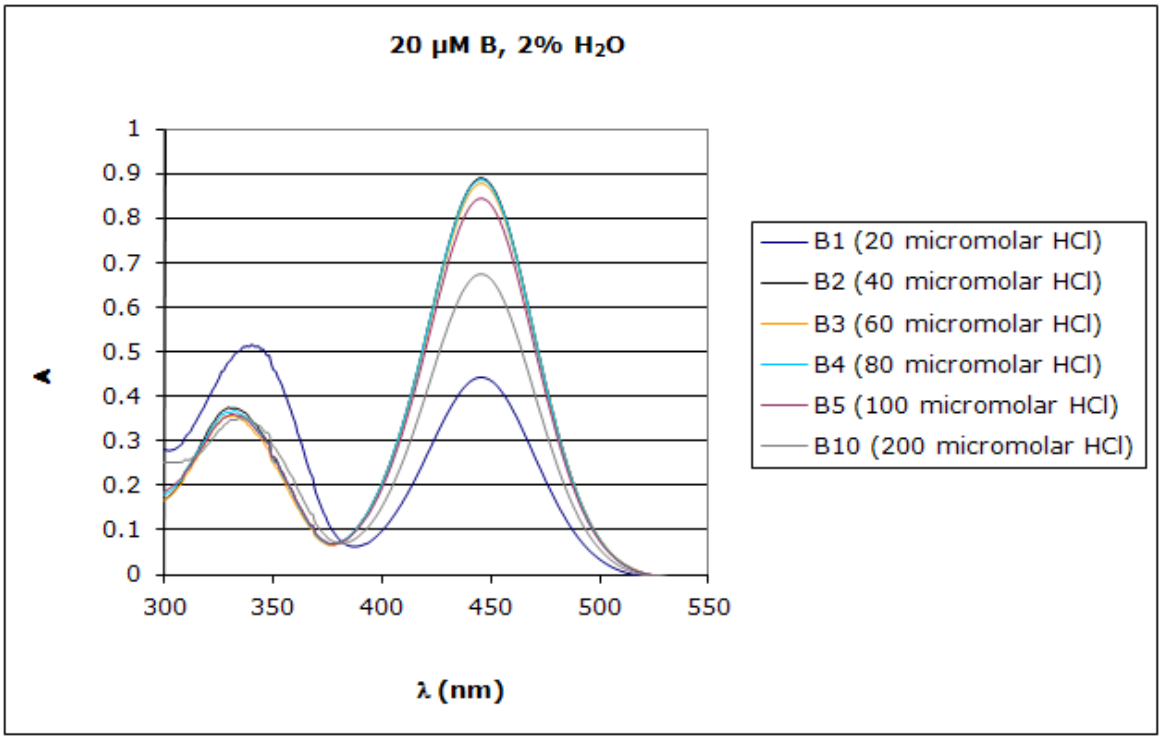

Figure B.1.3. Protonation study of B in HCl (20-200 µM)

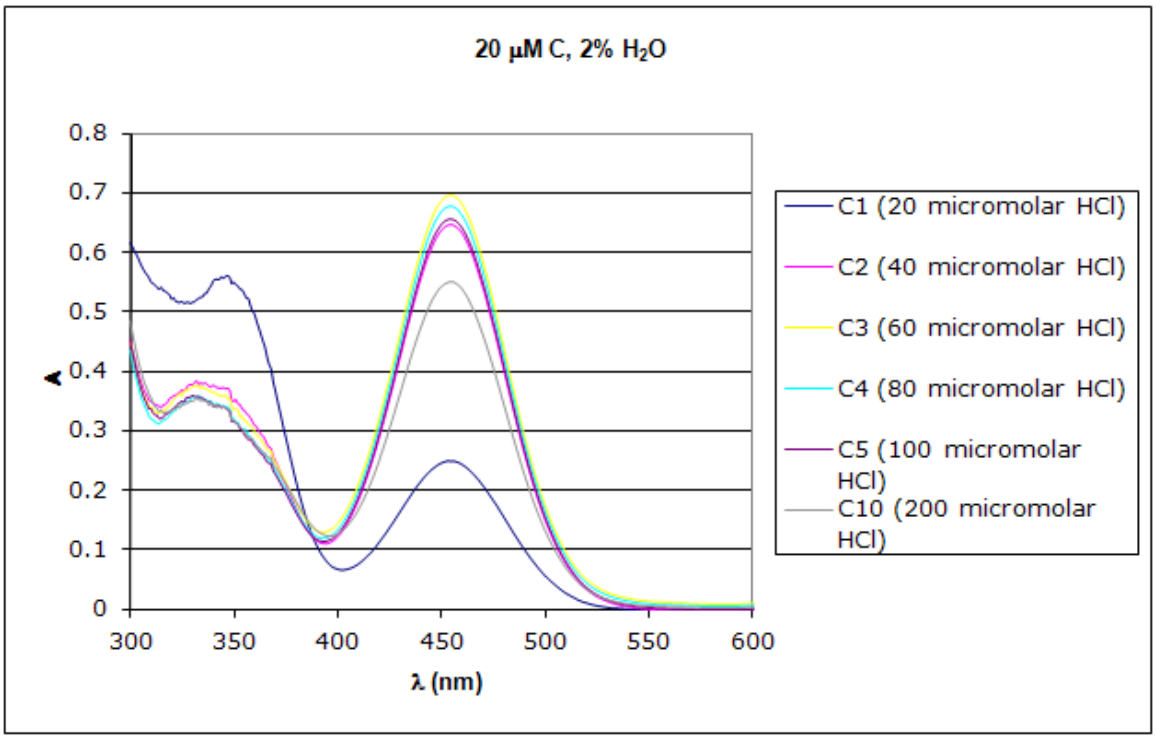

Figure B.1.4. Protonation study of C in HCl (20-200 µM)

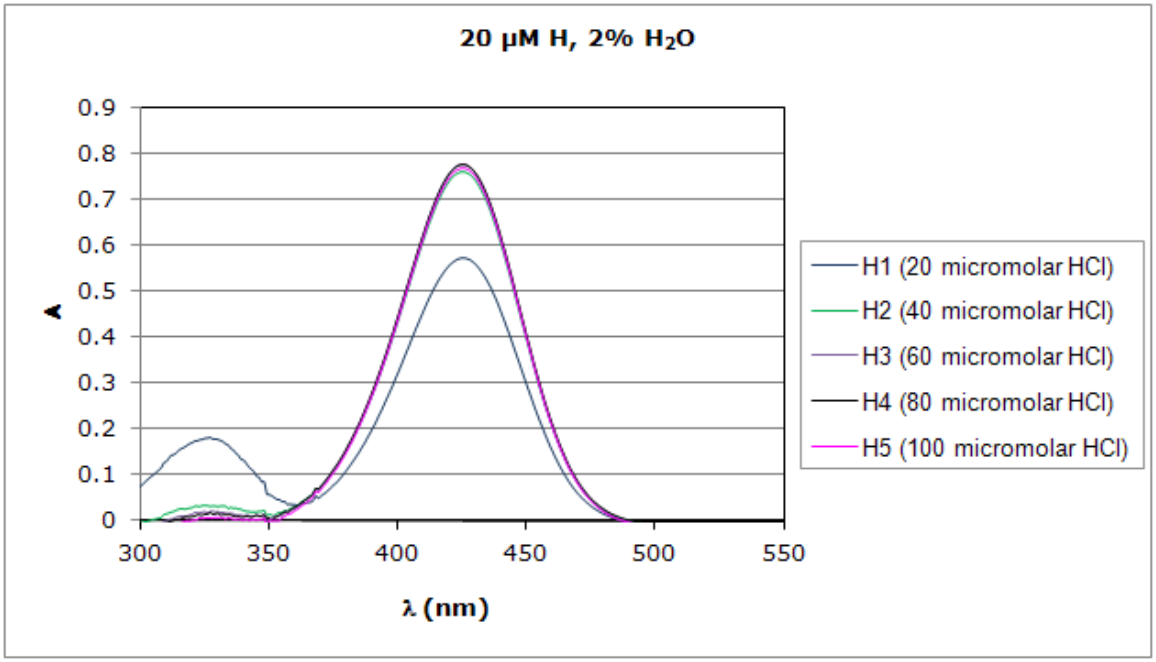

Figure B.1.5. Protonation study of H in HCl (20-100 µM)

For these dyes, the spectroscopic behavior discussed in B.1.1.1 is readily apparent. As the concentration of acid is increased, a red-shifted peak appears in the spectrum, indicating the presence of the singly protonated form of the dye (HB^+). This peak reaches a maximum, then begins to decrease as acid concentrations are further increased, indicating the second protonation equilibrium (the formation of H_2B^{2+}). At concentrations of HCl corresponding to the greatest observed absorptivity of the bathochromic peak, the absorption peak in the wavelength region near the λ_{MAX} of the base form disappears for dye H, but not for dyes B and C. Under these conditions, dyes B and C possess absorption peaks in this region that are slightly blue shifted and of lower intensity relative to those observed in the absence of added acid. This spectral feature was later observed in the protonation studies of all of the aryl-substituted dyes (A, B, C, D, E and G) with $HClO_4$, and was only absent in alkyl-substituted dye H, accordingly this second peak in the absorption spectrum is likely a result of the aryl D_1 and D_2 substitution.

Protonation studies to elucidate the effects of ionic strength and percent water were also carried out for dyes B and C protonated with HCl. The results of the protonation study carried out for dye B at constant ionic strength I = 100 μM are provided in Figure B.1.6. Comparison of the spectra for concentrations of HCl ranging between 20 – 100 μM when the ionic strength is not corrected for (Figure B.1.3) versus when the ionic strength is held constant (Figure B.1.6) indicates no appreciable difference in the extent of protonation and relative peak heights. The same behavior was observed for dye C (spectra not shown).

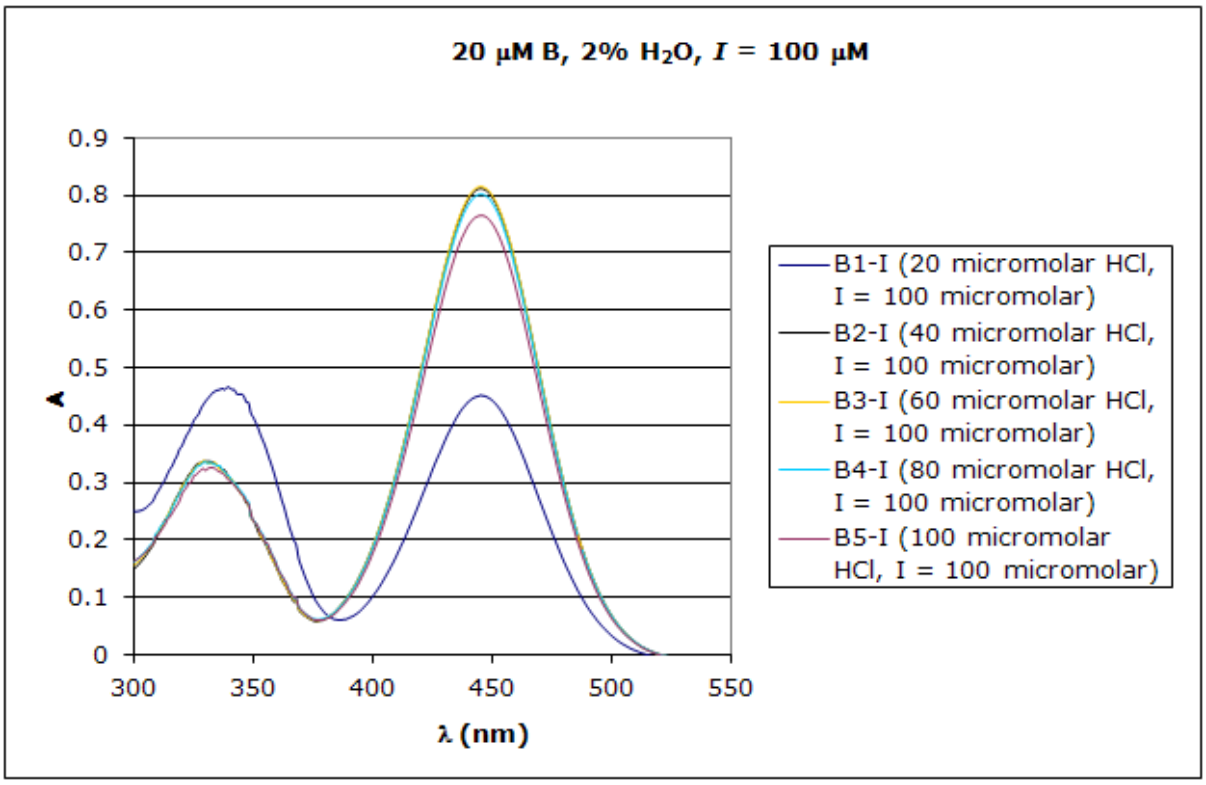

Figure B.1.6. Protonation study of B in HCl (20-100 µM) when the ionic strength is held constant at 100 µM

Provided in Figure B.1.7 are the results of the ionic strength study of dye B carried out when *I* was varied from 100 – 2000 µM (0.01 – 0.2 M) while [HCl] was held constant at 60 µM and [B] was held constant at 20 µM. When the ionic strength is increased substantially beyond 100 µM, it appears that the protonation equilibrium is perturbed slightly, as evidenced by the apparent decrease in the absorption of the red-shifted peak corresponding to the singly protonated form (HB^+) and a change in the relative peak heights. Accordingly, adjustment for ionic strength is necessary in the protonation studies only when higher concentrations of acid are used.

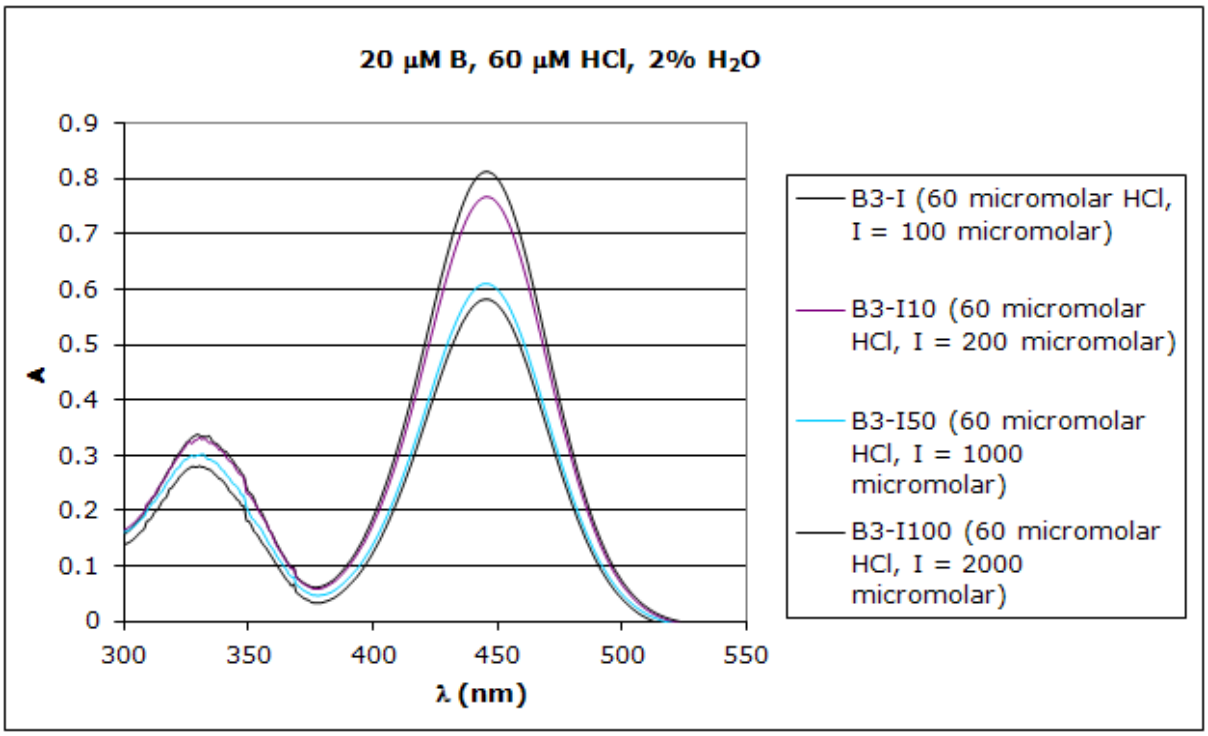

Figure B.1.7. Effect of increasing ionic strength from 100 – 2000 µM when concentrations of dye B and HCl are held constant

Provided in Figure B.1.8 are the results of the protonation study of dye B when [HCl] (and *I*) were held constant at 60 µM while the percentage of water was increased from 2 – 8%. Increasing the percentage of water also appears to perturb the equilibrium, as evidenced by similar spectral changes. Accordingly, even small changes in the solvent-water ratio must be accounted for when studying these dyes.

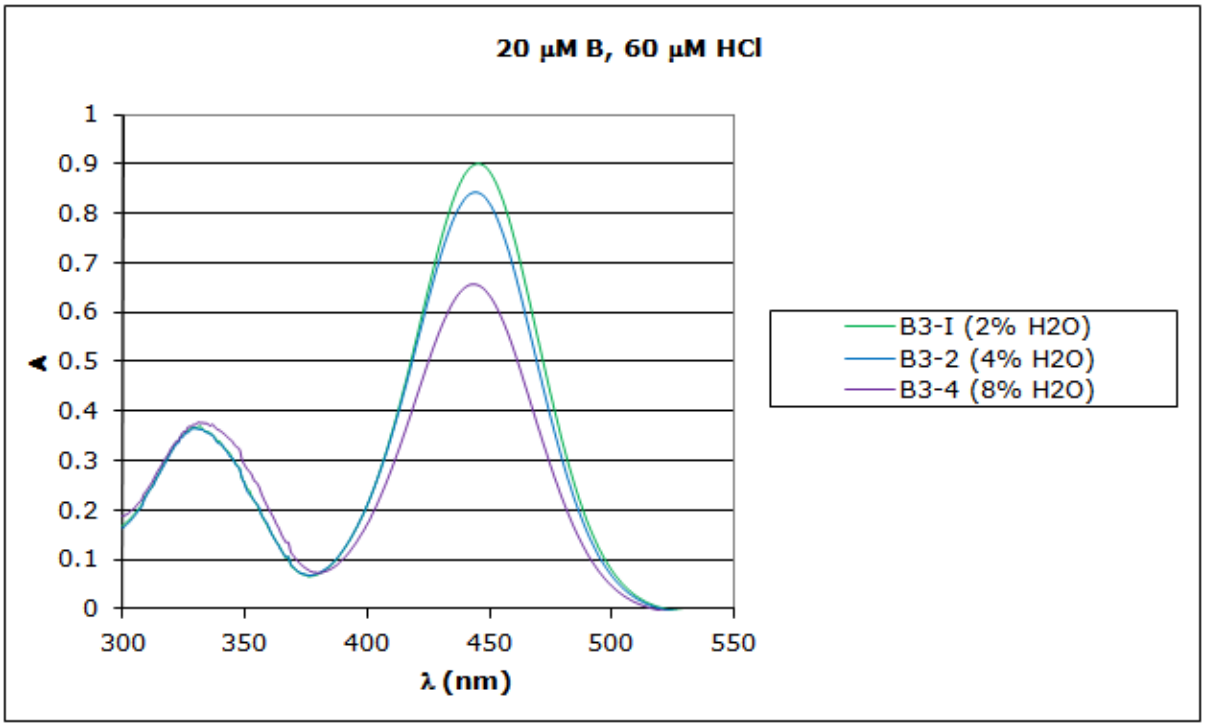

Figure B.1.8. Effect of increasing percentage of water in solvent-water mixture from 2%–8% when concentrations of dye B and HCl are held constant

B.1.3.2 Protonation studies using acetic acid, phenol, PTSA, and $HClO_4$

"Proton sharing" or complexation studies were carried out for dye C using phenol. It was expected that phenol would form hydrogen bonded complexes with the dyes, as the phenol and pyridine moieties of polymers bearing phenol and pyridine substituents are known to selectively form hydrogen bonds (in which the hydroxyl proton is shared) in solvents of sufficiently low polarity.[44,45] Such an interaction would be expected to result in a pronounced change in the UV-visible absorption spectrum,[46,47] however, no spectral evidence of hydrogen-bonding interactions between the phenol and pyridine group was observed, even when extremely high concentrations of phenol were used. The weak acid acetic acid was also tested in a protonation study of dye C, but like phenol, no color change or spectral shift was observed. Larger amounts of acid were added to the working solutions,

and working solutions were even prepared directly in the stock solutions of phenol and acetic acid, but still no evidence of protonation or hydrogen bonding was observed. The strong acid PTSA was also considered as a potential protonating agent for the dyes. Protonation studies using PTSA were carried out successfully for dyes C and H, as indicated by the previously discussed spectral changes associated with protonation. A representative protonation study of dye H using PTSA is provided in Figure B.1.9 However, protonation studies using PTSA were abandoned in favor of the stronger acid $HClO_4$.

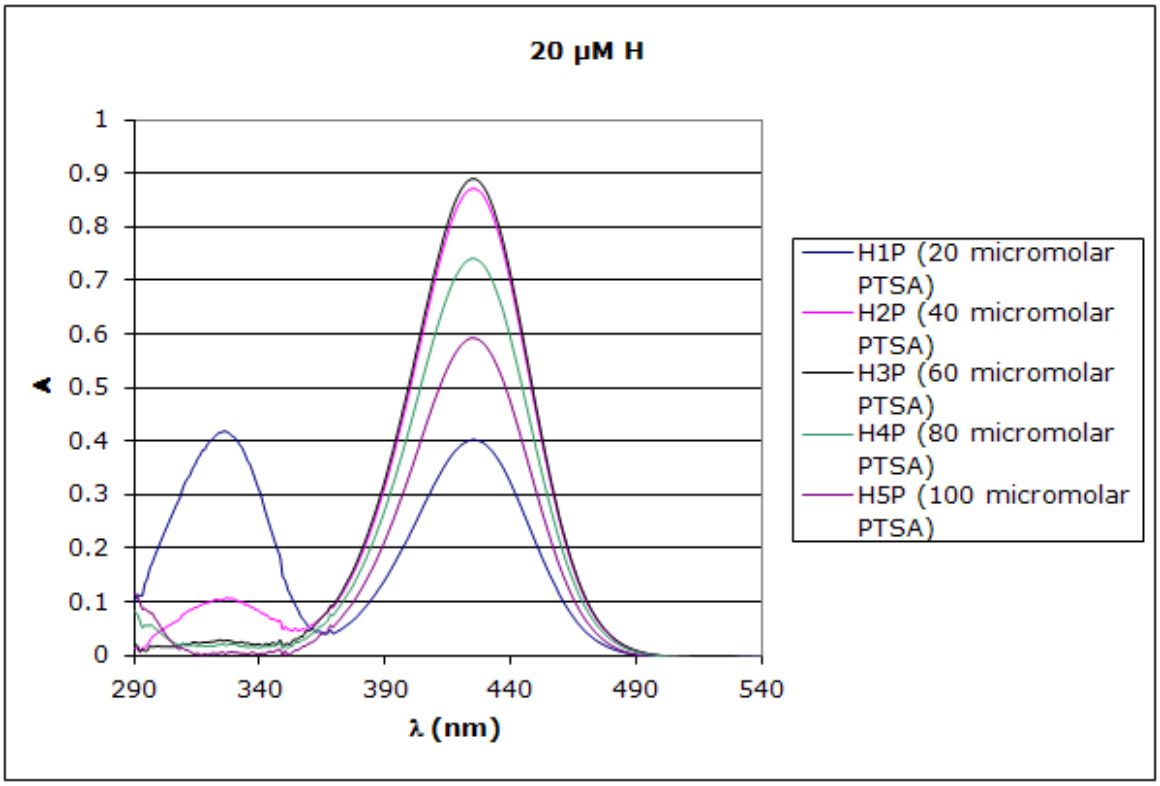

Figure B.1.9. Protonation study of dye H in PTSA (20-100 µM)

As discussed in B.1.1.2, acetonitrile has both a lower dielectric constant and lower donor number than water, therefore bases become significantly stronger and acids become significantly weaker in acetonitrile (i.e. an increase in pK_a is observed).[32] In acetonitrile, the weak acids phenol and acetic acid have pK_a values of 29 and 23.5, respectively, thus no dissociation is expected to occur, and even the strong acids HCl and PTSA have pK_a values of 8.9 and 8.45, respectively; thus neither of these acids are completely dissociated.[35] However, perchloric acid is fully dissociated even in acetonitrile.[32] Thus the use of $HClO_4$ ensures that the acid is fully dissociated and allows for estimation of solution pH (as it cannot be directly measured in acetonitrile using conventional electrodes) by ignoring the activity coefficient of the hydrogen ion and assuming that the pH is given solely by the concentration of hydrogen ion in solution; in other words, by assuming that the solution pH = p_cH.

Protonation studies were carried out for all of the dyes in $HClO_4$. Concentrations of acids used ranged from 20 – 200 µM, with corresponding p_cH values of 4.7 (20 µM), 4.4 (40 µM), 4.2 (60 µM), 4.1 (80 µM), 4.0 (100 µM), and 3.7 (200 µM). One of the first protonation studies was carried out for dye H, the results of which are presented in Figure B.1.10.

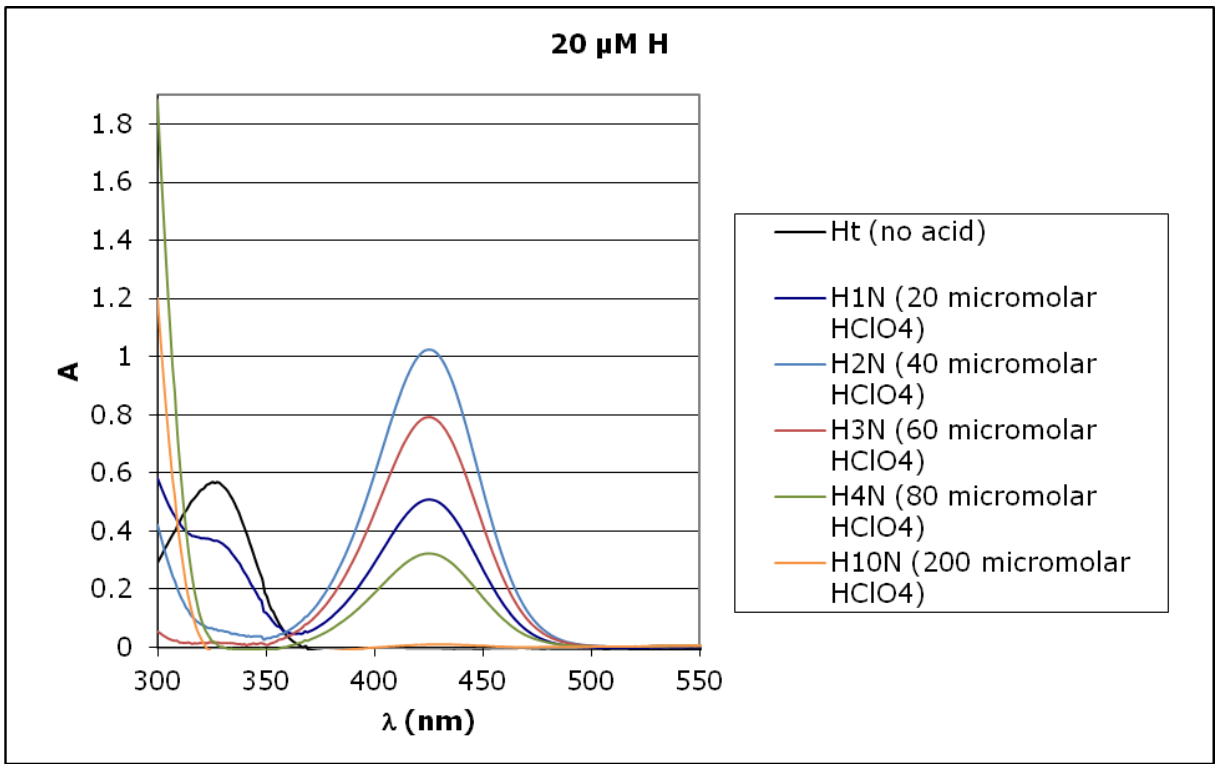

Figure B.1.10. Protonation of H using $HClO_4$ (20 – 200 µM) including base form peak Ht (in absence of acid)

The protonation study of dye H using $HClO_4$ clearly indicated spectral characteristics of both protonation equilibria. As the concentration of acid increased from 0 – 40 µM, the peak at 326 nm corresponding to the base form decreased almost to zero, while the bathochromic peak corresponding to the singly protonated form of the dye increased to a maximum absorption of approximately 1. When the acid concentration is further increased beyond the concentration required for maximum bathochromic peak absorption (60 – 200 µM), the bathochromic peak disappears fully, and a third peak with a hypsochromic shift relative to the base form peak appears, presumably corresponding to the doubly protonated form of the dye. When the study was carried out, the full disappearance of the bathochromic peak in the spectra had not been previously observed in our lab, and thus it was deemed necessary to ensure that the observed behavior was not a result of dye breakdown by the highly oxidizing perchloric acid.

To ensure the full disappearance of the bathochromic peak was not a result of dye decomposition, one additional study was carried out in which two samples were prepared. One sample was prepared that was 20 µM dye and 200 µM $HClO_4$, and a second sample was prepared in an identical fashion, except to this sample 160 µM NaOH (from a 1 mM solution prepared in deionized water) was added several minutes after the addition of acid but prior to diluting the solution to the mark. Both samples contained equal concentrations of dyes and acid, but the addition of base to the second sample resulted in an "effective" acid concentration of 40 µM. The results are shown in Figure B.1.11.

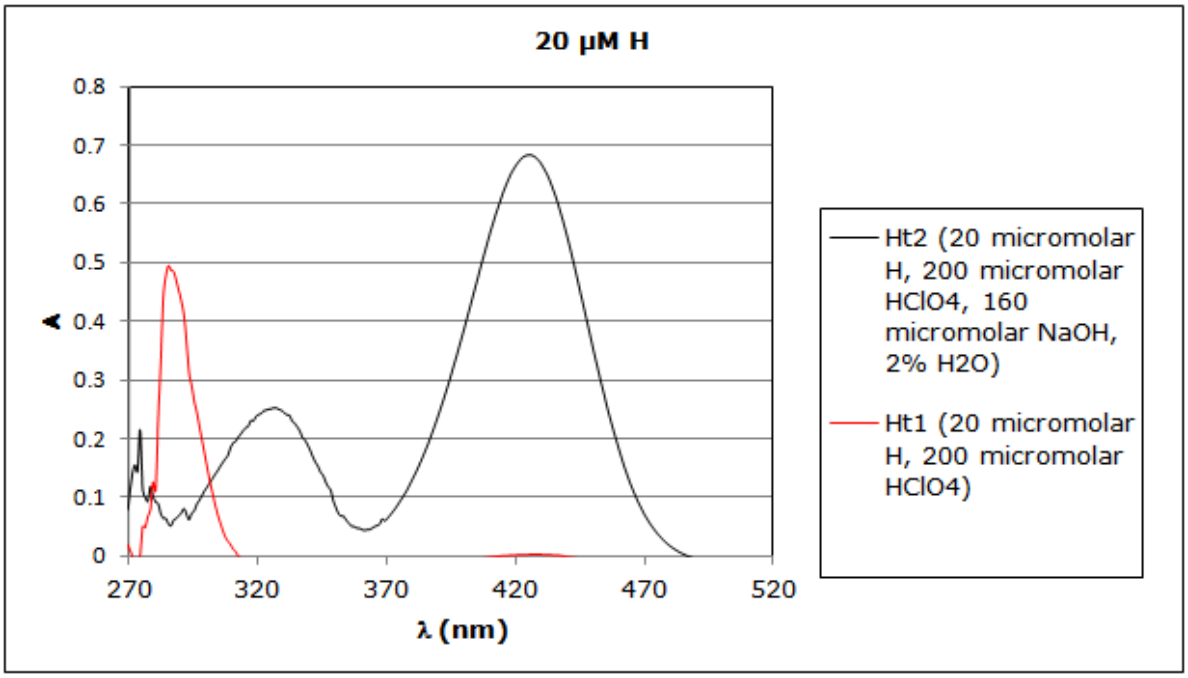

Figure B.1.11. The observed disappearance of the bathochromic protonation peak and appearance of the hypsochromic peak in Figure B.1.10 is reversible and not due to oxidation

For the first sample, the absorption behavior was the same as that observed in Figure B.1.10 (for the 200 µM acid sample), and for the second sample, the red-shifted peak (associated with the

singly protonated form of the dye) reappeared, along with the peak associated with the nonprotonated form of the dye. The second spectrum was not identical to that observed for 40 μM $HClO_4$ in acetonitrile, but this is to be expected because this sample contains NaOH and water in addition to the aforementioned species, and as found from previous studies both the increased ionic strength due to the NaOH and the presence of water have an influence on the extent of protonation observed for these compounds. The more important observation is that the disappearance of the bathochromic peak is reversible, and therefore not due to dye oxidation. It also reinforces the assumption that the presence of the bathochromic peak is solely indicative of the singly protonated form (HB^+), as the absorption in that region is zero both in the absence of acid and in the presence of adequately high concentrations of acid. This assumption is central to the method chosen to calculate the pK_a values of these dyes.

Protonation studies were carried out for all of the dyes using $HClO_4$. As two distinct equilibria are present in protonation spectra, the spectra from each of the studies except that of F were split into two groupings to simplify interpretation. The subsets of spectra belonging to group (I) correspond to the first protonation equilibrium, and include spectra of the base form of the dye and of the dye in the presence of increasing concentrations of $HClO_4$, up to the maximum observed absorptivity for the red-shifted peak (typically 40 – 60 μM $HClO_4$), at which point the concentration of the singly protonated form is thought to be at a maximum. The subsets of spectra belonging to group (II) correspond to the second protonation equilibrium, and include spectra obtained by increasing the concentration of acid past that corresponding to the maximum observed absorptivity of the red-shifted peak. Spectra from the protonation study of terpyridine dye F were split into three groupings to showcase its unique spectral behavior. As similar protonation behavior occurs in all of the non-terpyridine dyes, groups of peaks will be

distinguished by the conventions α [for the base form peak(s)], β [for the bathochromic peak that appears upon addition of smaller amounts of acid], χ [for the hypsochromic peak that appears upon addition of larger amounts of acid], and δ [for the peaks unaffected by concentration of acid added present in the spectra of the phenyl-substituted dyes at similar wavelengths to the α band].

Absorption spectra from the protonation study of dye B using $HClO_4$ are provided in Figure B.1.12 below. The protonation behavior exhibited by dye B is representative of the behavior exhibited by all of the aryl-substituted dyes with diethylaniline D_3 substituents (dyes A, B, C, D, E, and G).

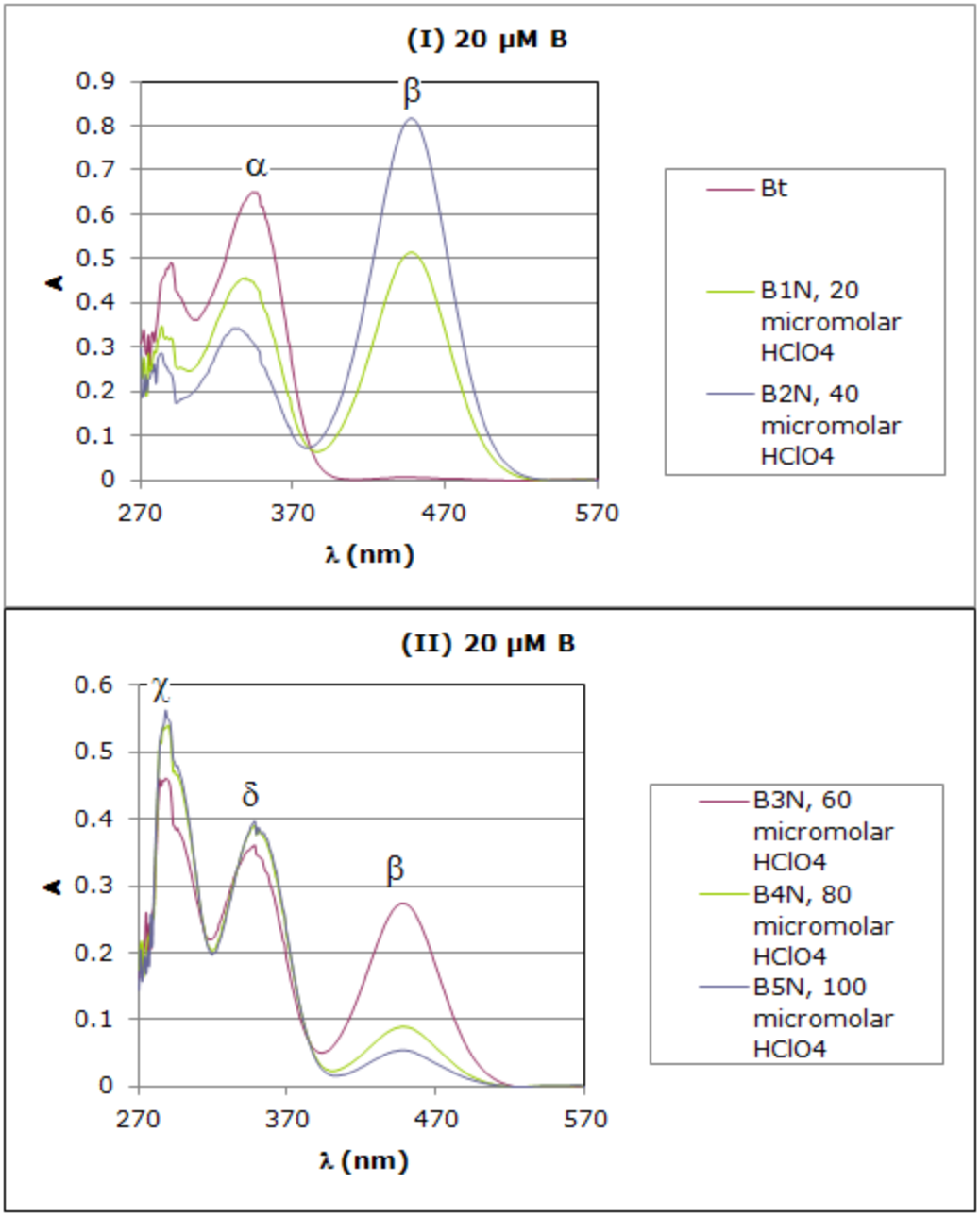

Figure B.1.12. Protonation study of B using $HClO_4$, with labeled α, β, χ, and δ bands. Bt = base form absorption of B (no added acid). (I): 0 – 40 µM H^+, (II): 60 – 100 µM H^+

In group (I) spectra, upon adding increasing concentrations of acid, dye B shows a decrease in the α band and an increase in the β band, as well as the appearance of the δ band in the same spectral region where the α band was previously present (but possessing a spectral shift relative to the α band). This behavior is associated with a color change from colorless to yellow.

In group (II) spectra, the β band decreases while the χ band increases and the δ band is unaffected. This behavior is associated with a disappearance of the yellow color and the bathochromic peak. The δ band is not a relic of the α band, but can instead be attributed to the phenyl substituents of the dyes A – E and G,[48] as it possesses a hypsochromic shift relative to the α band. Additionally, the δ band is not present in the spectrum of *tert*-butyl substituted dye H.

It is worth noting that most of the dyes possessing a diethylaniline D_3 substituent display greater absorptivity in the bathochromic β band relative to the base form α band when protonated with perchloric acid; the only exceptions are dyes E and G. These two dyes are expected to be the least basic, poorest nucleophiles of the dyes studied, as dye E possesses electron-withdrawing *para*-chlorophenyl D_1 and D_2 substituents, and dye G possesses an *ortho*-phenol group as its D_1 substituent that is capable of intramolecular hydrogen bonding with the pyridine nitrogen, as shown in Figure B.1.13. This correlation between electron-withdrawing functionality and absorptivity of the bathochromic protonation peak will be explored further in the conclusion.

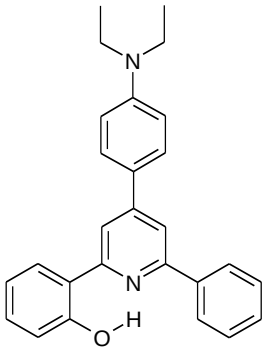

Figure B.1.13. The chemical structure of dye G facilitates intramolecular H-bonding

The terpyridine dyes ($D_1 = D_2$ = 2-pyridyl) showed distinctly different spectral behavior from the phenyl- and alkyl-substituted dyes. Terpyridine dye F displayed particularly unique spectral behavior (Figure B.1.14). In the group (I) spectra, upon addition of increasing amounts of acid, the α band decreased while the β band increased to a maximum (corresponding to a color change from yellow to red). However, when the acid concentration was increased further, only a slight hypsochromic shift (19 nm) was observed for the transition from the β to the χ band, corresponding to a slight change in the shade of red observed, as shown in the group (II) spectra. This behavior was unique among the aniline-substituted dyes studied; all other dyes with this functionality displayed a pronounced hypsochromic shift (>100 nm) upon addition of higher concentrations of acid. Further addition of acid beyond this point did not change the spectral characteristics significantly, as evidenced in the group (III) spectra.

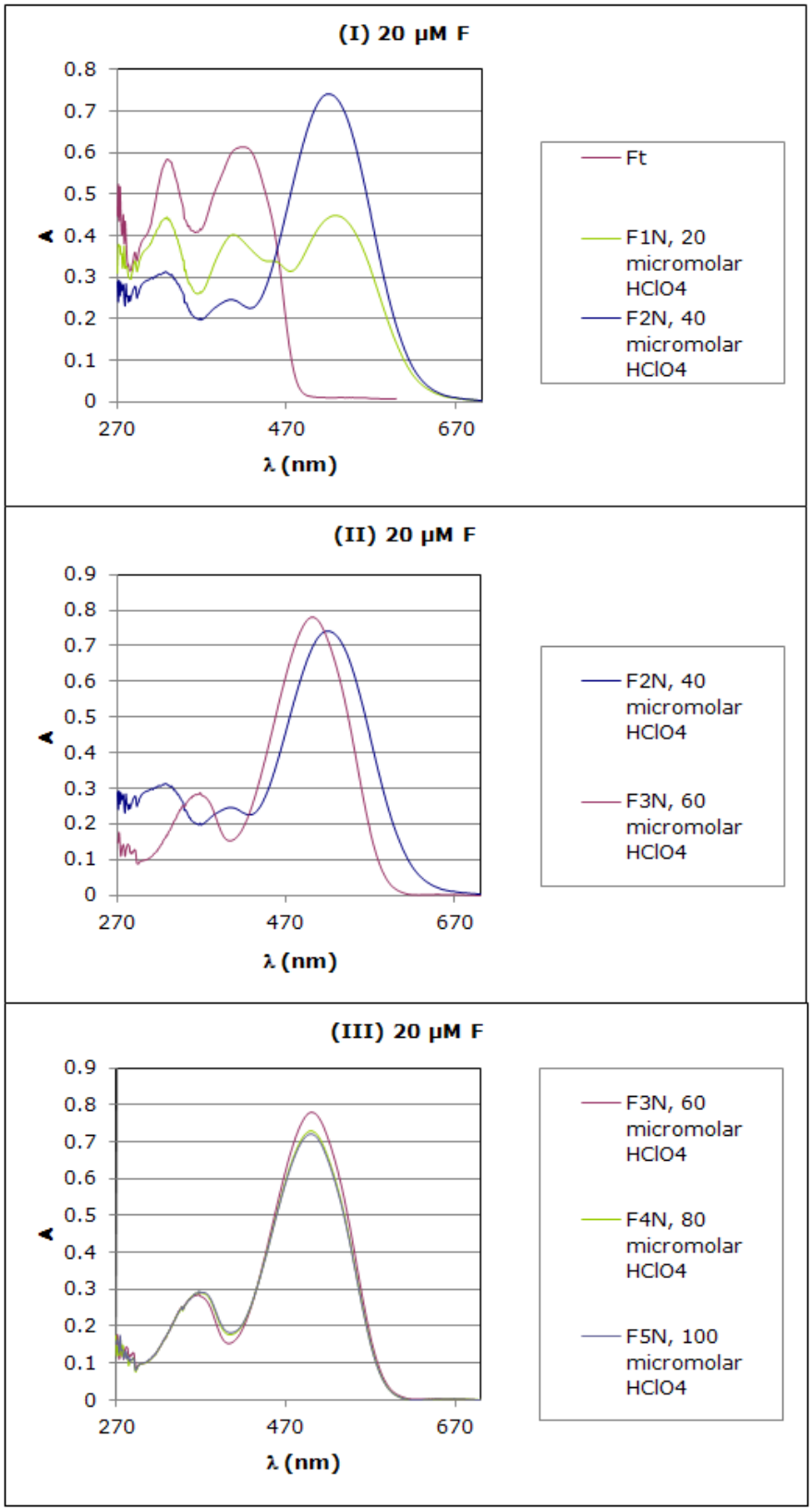

Figure B.1.14. Protonation study of F using $HClO_4$.
(I): 0 – 40 µM H^+, (II): 40 – 60 µM H^+, (III): 60 – 100 µM H^+

When the diethylaniline D_3 group of dye F is swapped for nonbasic ethoxyphenyl or toluene residues (in dyes I and J), the spectral behavior is changed dramatically. In both dyes I and J, the λ_{MAX} in the absence of added acid (α band) is decreased by more than 100 nm, and the red shift of the β-band is much smaller (~50 nm). Additionally, the β band demonstrates low absorptivity and is poorly resolved from the band at λ_{MAX} (which does not change as the pH is changed). Upon addition of higher concentrations of acid, the red-shifted peak blends into the λ_{MAX} band as a broad shoulder. Representative spectra from the protonation study of ethoxyphenyl-substituted terpyridine dye I are provided in Figure B.1.15 for comparison with that of dye F (Figure B.1.14). Toluene-substituted terpyridine dye J exhibited analogous behavior to that of dye I.

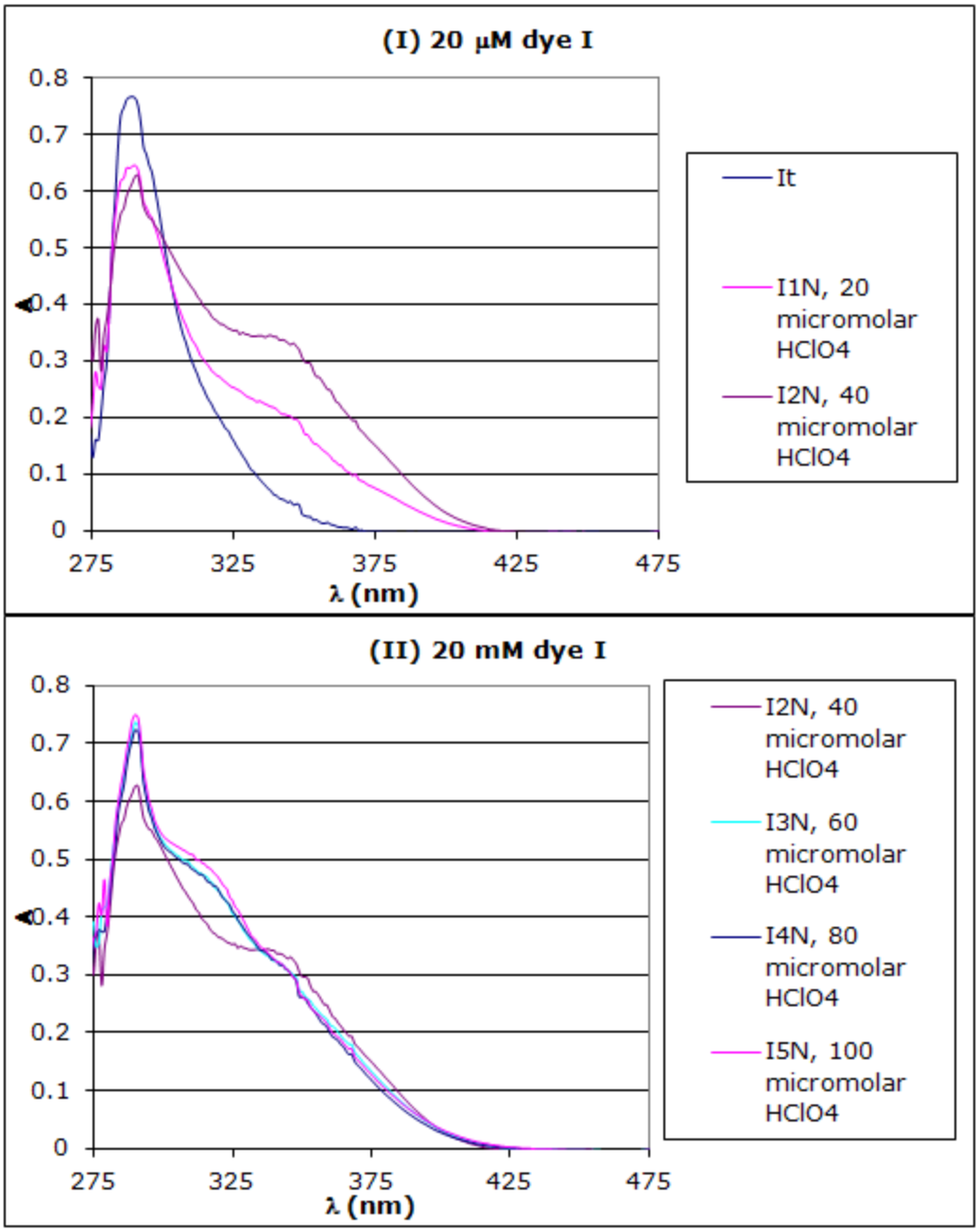

Figure B.1.15. Protonation study of I using $HClO_4$.
(I): 0 – 60 µM H^+, (II): 60 – 100 µM H^+

B.1.3.3 Aggregation studies of dyes F, I, and J

Attempts at determining the molar absorptivities of terpyridine dyes I and J failed, as the absorption as a function of concentration was extremely nonlinear. Additionally, it was observed that the absorption of a single solution could vary significantly over time. This observation

prompted a series of studies in which the spectra of both the protonated and nonprotonated forms of dyes I and J were measured over the course of an hour to see whether this behavior occurred for all forms of these dyes. The results of the absorption versus time studies for the non-protonated and protonated forms of dye I are provided in Figures B.1.16 and B.1.17, respectively; the results for the non-protonated and protonated forms of dye J are provided in Figures B.1.18 and B.1.19, respectively. It is clear from these spectral overlays that the absorption of both forms of both dyes is not stable over time. The observed spectral changes followed no discernible pattern; the absorption increased and decreased seemingly randomly over time. Moreover, the relative peak heights and peak shapes appear to change over time, indicating a likelihood that this instability is due primarily to aggregation rather than solubility issues, (which would be expected to result in an increase or decrease in the entire absorption spectrum without changing the peak shapes or relative peak heights).

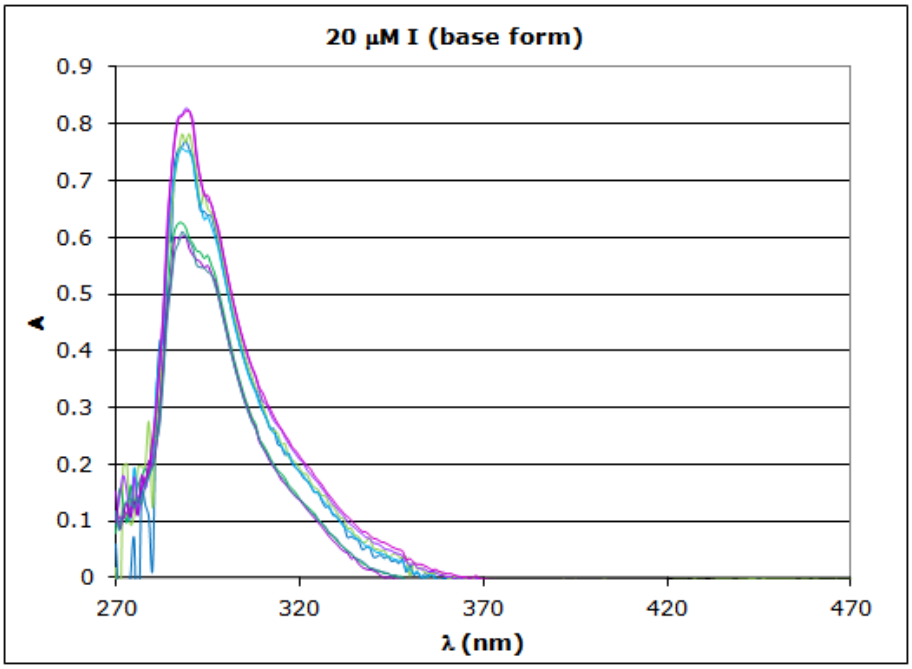

Figure B.1.16. Absorption of base form of dye I over the course of 1 hour

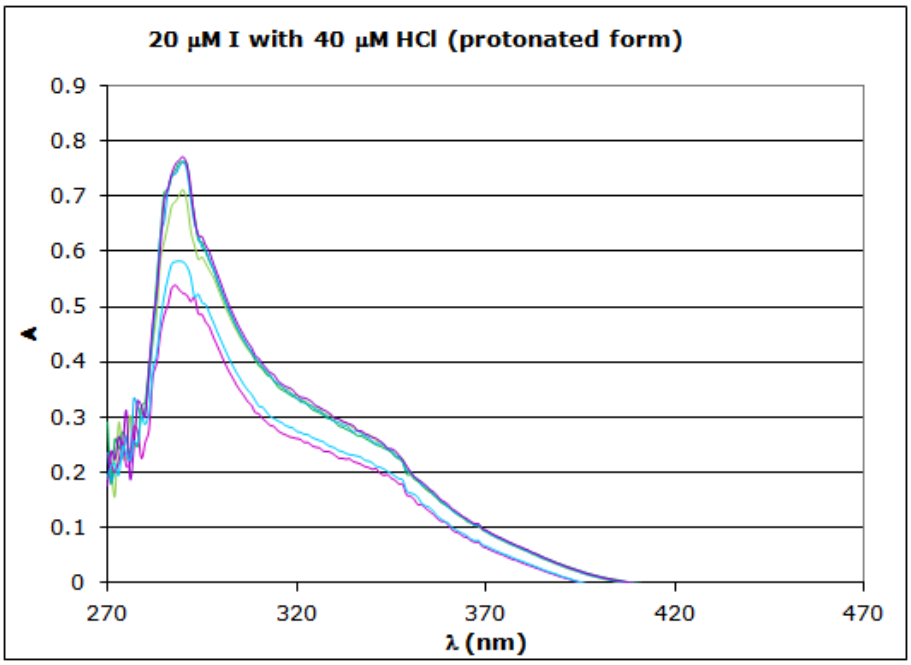

Figure B.1.17. Absorption of protonated dye I over the course of 1 hour

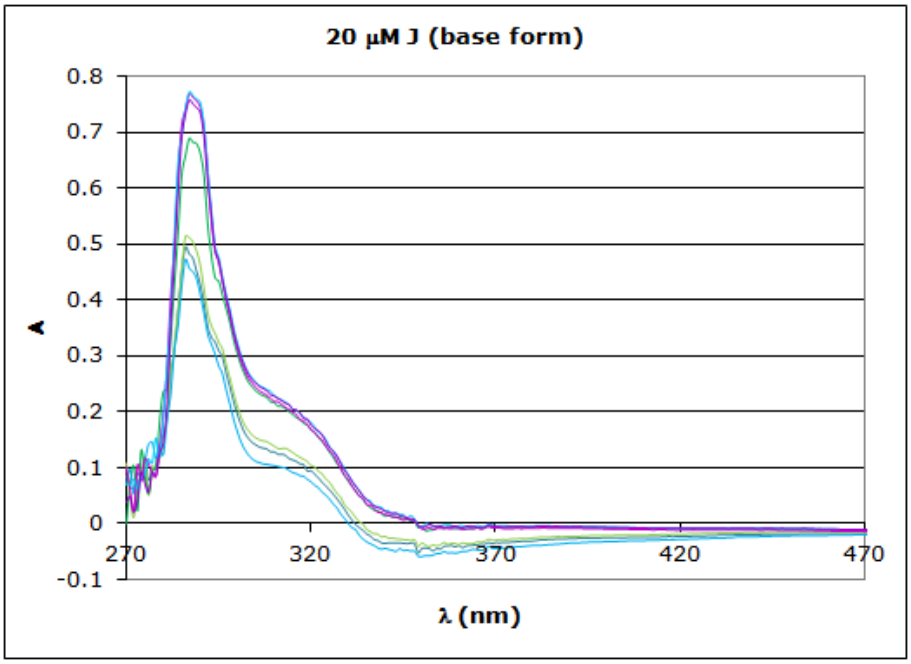

Figure B.1.18. Absorption of base form of dye J over the course of 1 hour

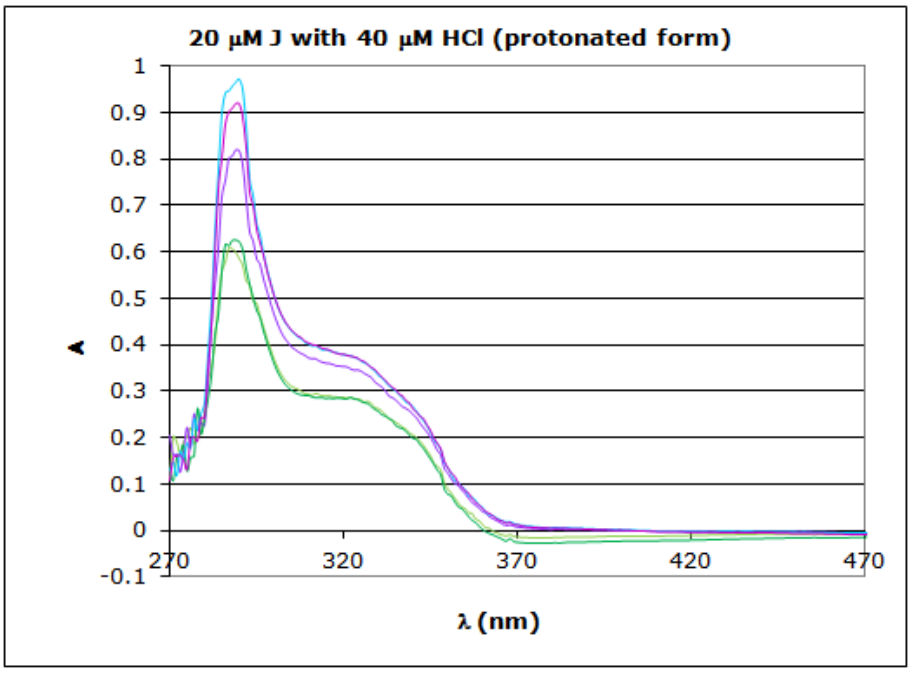

Figure B.1.19. Absorption of protonated dye J over the course of 1 hour

In contrast, both the non-protonated and protonated forms of dye F (also a terpyridine dye) show a very stable absorption over time, as illustrated by the spectra provided in Figures B.1.20 and B.1.21. The absorption of the non-protonated and protonated forms of the dyes at two wavelengths and the ratio of the absorptions at these wavelengths was also plotted as a function of time to further illustrate the time-dependence of the absorption and the relative peak heights. These plots are provided in Figures B.1.22 and B.1.23 for the non-protonated and protonated forms of the dyes, respectively. It is apparent from Figure B.1.22 that the absorption of the base form of dye F is more or less constant over the course of the hour (as evidenced by roughly linear behavior with no upward or downward trend in slope. For dye F in the presence of HCl, (Figure B.1.23) there was a slight reversion of the protonated form back to the non-protonated form over the course of an hour (the β peak at 526 nm decreases slightly in amplitude and the α peak at 402 nm increases slightly in amplitude), perhaps due to a slow establishment of

equilibrium. This slight change is still in stark contrast to the data for dyes I and J, for which there is no linearity or apparent trend in absorption.

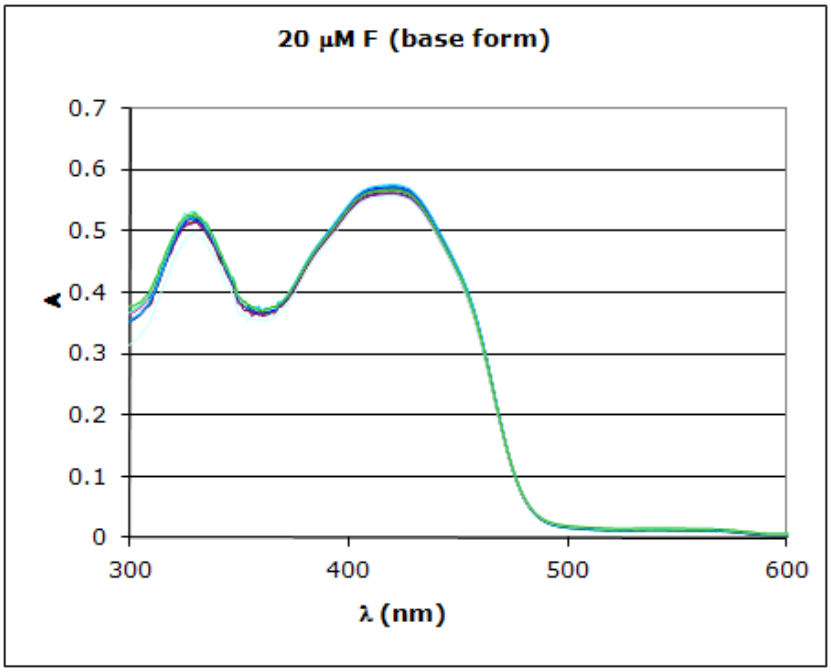

Figure B.1.20. Absorption of base form of dye F over the course of 1 hour

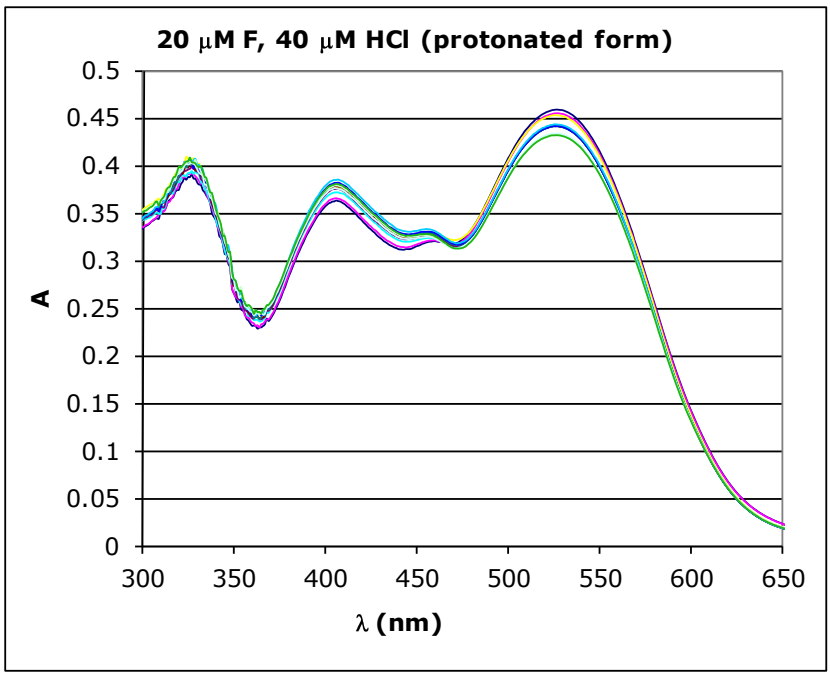

Figure B.1.21. Absorption of protonated dye F over the course of 1 hour

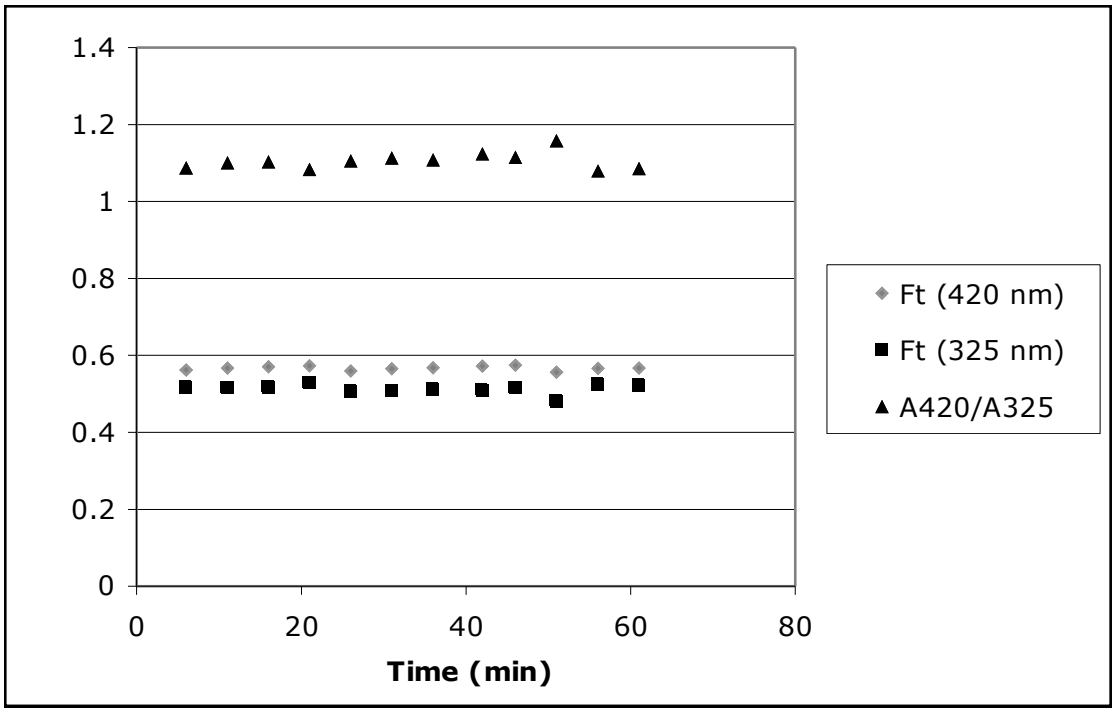

Figure B.1.22. Comparison of absorption of base form of dye F at two wavelengths (420 and 325 nm) over time, and ratio of absorption values at 420 and 325 nm over time (A420/A325)

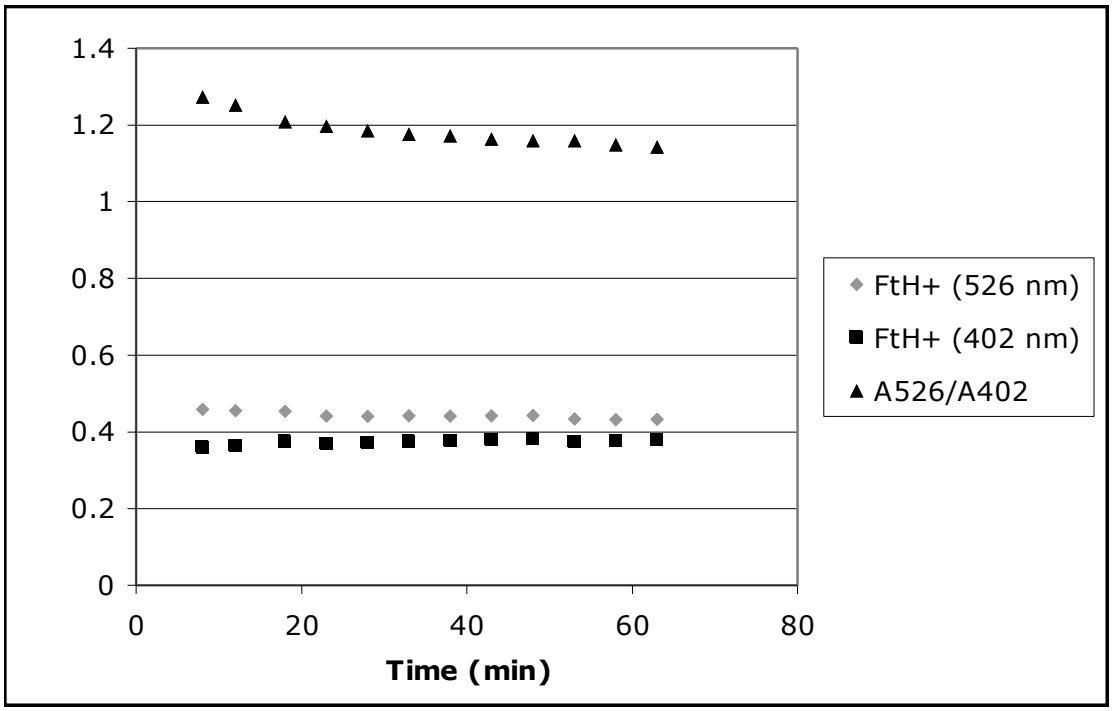

Figure B.1.23. Comparison of absorption of protonated dye F (20 µM HCl) at two wavelengths (526 and 402 nm) over time, and ratio of absorption values at 526 and 402 nm over time (A526/A402)

B.1.3.4 Molar absorptivities of 2,4,6-trisubstituted pyridines

Molar absorptivities were computed from the slope of the linear regression plots of absorption versus concentration as per Beer's law. As mentioned previously, absorptivities for the protonated forms of the dyes (except F) were determined by adding a constant concentration of HCl (in ACN, <0.1% H_2O) to all of the dye solutions and taking the absorption at the bathochromic peak λ_{MAX} corresponding to the singly protonated form of the dye. Concentrations of HCl corresponding to the maximum bathochromic peak absorptivity were determined by protonation studies using HCl in ACN prior to the first determination of absorptivity. Average molar absorptivities of the protonated and non-protonated forms of the dyes are provided in Table B.1.3, along with percent relative standard deviations.

Table B.1.3. Molar absorptivities of protonated and non-protonated 2,4,6-trisubstituted pyridines. Molar absorptivities of protonated form given for bathochromic peak in [HCl] associated with maximum extent of bathochromic absorptivity observed

Dye	Substituent			Base Form			Singly Protonated Form in HCl/ACN (<0.1% H_2O)			
	D_1	D_2	D_3	λ_{MAX} (nm)	Avg $\varepsilon(\lambda_{MAX})$ (M^{-1} cm^{-1})	%RSD	λ_{MAX} (nm)	Avg $\varepsilon(\lambda_{MAX})$ (M^{-1} cm^{-1})	%RSD	[HCl] (µM)
A	Ph	Ph	*N*,*N*-DEA	347	2.48E+04	0.62	450	2.2E+04	5.91	41.03
B	*p*-Toluene	*p*-Toluene	*N*,*N*-DEA	344	3.48E+04	2.62	448	4.06E+04	0.43	41.03
C	β-Np	β-Np	*N*,*N*-DEA	349	3.54E+04	0.55	456	2.561E+04	0.21	51.29
D	Ph	*p*-MeoPh	*N*,*N*-DEA	343	3.58E+04	1.96	448	3.77E+04	2.02	51.29
E	*p*-ClPh	*p*-ClPh	*N*,*N*-DEA	352	2.7E+04	6.45	456	8.7E+03	4.69	51.29
F	2-Pyridyl	2-Pyridyl	*N*,*N*-DEA	416	2.97E+04	2.12	524	3.4E+04	5.93	Varied*
G	*o*-Phenol	Phenyl	*N*,*N*-DEA	359	3.39E+04	0.77	447	5.77E+03	2.61	41.03
H	*tert*-Butyl	*tert*-Butyl	*N*,*N*-DEA	326	3.0E+04	6.44	425	4.12E+04	1.22	30.77
I	2-Pyridyl	2-Pyridyl	*p*-EtOPh	290	N/A	N/A	338	N/A	N/A	N/A
J	2-Pyridyl	2-Pyridyl	*p*-Toluene	287	N/A	N/A	323	N/A	N/A	N/A

*Varied from 35 - 17 µM as dye concentration varied from 30 - 10 µM

Abbreviations: Ph = phenyl, β-Np = β-naphthalene, *p*-MeOPh = *p*-methoxyphenyl, *p*-ClPh = *p*- chlorophenyl, *N*,*N*-DEA = *p*-*N*,*N*-diethylaniline, *p*-EtOPh = *p*-ethoxyphenyl

The percent relative standard deviations of the molar absorptivities indicated reasonably good reproducibility of the calculated values, with the highest %RSD corresponding the base form of dye E (6.45%). Additionally, correlation coefficients indicated reasonably good linearity, with the poorest R^2 value (0.995) corresponding to the protonated form of dye F. Improvement of this value is unlikely, as obtaining even a somewhat linear absorption versus concentration plot for this dye's protonated form proved quite challenging.

The base forms of these compounds had wavelengths of maximum absorption ranging from 287 – 416 nm, depending on substitution. Dyes with *para*-*N*,*N*-diethylaniline substituents at the 4-position of the pyridine ring and phenyl-based D_1 and D_2 groups (dyes A, B, C, D, E, G) had a comparatively narrow range of λ_{MAX} between 343 and 359, despite variation of the phenyl substitution. Dye H, which possesses *tert*-butyl D_1 and D_2 groups in place of the aryl groups possessed by all the other dyes studied, exhibits a λ_{MAX} of 326 nm, blue-shifted relative to those of dyes A-E and G. This is to be expected given that alkyl D_1 and D_2 substituents of H cannot contribute to energy-lowering conjugation, while aryl D_1 and D_2 substituents can. Terpyridine dye F ($D_1 = D_2$ = 2-pyridyl) possesses the same *N*,*N*-diethylaniline D_3 substituent as dyes A-E, G, and H, but exhibits a considerably red-shifted λ_{MAX} of 416 nm. Terpyridine dyes I and J ($D_1 = D_2$ = 2-pyridyl) possess *p*-ethoxyphenyl and *p*-toluene D_3 substituents, respectively, and demonstrate strongly blue-shifted λ_{MAX} values (290 nm for I and 287 nm for J) relative to the terpyridine dye F and the other dyes studied, which possessed *N*,*N*-diethylaniline D_3 substituents.

The singly protonated forms of all dyes possessing *N*,*N*-diethylaniline D_3 substituents are characterized by the appearance of a peak with a red shift of approximately 100 nm upon addition of acid, with a marked corresponding color change (from colorless to yellow for dyes A, B, C, D, E, G, and H, and from yellow to magenta for dye F. This shift has been attributed to

delocalization of the positive charge and increased conjugation within the π system of the molecule upon protonation.[26]

Upon addition of acid to dyes I and J, the spectra show a β peak with a significantly shorter red shift (48 nm and 36 nm, respectively) and a low absorptivity of the red shifted peak. Additionally the λ_{MAX} does not display a significant spectral shift away from that of the base form, instead exhibiting an increase in absorptivity. Pyridine is known to display an absorption band at 270 nm due to the $\pi \rightarrow \pi^*$ excitation, and upon protonation, the intensity of absorption of this band increases without any appreciable spectral shift.[49] The λ_{MAX} of this absorption band coincides closely with the unchanging overall λ_{MAX} of dyes I and J (around 260-270 nm) as well as the χ band of dyes A – H. The unchanging λ_{MAX} values of dyes I and J that demonstrate increased absorptivity upon protonation therefore most likely correspond to the pyridine $\pi \rightarrow \pi^*$ excitation, thus the spectral behavior of these compounds are straightforwardly attributable to pyridine protonation, as expected given the lack of other basic groups present in these dyes. For dyes A – H, the increased absorptivity around 270 nm as acid concentrations are increased in the second equlibrium is also most likely attributable to pyridine protonation and the localization of charge associated with protonation of the second site.

The marked difference in spectral behavior between the diethylaniline substituted dyes and the ethoxyphenyl and toluene substituted dyes I and J prompted the NMR studies in chapter B.2. The strongly red-shifted peak related to formation of the singly protonated form of the dye has been attributed to protonation of the pyridine moiety (which promotes delocalization of the positive charge throughout the chromophore),[26] however, if this were the case, it would be expected that terpyridine dyes I and J would also exhibit a substantial red shift and a spectral change similar to that observed for the other dyes. It would particularly be expected that dye I

would exhibit a substantial red shift, as the ether oxygen of the ethoxyphenyl D_3 substituent is capable of donating lone pair electrons to promote charge delocalization much like the amino nitrogen of a diethylaniline substituent.

Another interesting observation from these studies was that both the protonating acid and the solvent choice strongly affects the absorptivity of the bathochromic peak correlated to the singly protonated form of the dye. Although molar absorptivities for the bathochromic peak were only calculated by linear regression analysis using HCl as the protonating acid and acetonitrile as the solvent, absorptivities can be estimated from single point measurements of absorption spectra using Beer's law. A comparison of the maximum observed absorptivities of the bathochromic peak calculated from linear regression using HCl in acetonitrile with those calculated from single point measurements from the protonation studies of $HClO_4$ in acetonitrile for the diethylaniline substituted dyes is provided in Table B.1.4.

Table B.1.4. Comparison of observed maximum molar absorptivities of red-shifted peak for different acids in acetonitrile

Dye	λ_{MAX} (nm)	$\varepsilon(\lambda_{MAX})$ (M^{-1} cm^{-1}) in Acid/Solvent Combination: HCl/ACN	$HClO_4$/ACN
A	450	2.2E+04	2.4E+04
B	448	4.06E+04	4.1E+04
C	456	2.561E+04	4.1E+04
D	448	3.77E+04	4.7E+04
E	456	2.92E+03	1.7E+04
F	524	3.4E+04	3.7E+04
G	447	5.77E+03	1.3E+04
H	425	4.12E+04	5.1E+04

In acetonitrile, when $HClO_4$ is used as the protonating acid, there is an increase in the observed absorptivity of the red shifted peak corresponding to the singly protonated form for all of the diethylamino substituted dyes relative to those absorptivities measured using HCl as the

protonating acid. Additionally, molar absorptivities calculated from the protonation studies in ACN using PTSA as the protonating acid were found to be greater than those when HCl was used but less than those when $HClO_4$ was used; calculated absorptivities using PTSA were $3.9*10^4$ M^{-1} cm^{-1} for dye C and $4.4*10^4$ M^{-1} cm^{-1} for dye H. The reason for this difference in absorptivity is not entirely clear, although it may be an indication of the differential spectral responses to varying anions (as discussed in B.1.1.1), or it may be an indication of the difference in acid strengths, as of the acids studied in acetonitrile, HCl is the weakest, PTSA is slightly stronger, and $HClO_4$ is the strongest. However, the difference in acid strengths between PTSA and HCl is not substantial in acetonitrile, so this second explanation seems somewhat less plausible.

Solvent choices also substantially affected the absorptivities of the bathochromic peak correlated to the singly protonated form of the dye. When acetonitrile was swapped for 50% ethanol/water (v/v) in the pK_a studies (section B.1.3.5) or DMSO in the correlated NMR-absorption studies (section B.2.3.1), there was a marked decrease in the maximum absorptivity of the bathochromic peak when compared to the absorptivity when the same protonating acid was used in acetonitrile. In the pK_a studies in 50% ethanol/water (v/v), $HClO_4$ was used as the protonating acid, and the maximum absorptivity of the bathochromic peak was calculated to be $1.2*10^4$ M^{-1} cm^{-1} for dye B and $7.6*10^2$ M^{-1} cm^{-1} for dye E; both absorptivities are substantially lower than those calculated in acetonitrile using $HClO_4$ ($4.1*10^4$ M^{-1} cm^{-1} for dye B and $1.7*10^4$ M^{-1} cm^{-1} for dye E). In the correlated NMR-absorbance studies in DMSO, HCl was used as the protonating acid, and the maximum absorptivity of the bathochromic peak was calculated to be $7.2*10^3$ M^{-1} cm^{-1} for dye A; this absorptivitiy is substantially lower than that calculated in acetonitrile using HCl ($2.2*10^4$ M^{-1} cm^{-1}). The reasons for this are similarly unclear, and no

concrete conclusions may be drawn, although at this point it can be generalized that the absorptivity seems to decrease with increasing dielectric constant of the solvent or solvent mixture. It is interesting to note that the base form peaks of the dyes around 320 – 360 nm for the non-terpyridine dyes and at 416 nm for terpyridine dye F did not show any pronounced dependence of absorptivity on solvent content.

B.1.3.5 Spectroscopic pK_a determination

Molarities of $HClO_4$ solutions prepared in 50% EtOH/H_2O were determined by indirect triplicate standardization of the 1 M $HClO_4$ solution. Molarities of the solutions were found to be 1.005$\pm$0.002 M for the "1 M" solution, 0.1005$\pm$0.0002 M for the "0.1 M" solution, and 10.05$\pm$0.02 mM for the "0.01 M" solution (percent relative standard deviations of these values were 0.21%). Note that these values do not take dilution error into account. Ionic strengths were equal to concentrations of $HClO_4$ in the "1 M" and "0.1 M" solution, and the ionic strength of the "0.01 M" solution was 0.100 M (adjusted using 2 M NaCl prepared in deionized H_2O).

The spectral results of the pK_a studies of dye B in 50% EtOH/H_2O are provided in Figure B.1.24. For ease of interpretation, the spectra have been grouped into two plots, the first plot (I) depicting spectra corresponding to the first equilibrium, and the second plot (II) depicting spectra corresponding to the second equilibrium. In both spectra, arrows indicate the spectral changes associated with decreasing pH.

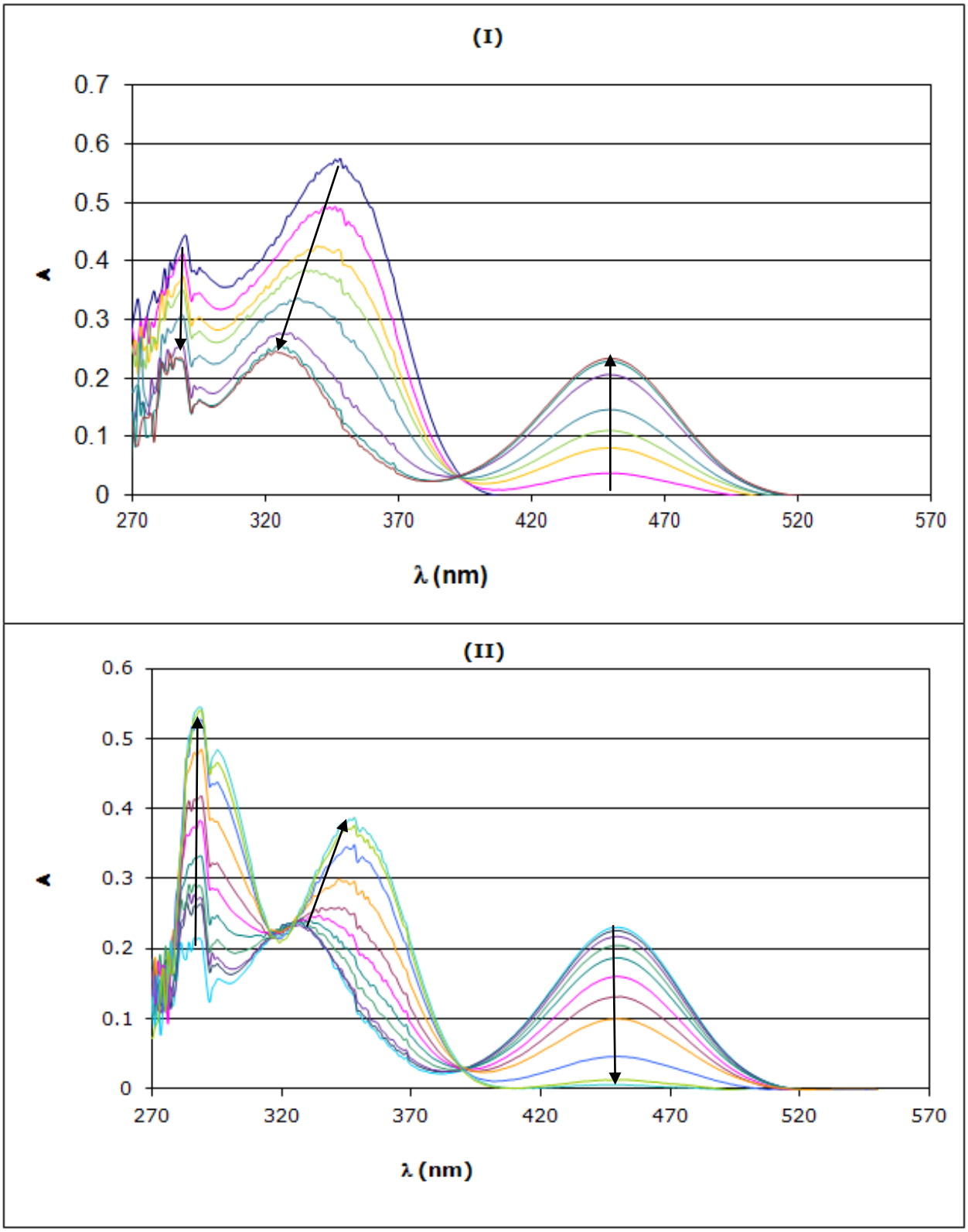

Figure B.1.24. Absorption spectra from pK_a determination of dye B (20 μM) in 50% EtOH/H_2O (25°C, I = 0.100 M except for pH < 1.00)

Both equilibria in both sets of spectra show clear isosbestic behavior, reinforcing the assumption that the pK_a values are at least two units apart and validating the approach to calculating pK_a used in this section. Furthermore, the absorption of the red-shifted peak at 449 nm goes from zero to a maximum in the first equilibrium and decreases back to zero in the second equilibrium, further validating the approach for calculating pK_a. The absorption at 449 nm was plotted as a function of pH; this plot is provided in Figure B.1.25.

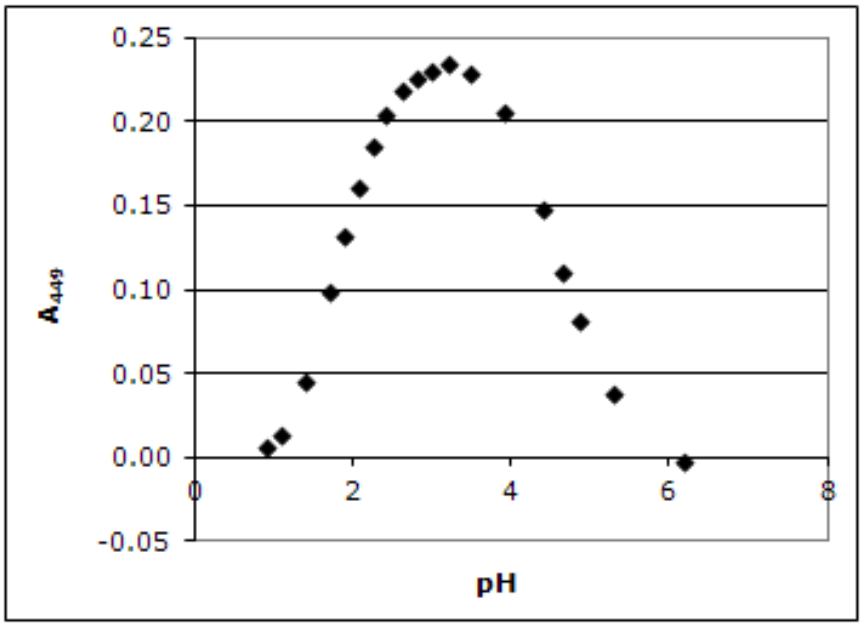

Figure B.1.25. Absorption of dye B (20 μM) at 449 nm as a function of pH from pK_a determination in 50% EtOH/H_2O (25°C, I = 0.100 M except for pH < 1.00)

As discussed in the experimental (section B.1.2.8.), the p_sK_{a1} and p_sK_{a2} values were determined by by drawing the linear regression for the two linear regions on either side of the maximum absorption at 449 nm ($A_{449\ MAX}$) and solving for pH when the absorption at 449 nm was half the maximum observed absorption (½ $A_{449\ MAX}$). The experimentally determined p_sK_a values were then used to calculate aqueous pK_a values, which were corrected for ionic strength as outlined in the experimental section.

The spectral results of the pK_a studies of dye E in 50% EtOH/H_2O are provided in Figure B.1.26. As with dye B, the spectra have been grouped into two plots, the first plot (I) depicting spectra corresponding to the first equilibrium, and the second plot (II) depicting spectra corresponding to the second equilibrium. In both spectra, arrows indicate the spectral changes associated with decreasing pH.

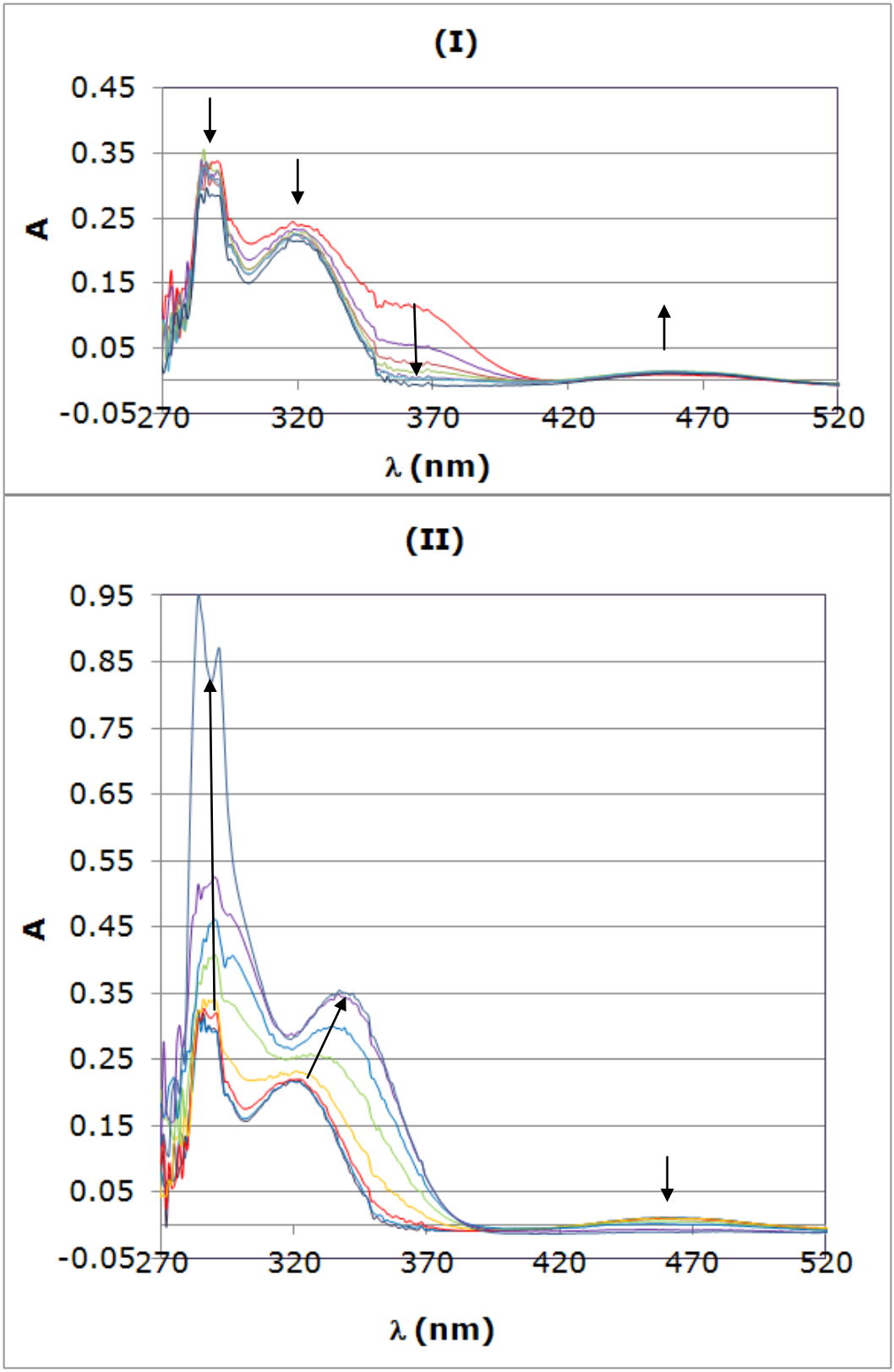

Figure B.1.26. Absorption spectra from pK_a determination of dye E (20 μM) in 50% EtOH/H_2O (25°C, I = 0.100 M except for pH < 1.00)

Both equilibria in both sets of spectra show clear isosbestic behavior, reinforcing the assumption that the pK_a values are at least two units apart and validating the approach to calculating pK_a used in this section. As mentioned in section B.1.3.4, the molar absorptivity of the bathochromic peak corresponding to the singly protonated form of dye E is substantially lower when the solvent is changed from acetonitrile to the ethanol-water mixture, so much so that the instrumental error inherent in the measured absorption of this peak is quite substantial. Accordingly, although the bathochromic peak at 456 nm increases from zero to a maximum in the first equilibrium and decreases back to zero in the second equilibrium, the plot of absorption as a function of pH at 456 nm (provided in Figure B.1.27) is extremely noisy and cannot be interpreted with any real certainty.

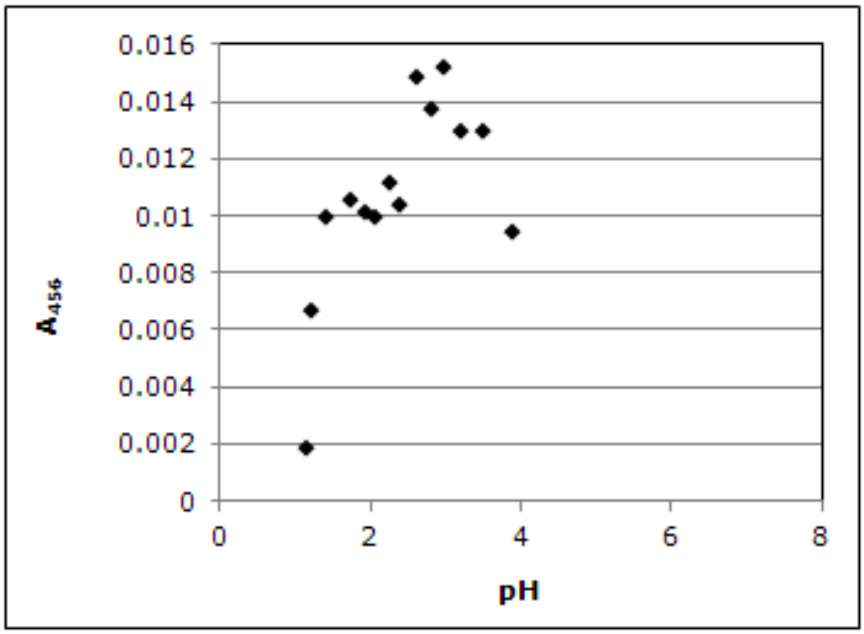

Figure B.1.27. Absorption of dye E (20 μM) at 456 nm as a function of pH from pK_a determination in 50% EtOH/H_2O (25°C, I = 0.100 M except for pH < 1.00)

Fortunately, the absorption behavior of a different peak can also be used to calculate the p_sK_a values, provided that it exhibits different absorption behaviors in the two equilibria. It was observed in Figure B.1.26 that absorption at 360 nm decreases to zero in the first equilibria, then increases in the second equilibrium. Accordingly, p_sK_a values were calculated using the absorption at 360 nm (A_{360}) following the same logic as described in section B.1.2.8 (except that when $[HB^+]$ is at a maximum, A_{360} is at a minimum and A_{360} when [B] is at a maximum is not equal to A_{360} when $[H_2B^{2+}]$ is at a maximum). Specifically, p_sK_{a1} is found by solving for pH when $A_{360} = ½\ A_{360\ MAX}$ (at lower pH), and p_sK_{a2} is found by solving for pH when $A_{360} = ½\ A_{360\ MAX}$ (at higher pH). Absorption as a function of pH at 360 nm is provided in Figure B.1.28.

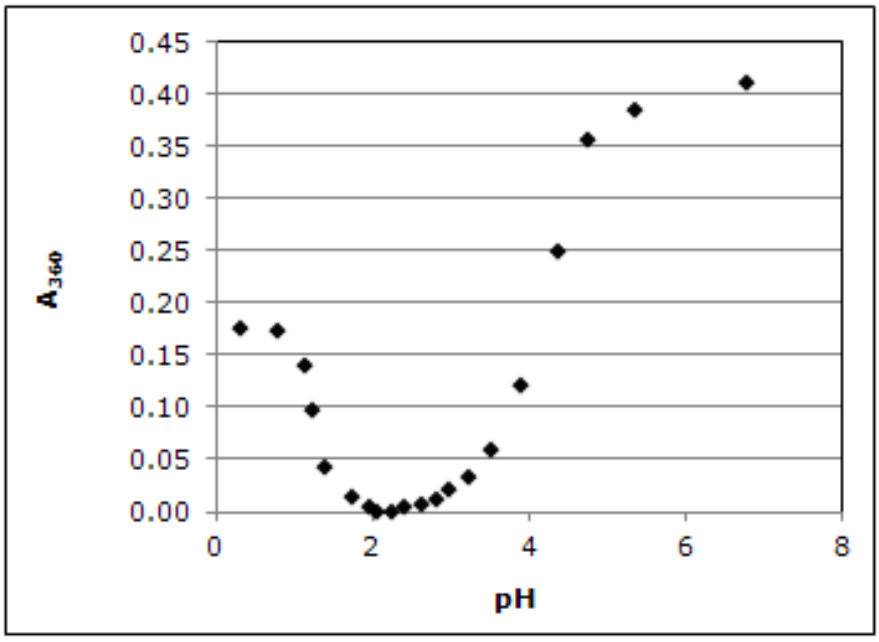

Figure B.1.28. Absorption of dye E (20 μM) at 360 nm as a function of pH from pK_a determination in 50% EtOH/H_2O (25°C, I = 0.100 M except for pH < 1.00)

Provided in Table B.1.5 are the experimentally determined p_sK_a values for the compounds in 50% EtOH/H_2O, calculated aqueous pK_a' values (for I = 0.1 M) and aqueous pK_a values corrected for ionic strength.

Table B.1.5. Calculated p_sK_a values in 50% EtOH/H_2O, aqueous pK_a' values for I = 0.1 M, and aqueous pK_a values corrected for ionic strength of diethylaniline substituted dyes correlated to substitution at the 2 and 6 positions of pyridine (D_1 & D_2)

Dye	D_1 & D_2	p_sK_{a1}	pK_{a1}'	pK_{a1}	p_sK_{a2}	pK_{a2}'	pK_{a2}
B	*p*-Toluene	1.8	-0.013	-0.053	4.6	2.8	2.8
E	*p*-Chlorophenyl	1.3	-0.57	-0.61	4.2	2.3	2.3

The data provided in Table B.1.5 indicates that, for 2,4,6-trisubstituted pyridine dyes possessing *N*,*N*-diethylaniline substituents at the 4 position (D_3), when electron donating substituents (such as *p*-toluene) are interchanged for electron withdrawing substituents (such as *p*-chlorophenyl) at the 2 and 6 positions of pyridine (D_1 & D_2), neither the pK_{a1} nor the pK_{a2} are decreased substantially (the decrease for both in this case is approximately 0.4 - 0.5 units). This modulation of pK_a by changing substitution follows the expected pattern (as electron withdrawing substituents are expected to make the dye less basic), but the observed change in pK_a is not as large as our group had initially expected.

B.2. Determination of Site of First Protonation by NMR Spectroscopy

B.2.1 Introduction

B.2.1.1 Goal of this study

As discussed in chapter B.1, the absorption studies in acetonitrile of dyes possessing a *N*,*N*-diethylaniline D_3 substituent indicated the presence of two distinct equilibria associated with protonation (as indicated by two sets of isosbestic points and two distinct types of spectral changes). The first equilibrium was observed with addition of lower concentrations of acid and associated with the singly protonated form of the dye. This equilibrium involved the appearance of a red-shifted peak in the absorption spectrum and a visible color change (from colorless to yellow or from yellow to red) of the dye solution. The second equilibrium was observed with the addition of higher concentrations of acid and presumably related to the doubly protonated form of the dye. This equilibrium was associated with the reduction of the red-shifted absorption peak and the increase of a blue-shifted absorption peak, as well as a visible color change (disappearance of yellow color or change in hue of red).

Those dyes possessing nonbasic *p*-toluene and *p*-ethoxyphenyl D_3 substituents exhibited distinctly different spectral behavior than those possessing *p*-*N*,*N*-diethylaniline D_3 substituents and did not demonstrate any visible color change upon protonation. Accordingly, it was of interest to determine whether the large bathochromic shift exhibited in the first equilibrium by dyes possessing a diethylaniline D_3 substituent was possibly due to protonation of the basic diethylamino substituent or simply a result of pyridine protonation (with the auxochromic properties of the amino nitrogen being responsible for the bathochromic shift).

The bathochromic shift observed in the first equilibrium is thought to be attributable to delocalization of the positive charge and increased conjugation within the π system of the molecule upon protonation. This delocalization is only possible if the first protonation occurs at the pyridine nitrogen. However, since a strong red shift (~100 nm) only occurs for those dyes possessing a basic diethylaniline D_3 substituent, it is important to determine with certainty that the first protonation actually occurs at the pyridine substituent in order to verify that the red shift is due to widespread charge delocalization from pyridine protonation rather than protonation of the other basic substituent (diethylamino group).

To determine this information, proton NMR studies were carried out on solutions containing dye A and HCl that demonstrate absorption characteristics corresponding to the first equilibrium in order to determine which basic site is protonated first. Dye A was chosen as representative of the diethylaniline substituted dyes because a large sample was available for study, and its simple phenyl D_1 and D_2 substitution (Figure B.2.1) simplify the interpretation of NMR spectra and makes it structurally representative of most of the dyes studied in chapter B.1. Deuterated dimethylsulfoxide (DMSO-*d*6) was chosen as the NMR solvent for these studies as it was already available within our lab and was a suitable solvent for these dyes, however, important differences between this solvent and acetonitrile were observed, which will be discussed in greater detail with respect to the results obtained.

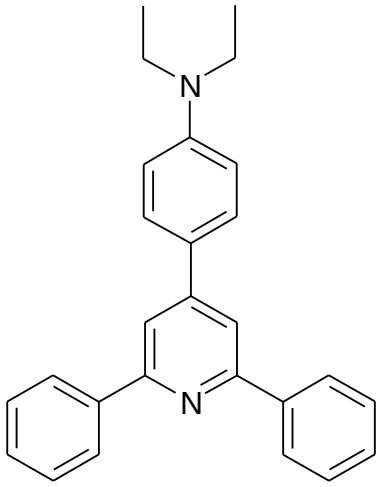

Figure B.2.1. Structure of Dye A

B.2.1.2 NMR spectroscopy: basic principles and optimization of parameters

Nuclear magnetic resonance spectroscopy is an invaluable instrumental technique for analytical applications and may be used to determine structural information about compounds, as the chemical shift of a particular nucleus provides information about functional groups and the electron density of the environment surrounding a particular nucleus.[50] NMR makes use of the properties of magnetic nuclei to determine quantitative and qualitative information about compounds. Stable isotopes of elements containing an odd number of protons and/or neutrons have a nonzero nuclear spin and therefore an intrinsic magnetic moment, and are accordingly responsive to an applied magnetic field, absorbing and reemitting energy at a specific frequency. The resonant frequency for a given magnetic nucleus is proportional to the magnetic field strength, as is the intensity of the signal. For a given magnetic field strength, each nucleus absorbs at a frequency characteristic to the isotope, known as the Larmor frequency. Although NMR may be applied to any magnetic nucleus, the most common forms currently in use are carbon-13 (^{13}C) NMR and proton (^{1}H) NMR.[51]

When a sample comes into contact with the magnetic field (along the "z" axis) in the probe, the spin of a dipolar (I = ½) nucleus splits into two distinct energy levels. The lower energy level n_α is associated with a "+z" spin oriented parallel to the magnetic field, and the higher energy level n_β is associated with a "-z" spin oriented antiparallel to the magnetic field. The energy difference ΔE between the two levels is a function of the magnetic field strength B_0 as well as the gyromagnetic ratio γ of the nucleus, as per the equation[52]

$$\Delta E = h \gamma B_0 / 2\pi$$

where h is Planck's constant. The populations of the two energy levels are governed by the Boltzmann distribution, and the net magnetization of the sample (population excess) is always along the lower energy "+z" axis. The amount of time it takes to establish the equilibrium Boltzmann distribution is a factor of the spin-lattice relaxation time T_1, which in turn depends on the nucleus, the temperature, and state of matter of the sample. The spin-lattice relaxation time also describes the time it takes for a proton perturbed by a RF pulse to return to its original orientation in the magnetic field (along the "+z" axis). For a sample with net magnetization along the xy plane, the relationship between magnetization (M) and T_1 is given by

$$M = M_0 (1 - e^{-t/T_1})$$

where M_0 is the equilibrium magnetization (along the z axis).[53] According to this equation, after one time constant T_1, the magnetization is recovered to approximately 63% of its equilibrium

value. It is important to establish this distribution prior to acquiring the NMR spectrum, as well as to reestablish it between RF pulse repetitions in order to obtain good data.

A simple one pulse NMR experiment consists of three distinct events: the delay, the pulse, and the acquisition. The delay is employed to establish (and reestablish) the Boltzmann distribution between energy levels discussed previously. Ideally, a delay (d_1) of least $5T_1$ should be employed both prior to acquiring the spectrum and between pulse repetitions to ensure a return to equilibrium (as this allows for a recovery of 99% of the original magnetization along the z-axis). The pulse event involves the application of a short pulse of RF energy from the probe coils at a perpendicular to the magnetic field. When the sample is pulsed with RF energy, the net magnetization is perturbed from the z axis and rotates about its origin. The extent of perturbation is dependent on both the pulse power (PL1) and length of time the pulse is turned on (P1). The signal intensity depends on the distance from the xy axes (i.e. how much of the sample magnetization vector lies in the xy plane), reaching a maximum when the magnetization vector lies along the xy plane, i.e. at angles of 90˚ and 270˚ from the +z axis. The combinations of pulse power and pulse width that result in these signal intensity maxima are known as the 90˚ pulse width (PW90) and the 270˚ pulse width. When the RF pulse is turned off, the acquisition event occurs. Acquisition is accomplished by the probe receivers, which detect the signal from the Larmor precession of the spin back to the +z axis. The frequency of this precession is reduced from the Larmor frequency of the nucleus by a difference dependent on the electronic environment of each nucleus in the sample, which essentially dictates how much of the applied magnetic field is "experienced" by each nucleus. This difference gives rise to the chemical shift. The signal acquired is known as the free induction decay (FID), which is essentially the signal as

a function of time. This signal is processed through a Fourier transform algorithm, which results in the familiar NMR spectrum in which the signal consists of peaks as a function of frequency.[52]

Developing and optimizing an NMR experiment for a given sample in a particular solvent requires the determination of the PW90, as well as the T_1 values of each (or at least most) of the nuclei in the sample. This becomes especially important for obtaining NMR spectra of low concentration samples. One other important consideration for samples of lower concentration is the signal-to-noise (S/N) ratio in NMR experiments, which increases as the square root of the number of scans; [52] for example, to double the signal to noise ratio, the number of scans must be quadrupled.

B.2.1.3 Special considerations in correlated NMR-absorption studies

Proton NMR spectra are typically obtained for higher concentrations of analytes (millimolar to molar range) than absorption spectra (micromolar). To obtain absorption and NMR spectra of a single solution, one option is to prepare a solution of intermediate concentration, higher than that typically used for absorption measurements and lower than that typically used for NMR measurements. Perhaps the simplest way to obtain a usable absorption spectrum of a high concentration sample is to decrease the pathlength of light through the sample by using a short pathlength cuvette. Absorption is related to pathlength (b) and concentration (c) by Beer's law, as described in section B.1.2.5. Using a reduced pathlength cell (b = 0.2 cm), the maximum concentration of a solution appropriate for a UV experiment in a standard 1.0 cm pathlength cell can be multiplied by five. Absorbance of light is related to transmittance (T) by the equation

$$A = \log (P_0/P) = -\log T$$

where P_0 is the irradiance of the beam prior to striking a sample of pathlength b, and P is the irradiance of the beam exiting the sample.[54] When A = 1, 90% of the incident light is absorbed (10% is transmitted), when A = 2, 99% of the incident light is absorbed (1% is transmitted), and when A = 3, 99.9% of the incident light is absorbed (0.1% is transmitted). Beer's law (which posits a linear relationship between absorption and concentration) is most accurate for intermediate absorption values between 0.4 and 0.9, and begins to fail substantially when the solution is too concentrated (i.e. for absorption values above two).[54] For samples with absorption greater than two, absorption spectra are still obtainable, although these spectra are not appropriate for quantitative studies as the error resulting from the low intensity of detected light and the dark current noise is far more significant in this range than at intermediate absorption values.[55]

With respect to the 2,4,6-trisubstituted pyridines studied (most of which were found in the previous chapter to possess absorptivities ranging between approximately of 20,000 M^{-1} cm^{-1} to 40,000 M^{-1} cm^{-1}), for a maximum absorption of 3 in a reduced pathlength cell with b = 0.2 cm, the maximum concentration of a sample used for absorption measurements should range between 0.375 mM and 0.75 mM. Accordingly, a concentration of 0.5 mM was chosen for the correlated absorption-NMR studies of dye A.

While NMR spectra of solutions significantly less concentrated than 0.5 mM are readily obtainable,[56] it is more practical (in consideration of experiment time and obtaining reasonable S/N values) to work with a more concentrated solution. The signal in an NMR experiment is proportional to the concentration of the species present, and as noted in the previous section, S/N increases as the square root of the number of scans;[52] thus for every halving of concentration, the

number of scans (and experiment time) must be quadrupled to maintain the S/N ratio (assuming all other experimental parameters affecting the pulse repetition time are held constant). Additionally, an analyte concentration less than 1 mM is still considered to be on the low end of NMR sample concentrations, thus care must nonetheless be taken to maximize the signal. The primary considerations in maximizing the NMR signal are using a combination of RF pulse length and pulse power that corresponds to a perturbation of 90° from the z-axis (i.e. using the PW90), programming delays (d_1) that are greater than or equal to $5T_1$ for the nucleus possessing the longest T_1 values in the compound, and running an adequate number of scans to obtain a reasonable S/N.

B.2.2 Experimental

B.2.2.1 Materials and instrumentation

Dimethylsulfoxide (DMSO; $\geq$ 99.8%, UV grade) was obtained from Sigma-Aldrich (St. Louis, MO). Deuterated dimethylsulfoxide (DMSO-*d*6; 99.9% +0.05% V/V TMS) was obtained from Cambridge Isotope Laboratories (Andover, MA) and stored under dry N_2 (replenished after each use). Quartz cuvettes of 1.000 cm pathlength were obtained from Starna Cells, Inc. (Atascadero, CA). A quartz cuvette of 0.200 cm pathlength (and a spacer to adjust the effective sample compartment size) was obtained from NSG Precision Cells (Farmingdale, NY). Standard 5 mm NMR tubes were obtained from Wilmad-LabGlass (Vineland, NJ). NMR studies were carried out on a 400 MHz Bruker NMR spectrometer (Bruker BioSpin Corporation, Billerica, MA). T_1 calculations were carried out using Topspin Software (Bruker BioSpin Corporation, Billerica,

MA). NMR spectra were processed using Mnova Software (Mestrelab Research, Escondido, CA). Other materials and instruments used in this chapter were discussed in B.1.2.1.

B.2.2.2 Preparation of stock solutions

Stock solutions (2-3 mM) for the correlated NMR-absorbance studies were prepared by weighing the solid dye on a 5-digit analytical balance directly into a glass vial and adding DMSO (for initial protonation studies) or DMSO-*d*6 (for NMR studies and correlated NMR-absorbance studies) via a class A volumetric pipette and/or an adjustable volume micropipette. The contents of the vial were sonicated for 10 minutes, then vortexed for 20 seconds to ensure complete solvation. The stock solutions were protected from light and stored at room temperature under N_2 when not in use.

Initial protonation studies were carried out using HCl. A parent stock solution of 1 M HCl was prepared in DMSO, from which secondary HCl stock solutions (10-100 mM) were prepared in DMSO for protonation studies. A second set of HCl stock solutions and secondary stock solutions identical to those discussed immediately prior were also prepared in DMSO-*d*6 for the correlated NMR-absorbance protonation studies.

B.2.2.3 Initial protonation studies in DMSO using HCl

Hydrochloric acid was used as the protonating agent for the dye. HCl was chosen instead of $HClO_4$ despite the fact that HCl is not fully dissociated in DMSO because concentrated $HClO_4$ is capable of reacting explosively with DMSO.[57,58] Solutions for the protonation studies of dyes using these other acids were prepared by adding varying amounts of acid stock solutions (prepared in DMSO) and adequate dye stock solution and diluted to a total volume of 1.00 mL

with non-deuterated DMSO such that the concentration of dye was 0.500 mM. Absorption spectra were obtained using the 0.2 cm pathlength quartz cuvette. The spectra obtained were characterized and compared to those observed in the acetonitrile studies. An additional protonation study was carried out for a more justifiable comparison of the spectral properties in the two solvents by preparing solutions in DMSO containing the same concentration of dye (20 μM) used in the protonation studies with acetonitrile while varying the concentration of HCl.

B.2.2.4 General notes on acquisition of NMR spectra and NMR sample preparation

Acquisition of all NMR spectra involved setting a proper spectral width and number of points (i.e. acquisition time) so as to fully encompass the FID without an excess of "dead space," setting the receiver gain to an appropriate value, and shimming to obtain a proper Lorentzian lineshape. Peaks were calibrated against the TMS peak (which was set to 0.000 ppm).
All NMR samples (dyes and acid stock solutions) were prepared under N_2 and protected from light. NMR tubes were purged with N_2 before and after filling with solutions.

B.2.2.5 NMR parameter optimization: PW90 determination

NMR samples for parameter optimization were of higher concentrations than those used in later analytical studies (to reduce the number of scans required to obtain reasonable S/N values). Samples were prepared by adding 650 μL DMSO-d6 to a few mg of dye A in a glass vial and transferring the sample to a standard NMR tube. All sample preparation was done under N_2 and NMR tubes were purged with N_2 before and after filling.

The PW90 was determined by first setting the pulse power PL1 to -3.00 dB and acquiring an initial NMR spectrum using a short pulse length P1 < 10 μs known to be shorter than that

corresponding to the PW90. The transmitter offset was then set to the DMSO peak at 2.509 ppm and the spectrum was obtained again using the same parameters. This spectrum was phased to positive, after which no phasing was carried out (so the peak intensity and sign could be observed as a function of pulse length). NMR scans were then carried out by increasing the pulse length until the sinusoidal progression of the peaks approached the null peak at 360° (Figure B.2.2).

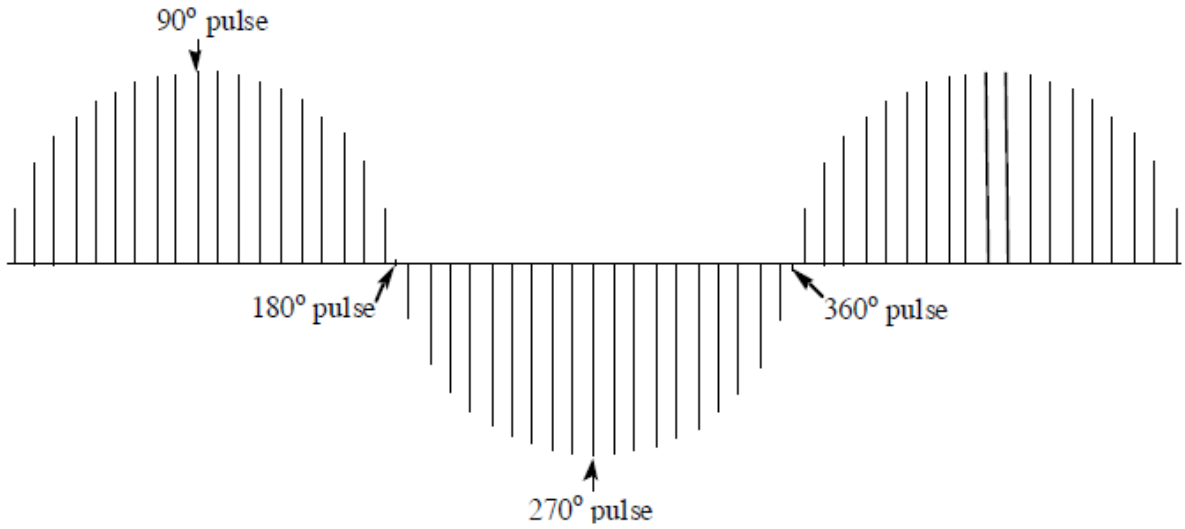

Figure B.2.2. Amplitude and sign of a single NMR peak as a function of pulse length (P1) when pulse power held constant, with 90°, 180°,270°, and 360° pulses indicated[59]

At this point the pulse lengths were adjusted in small increments until the null signal (where the peak possesses both positive and negative portions of equal amplitude) was observed; this signal

was taken to be the true 360° pulse length. The iteratively determined 360° pulse length for PL1 = -3.00 dB was then divided by two to determine the 180° PW and by four to determine the PW90.

B.2.2.6 NMR parameter optimization: T_1 determination

Spin lattice relaxation times T_1 for a given compound can be approximated from the molecular weights. It can be generalized that, for molecules with molecular weights between approximately 10 and 1000 g/mol, the smaller the molecule, the longer the T_1 value. The relationship between molecular weight and T_1 is illustrated in Figure B.2.3.

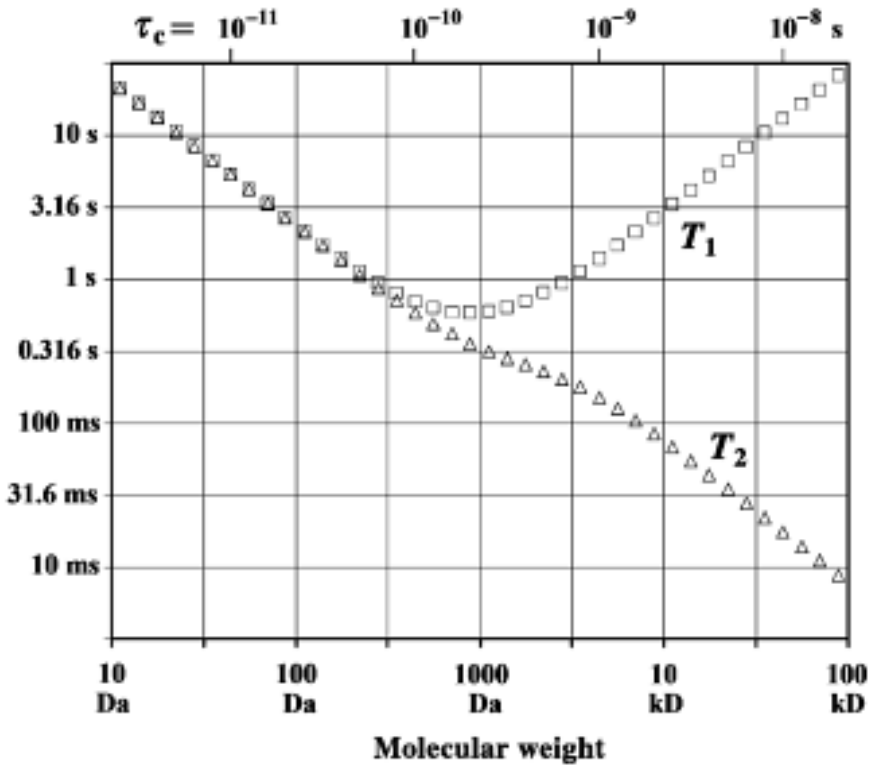

Figure B.2.3. Relationship between spin-lattice relaxation time T_1, spin-spin relaxation time T_2, and molecular weight[60]

The data provided in Figure B.2.3 indicates that for the 2,4,6-trisubstituted pyridines studied (which have molecular weights between 323 and 479 g/mol, the expected T_1 values should be approximately 1 s. However, the actual T_1 values require experimental determination (as there are other environmental factors that affect the T_1 of a given nucleus).

The T_1 values of selected nuclei in the dye molecule were determined following determination of the PW90 by the inversion-recovery method, as depicted in Figure B.2.4.

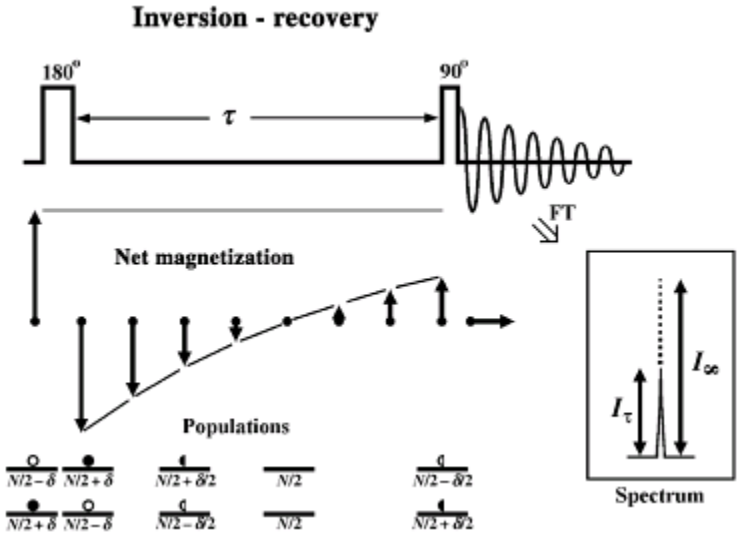

Figure B.2.4. Depiction of inversion-recovery procedure for determination of T_1[60]

This method involves setting up a two-pulse program with a variable delay (τ) between the pulses. The first pulse (P1), known as the inversion pulse, corresponds to the 180° pulse (PL1 was set to -3.00 dB and P1 was set to double the PW90) and results in an inversion of sample magnetization to the –z axis. The second pulse (P2), known as the read pulse, corresponds to the 90° pulse (PL1 was set to -3.00 dB and P1 was set to double the PW90). A number of τ values

were set, ranging from 1 ms to 10 s (to ensure that delays correspond to values significantly smaller and larger than the expected T_1 values). For long delay times ($>T_1$) for which the magnetization along the z axis M_z has recovered all the way to M_0, the intensity of the signal I_{inf} corresponds to the maximum positive signal given by the PW90. The relationship between signal intensity at delay $I(\tau)$, the delay time τ, and the T_1 value is given by the following equation.[60]

$$I(\tau) = I_{inf}(1 - 2e^{-\tau/T_1})$$

Determination of T_1 can accordingly be obtained by a nonlinear least squares fit of the signal intensity $I(\tau)$ as a function of the delay time. Spin-lattice relaxation times T_1 for selected nuclei in dye A (those that demonstrated NMR peaks that were resolved from surrounding peaks) were obtained by this curve fitting method, which was carried out following acquisition of all NMR spectra by phasing the first spectrum (τ = 1 ms) to negative (corresponding to the 270° pulse) then fitting the curves using the Bruker Topspin software.

B.2.2.7 ^{1}H NMR of dye A (base form)

Following determination of the PW90 and T1 values, an optimized ^{1}H NMR spectrum of the base form of dye A was obtained. Approximately 3 mL of a solution that was 3.00 mM A in DMSO-*d*6 was prepared under N_2 in a glass vial by weighing out a sample of dye A and adding an appropriate volume of deuterated solvent via volumetric pipettes. Approximately 0.6 mL of this sample was transferred into an NMR tube and the spectrum was run by setting the parameters discussed previously to their optimum values. Pulse power PL1 was set to -3.00 dB,

pulse length P1 was set to 29.375 μs (the PW90), and d_1 to 12.5 s ($d_1 > 5T_1$ for the largest T_1 measured in the previous section). The number of scans was set to obtain reasonable S/N.

B.2.2.8 Correlated ^{1}H NMR and absorption spectra of dye A (protonated form)

A secondary sample containing 0.5 mM dye A and 10 mM HCl was prepared in DMSO-*d*6 from the solution described in B.2.2.7. The concentration of HCl was chosen from the results of the protonation studies of 0.5 mM A in DMSO described in B.2.2.3, which indicated that the addition of 10 mM HCl results in absorption spectra displaying only the characteristics of the first equilibria. The solution was prepared by pipetting 0.500 mL of the 3.00 mM dye solution into a second vial, adding 0.300 mL of a secondary 100 mM solution of HCl in DMSO-*d*6, and diluting to a total of 3.00 mL. The final concentrations of dye A and HCl in this solution were 0.500 mM and 10.0 mM, respectively. For both samples, approximately 1 mL was transferred into the 2 mm pathlength quartz cuvette and an absorption spectrum was taken. Concurrently, 0.6 mL of this sample was transferred into an NMR tube, and the NMR spectrum was run under the same conditions as the spectrum obtained in B.2.2.7 except that the receiver gain and the number of scans were increased (as the sample contained one-sixth the concentration of dye as the 3 mM sample in B.2.2.7). The absorption spectrum was compared to the NMR spectrum to determine structural information about the first equilibrium.

B.2.3 Results and discussion

B.2.3.1 Protonation studies of dye A in DMSO

Provided in Figure B.2.5 are the absorption spectra from the protonation study of 0.5 mM A in DMSO using HCl. Inspection of the data reveals a single set of isosbestic points, corresponding to only a single equilibrium. The absorption of the bathochromic peak increased with increasing acid concentration up to the addition of 15 mM HCl (30 equivalents of HCl per equivalent of dye). Addition of 20 mM HCl (40 equivalents) yielded a slightly lower bathochromic peak absorption, indicating the beginning of the transition to the second equilibrium as discussed repeatedly and in detail in chapter B.1. Arrows in the spectrum indicate changes in intensities of various peaks as acid concentration is increased.

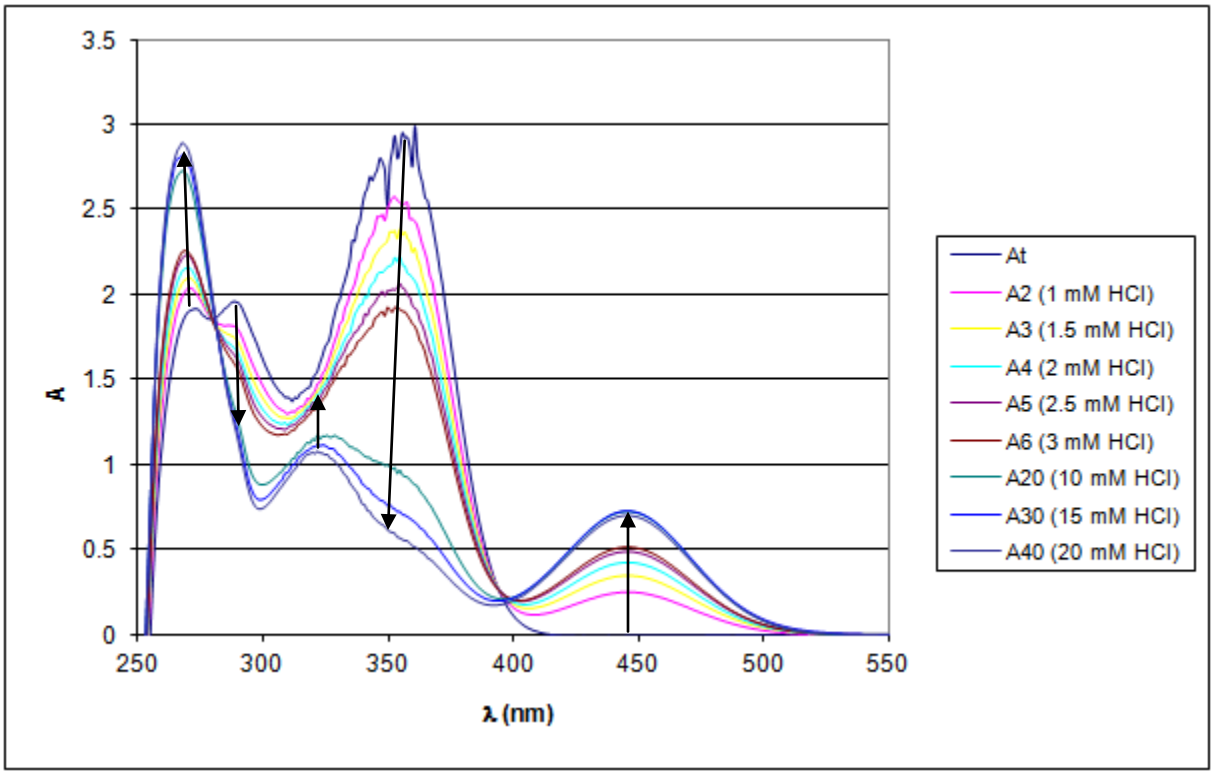

Figure B.2.5. Absorption spectra from protonation study of 0.5 mM A using HCl (in DMSO). Sample At is the absorption spectrum of a 0.5 mM sample of dye A in absence of acid

Product specifications provided by the supplier of the UV grade DMSO (Sigma-Aldrich) indicated that for this grade of DMSO, the intrinsic absorption of the solvent is significant at wavelengths lower than 290 nm. This grade of DMSO has $A_{290} = 0.16$ and $A_{300} = 0.10$ (presumably in a 1.000 cm pathlength cuvette); accordingly, absorption spectra of lower concentration samples of dye A in DMSO may be subject to interference from the DMSO absorption peak at wavelengths near or below 290 nm.

Provided in Figure B.2.6 are the absorption spectra from the protonation study of 20 µM A in DMSO using HCl. Note that the low end of the spectral window was cut off at 300 nm (as the absorption data below this point was complicated by the intrinsic absorption of DMSO). The absorption spectra of 20 µM dye A protonated with varying concentrations of HCl demonstrate less well-defined isosbestic behavior than those of the 0.5 mM A, but the spectral behavior of the two concentrations when [HCl] is varied are comparable. As with the 0.5 mM A, the addition of concentrations of acid far greater than that of the dye results in spectral behavior corresponding primarily to the first equilibrium ($B \rightleftharpoons HB^+$); the bathochromic peak intensity increases for acid concentrations as high as 10 mM (500 equivalents of acid per dye molecule), although the absorption spectrum for this solution may be indicative of the beginning of the transition to the second equilibrium (as indicated by a sharp increase in absorption around 260 nm, full peak not shown). Provided in Figure B.2.7 are the absorption spectra from the protonation study of 20 µM A in ACN using HCl (from the preliminary protonation studies used in the molar absorptivity experiments described in section B.1.2.5) for comparison with the results obtained in DMSO (Figure B.2.6). Arrows in the spectra in Figures B.2.6 and B.2.7 indicate changes in intensities of various peaks as acid concentration is increased.

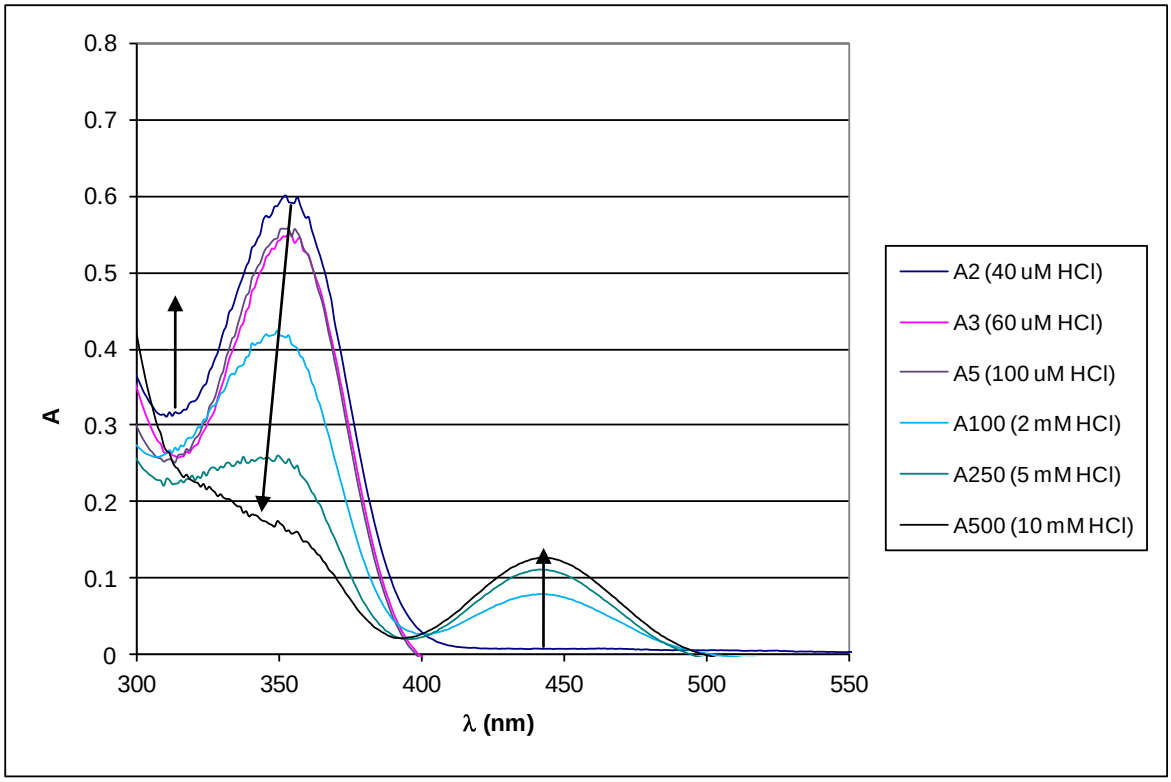

Figure B.2.6. Absorption spectra from protonation study of 20 µM A using HCl (in DMSO)

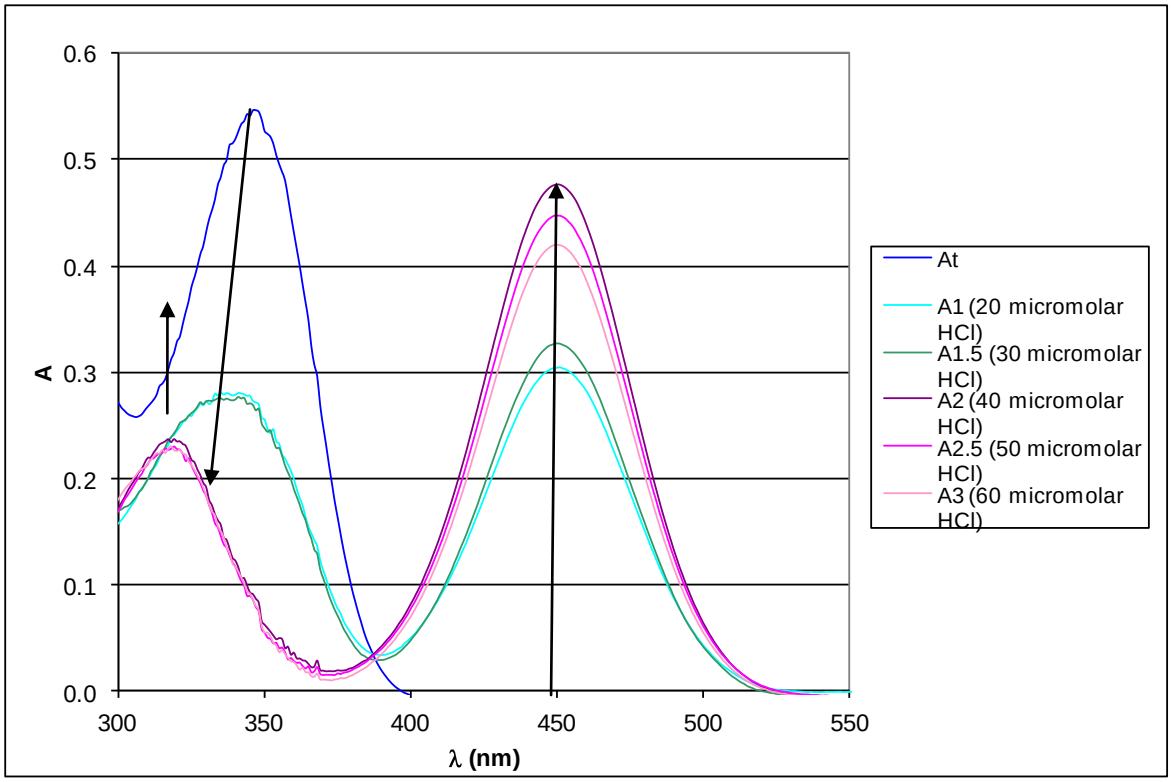

Figure B.2.7. Absorption spectra from protonation study of 20 µM A using HCl (in ACN)

Comparison of the spectroscopic behavior of 20 µM A protonated with HCl in DMSO to that of the same concentration of A protonated with HCl in acetonitrile (ACN) reveals differences that primarily reflect the difference in donor number (i.e. basicity) of the two solvents and the effects that these differences have on acid and base strength in as discussed in B.1.1.2. While the spectroscopic behavior of the dye in the two different solvents is comparable as increasing concentrations of acid are added, there are two apparent differences: the concentration of acid required to protonate the dye, which is much higher in DMSO, and the absorptivity of the bathochromic peak corresponding to the singly protonated form (HA^+).

In DMSO, HCl behaves as a moderately strong acid ($pK_a = 1.8$),[34] whereas in ACN, HCl behaves as a weak acid ($pK_a = 8.9$).[35] As a point of reference for the dye studied, the pK_a of pyridine (as pyridinium) in DMSO is known to be 3.4,[34] whereas in acetonitrile it is known to be 12.5.[37] The equilibrium observed in Figure B.2.6 thus represents the protonation of a very weak base with a moderately strong acid. Conversely, the equilibrium observed in Figure B.2.7 represents the protonation of a strong base with a weak acid. This difference would explain why the addition of as much as 500 equivalents of acid per dye molecule in DMSO results in the formation of only a small concentration of HB^+ relative to the significantly larger amount formed in acetonitrile upon addition of just two equivalents of acid per dye molecule. This difference also explains why the second equilibrium ($HB^+ \rightleftharpoons H_2B^{2+}$) is observed in ACN for acid concentrations greater than 40 µM but not observed to any real extent in DMSO even at acid concentrations of 10 mM. The similarity of the spectra (absorption wavelengths and spectral changes observed upon changing acid concentration) probably indicates that the first equilibrium observed in both solvents corresponds to protonation of the same site, but correlated absorbance-NMR studies in deuterated acetonitrile are required to fully substantiate this claim.

B.2.3.2 Initial NMR studies

The experimentally determined PW90 was found to correspond to a pulse length P1 = 29.375 μs and pulse power PL1 = -3.00 dB. Provided in Table B.2.1 are the T_1 values determined by the inversion recovery procedure and the chemical shifts (δ), multiplicities, and peak areas from the optimized ^{1}H NMR spectrum of dye A (obtained following the T_1 values) for the basic form of dye A in DMSO. Also included are the peak assignments and the structure with the peak assignment positions labeled.

Table B.2.1. ^{1}H NMR data obtained for the base form of dye A: chemical shifts (δ), multiplicities, integration (number of protons/peak), peak assignments to specific nuclei, and experimentally determined spin-lattice relaxation times T_1 for particular peaks

Dye A Structure With Labeled Positions	Assignment to Position	δ (ppm)	Multiplicity	Integration	T_1 (s)
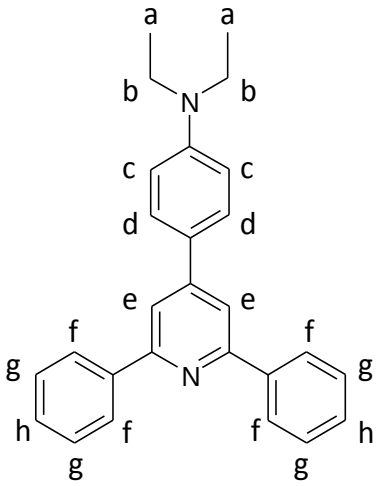	a	1.148	triplet	6	0.907
	b	3.434	quartet	N/A*	0.305*
	c	6.805	doublet	2	0.630
	d	7.902	doublet	2	0.877
	e	8.091	singlet	2	0.770
	f	8.299	doublet	4	1.227
	g	7.527	triplet	4	1.432
	h	7.457	triplet	2	1.557

*Not resolved from water peak, therefore integration was not possible. Experimentally determined T_1 value may also be inaccurate for this reason.

The optimized ^{1}H NMR spectrum of dye A was obtained by setting the pulse length and power to the PW90 settings (P1 = 29.375 μs, PL1 = -3.00 dB) and the delay d_1 to 12.5 s (>5T_1 for the largest T_1 measured = 1.557 s). Assignment of peaks to the structure allows us to single out the quartet at 3.43 ppm (assigned to the methylene protons neighboring the diethylamino nitrogen) and the doublets at 8.09 and 8.30 ppm (assigned to the aryl protons nearest the pyridine nitrogen) as being of particular interest in determining where the proton adds in the upcoming correlated NMR-absorption study.

B.2.3.4 Correlated NMR-absorption studies

The absorption spectra of the 0.5 mM NMR sample of dye A protonated with 10 mM HCl in DMSO-*d*6 falls within the first protonation equilibrium, as evidenced by overlaying the spectrum obtained for this sample onto the spectra obtained for the first equilibrium in the protonation study of dye A in DMSO (Figure B.2.5); this spectral overlay is provided in Figure B.2.8. The absorption spectrum of this sample remained almost constant when monitored every 60 minutes over the course of two hours (approximately the amount of time it took to run the experiment), as indicated in Figure B.2.9. Accordingly, the NMR spectra obtained can be correlated directly to the first equilibrium (associated with the formation of the red shifted peak) and the position within this equilibrium remains constant during the course of the NMR experiment.

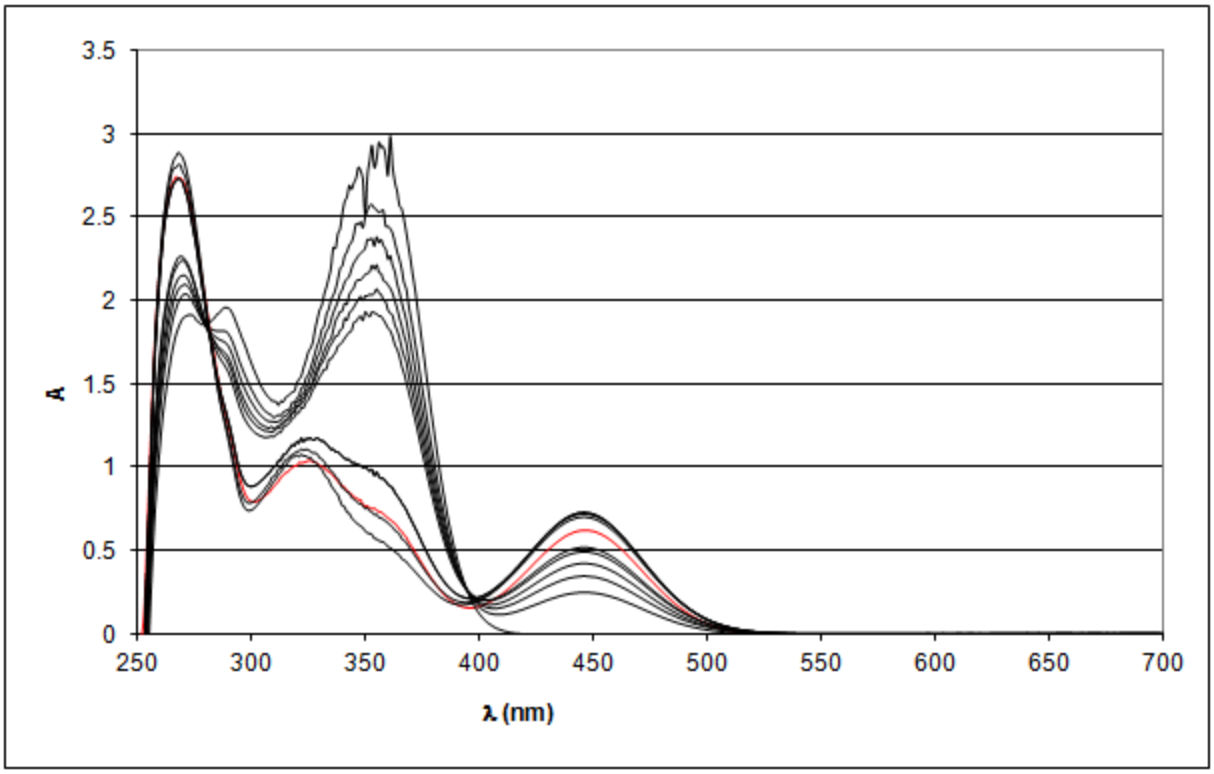

Figure B.2.8. Overlay of absorption spectra from protonation study in Figure B.2.4 (black) with spectrum obtained for NMR sample containing 0.5 mM A and 10 mM HCl in DMSO-*d*6 (red)

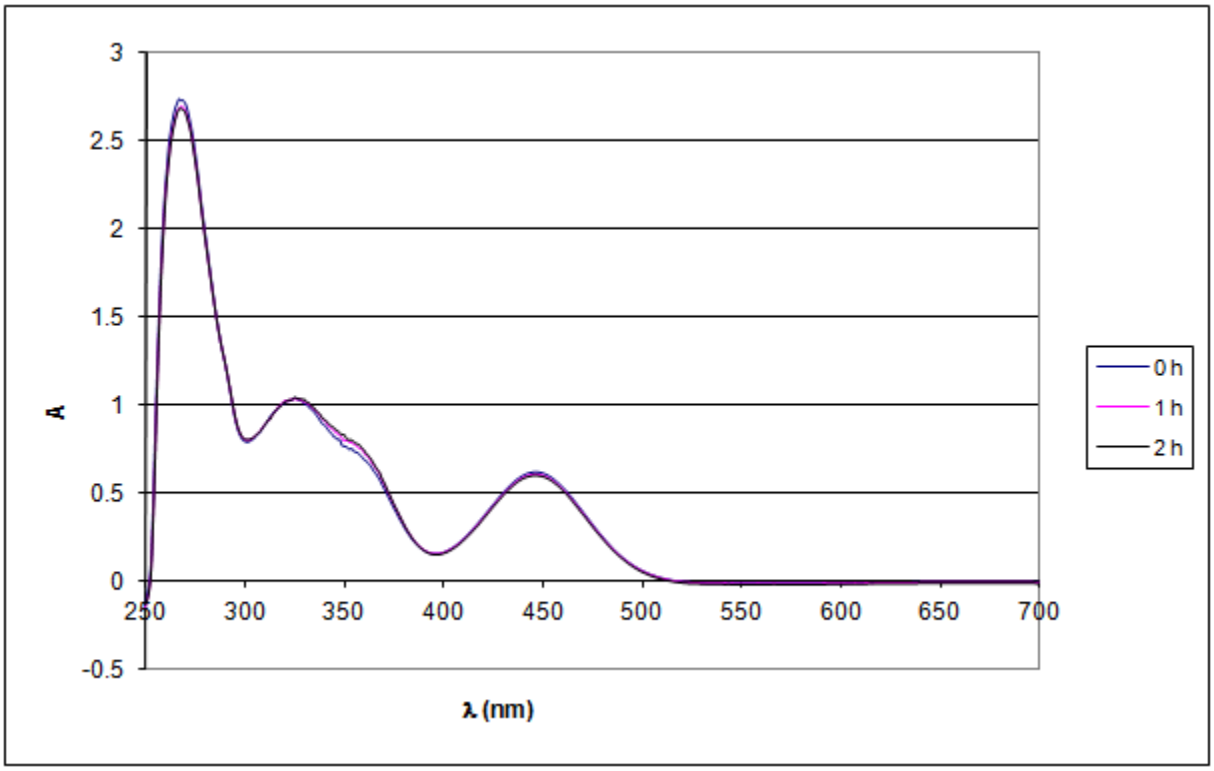

Figure B.2.9. Absorption spectrum of NMR sample taken during the course of the NMR experiment exhibits no significant change over time

The NMR spectra from the correlated NMR-absorption study of 0.5 mM dye A with 10 mM HCl added is provided in Figure B.2.10. The NMR spectrum has been stacked with that of the 3 mM (base form) sample. A second set of stacked spectra from this same experiment is provided in Figure B.2.11, in which only the aryl regions from the spectra shown in Figure B.2.10 are shown. Peaks are assigned to the structure in both sets of spectra.

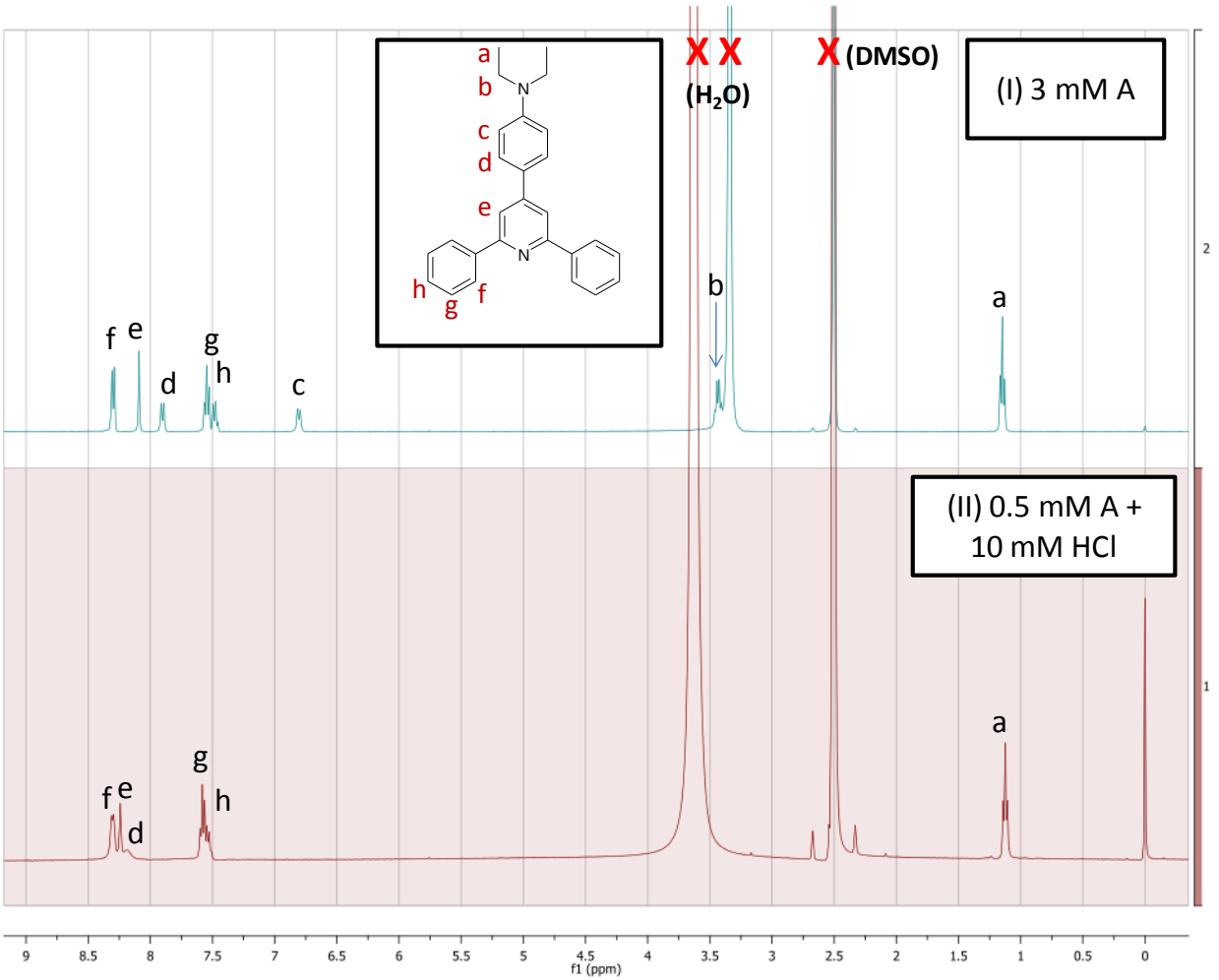

Figure B.2.10. Stacked NMR spectra corresponding to (I) base form of A (3 mM in absence of acid) and (II) A (0.5 mM) protonated with 10 mM HCl. Structure is inset and peak assignments to structure are shown

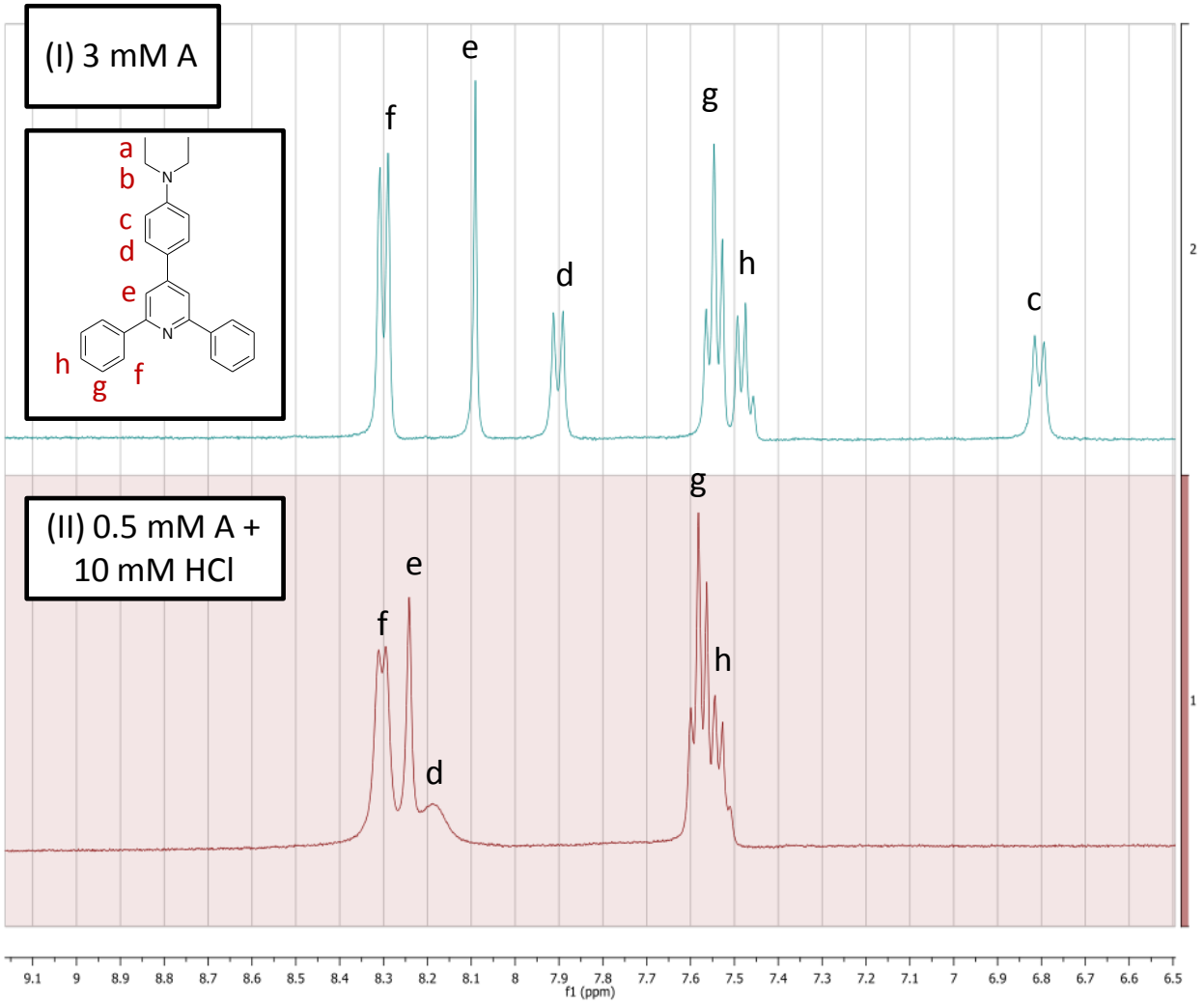

Figure B.2.11. Zoom view of aryl region from Figure B.2.10. Stacked NMR spectra corresponding to (I) base form of A (3 mM in absence of acid) and (II) A (0.5 mM) protonated with 10 mM HCl. Dye structure inset, with peak assignments indicated.

As mentioned previously, the quartet at 3.43 ppm (assigned to the methylene protons neighboring the diethylamino nitrogen) and the doublets at 8.09 and 8.30 ppm (assigned to the aryl protons nearest the pyridine nitrogen) are of particular interest in determining which nitrogen the first proton adds to. However, when looking at the effects of protonation in these

spectra, it is important to take into account both inductive and resonance effects on chemical shift., The origin of the bathochromic shift is thought to be increased conjugation within the π system of the molecule due to widespread delocalization of the positive charge throughout the molecule, as a result of protonation of the pyridine substituent.[26] Accordingly, the effects of pyridine protonation should result in a downfield shift of many of the protons attached to this conjugated system via resonance effects (as the delocalized charge results in decreased electron density and less shielding). Additionally, for protons close to the site of protonation, a stronger downfield shift would be expected due to inductive deshielding effects. If the pyridine nitrogen is protonated first, downfield shifts due to resonance effects would be expected at the "d" "f" and "h" positions and a downfield shift due to inductive effects might be observed at the "e" position. Protonation of the aniline nitrogen cannot result in resonance delocalization of the charge, accordingly, one would expect to observe only inductive effects. In other words, a perturbation of chemical shifts would be expected only for those protons in close proximity to the diethylaniline nitrogen, specifically those at the "a" "b" and "c" positons, and a more complex splitting pattern for the "b" position would be expected to occur due to spin-spin coupling between nonequivalent protons.

The results seem to verify initial protonation of the pyridine substituent, as significant downfield shifts are observed for many of the aryl protons. The downfield shift observed for the peak corresponding to position "h" is particularly diagnostic, as it is indicative of extensive charge delocalization through the conjugated system (which is only possible given pyridine protonation). It is unfortunate that the quartet corresponding to the "b" position (protons neighboring the diethylamino group) is obscured by the large water peak around 3.4 ppm in the protonated NMR spectrum (originating from the water content of the 12 M HCl used to prepare

the acid stock solution). Further complicating the situation is the apparent "disappearance" of the peak corresponding to the proton at the "c" position, which may be due to a downfield shift of the peak, (seemingly less likely because this peak area did not integrate into any of the remaining peaks present) or possibly proton exchange with the solvent. Additionally, the broadening and loss of fine structure of the signal for the "d" position is puzzling. The behaviors of the "c" and "d" peaks need to be accounted for by additional NMR studies utilizing lower concentrations of acid (to observe the behavior of the peaks as acid concentrations are increased). Additionally, if proton exchange is implicated, the assignment of these peaks to the "c" and "d" positions of the compound should be verified by two dimensional correlation spectroscopy (COSY or TOCSY), as the reason for proton exchange at these positions is unclear. One additional surprising observation is that there is a downfield shift in the signals for the "g" and "h" positions but no change in chemical shift for the "f" position, as the resonance structures for charge delocalization in these positions when pyridine is protonated indicate that the positive charge should be concentrated at both the *para* (h) and *ortho* (f) positions. Provided in Figure B.2.12 are three representative resonance structures of the dye protonated at the pyridine nitrogen to illustrate the preceding discussion.

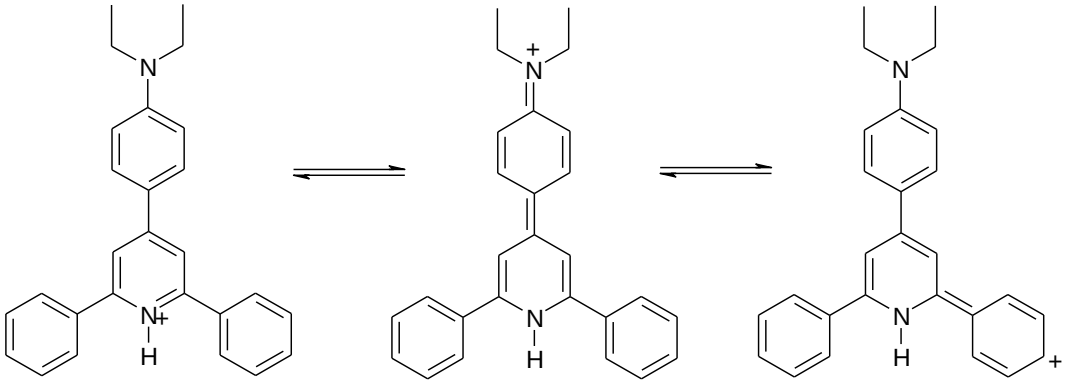

Figure B.2.12. Representative resonance structures illustrating extent of charge delocalization resulting from pyridine protonation

Overall, the fact that there are changes in chemical shift for most of the aryl protons (and even the protons at the "g" and "h" positions) while there is no change in the chemical shift of postion "a" (methyl protons of diethylamino group) supports protonation of the pyridine nitrogen as being responsible for the bathochromic shift observed in the first protonation equilibrium. This is in good agreement with published results of NMR studies of metal complexes of similar dyes, in which complexation at the pyridine nitrogen was found to be responsible for the observation of red-shifted spectral features.[26] Given the large concentrations of acid required to protonate the dye in DMSO, it is apparent that deuterated acetonitrile is the better solvent for observing this protonation (as much lower acid concentrations may be used and the interfering peaks associated with addition of acid will accordingly be lower). Additionally, given the greater base strength of the dyes and the spectroscopic observation of the second protonation state in this solvent, deuterated ACN will be far more appropriate for the study of both equilibria.

B.3 Conclusions

Dyes A – H (with *N*,*N*-diethylaniline D_3 substituents) all display a bathochromic shift of approximately 100 nm upon addition of acid, with a marked corresponding color change. Upon further addition of acid to dyes A – E and H, (D_1 & D_2 = alkyl or substituted phenyl groups) there is a reversal of the color change and a corresponding hypsochromic shift, with the new peak demonstrating a λ_{MAX} around 270-280 nm. For terpyridine dye F, ($D_1 = D_2$ = 2-pyridyl), the magnitude of the hypsochromic shift is far smaller (approximately 25 nm), with the new peak demonstrating a λ_{MAX} at 500 nm. As mentioned before, this spectral behavior corresponds to two protonation equilibria. The presence of clear isosbestic points suggests that these two equilibria

are distinct and well-resolved (i.e. pK_{a1} and pK_{a2} are separated by at least 2 pH units); results of pK_a studies confirm this.

Ethoxyphenyl substituted terpyridine dye I and toluene substituted terpyridine dye J possess absorption maxima in their nonprotonated forms at substantially lower wavelengths than those observed for diethylaniline-substituted dyes (the difference is almost 200 nm when compared to diethylaniline substituted terpyridine dye F). Additionally, upon addition of acid to dyes I and J, the spectra demonstrate a red-shifted peak broadening with a substantially smaller bathochromic shift than those observed for the diethylaniline substituted dyes, and the λ_{MAX} does not display a significant spectral shift away from that of the base form, instead exhibiting an increase in absorptivity. These unchanging λ_{MAX} values that demonstrate increased absorptivity upon protonation most likely correspond to the pyridine $\pi \rightarrow \pi^*$ excitation.[49] These spectral differences correlated to the presence of a second basic group (the aniline amine) led our group to suspect that the site of the first protonation in the aniline substituted dyes might actually be the aniline amino group rather than the pyridyl nitrogen, but NMR studies of this first equilibrium supported the idea that the pyridine nitrogen is in fact the site of the first protonation. Accordingly, the origin of the bathochromic shift is probably resonance delocalization of the positive charge throughout the conjugated chromophore, and role of the diethylamino group is to act as an auxochrome that both increases the wavelength of absorption of the nonprotonated form of the dye and increases the magnitude of the red shift such that visible color indication of the presence of acid is observed.

One other interesting characteristic of dyes I and J relative to dyes possessing diethylaniline substituents is their unstable absorption over time, which is likely attributable to aggregation. Pyridine is well known for its π-stacking capability, and terpyridine is well known

for its ability to form supramolecular aggregates through π-stacking and other noncovalent interactions, especially in complexes with metals.[49,61,62] Thus aggregation of dyes I and J certainly seems likely, and in fact it is surprising and fortunate that the same behavior is not observed for dye F (or any of the other dyes for that matter), as a change in absorption with time precludes the determination of molar absorptivity. One might speculate that the diethylaniline D_3 substituent assists in preventing aggregation as well as providing the large bathochromic shift that allows color indication of protonation.

The presence of electron withdrawing groups or groups that can form intramolecular hydrogen bonds with the pyridine acceptor in the D_1 or D_2 positions was correlated to a reduction in the color intensity (absorptivity) of the red-shifted protonation peak. This reduction in absorptivity may be due to hindered ICT behavior of the donor-acceptor structure of these compounds resulting from the reduced ability of the "donor" groups to donate electrons. Similarly, substitution with electron donating groups was correlated to an increase in the color intensity (absorptivity) of the red-shifted protonation peak, which may also be explained in terms of charge transfer behavior; as the electron-donating nature of the substituents increases, more extensive delocalization of the positive charge throughout the structure is possible, resulting in a greater absorptivity. Surprisingly, despite the large differences in absorptivity of the bathochromic protonation peaks for dyes substituted with electron withdrawing groups versus electron donating groups, pK_a values of the dyes are not strongly modulated by interchanging electron-withdrawing substituents for electron-donating substituents at the 2 and 6 positions of the pyridine ring (D_1 and D_2 positions).

It was also found that both the solvent and the protonating acid have a strong influence on the absorptivity of the bathochromic protonation peak. Absorptivities of the protonation peak in

acetonitrile were substantially higher than those found in either DMSO or 50% EtOH/H_2O when the same protonating acid was used, this observation requires further study to determine the origin of this behavior. Additionally, it was found that in acetonitrile, perchloric acid resulted in the greatest absorptivity of the bathochromic peak, followed by PTSA, followed by HCl. This trend follows the trend of acid strengths in this solvent but it may also be due to differential spectral responses to anions. As with the observed solvent effects, this behavior requires further study.

Generally speaking, it was found that the structural characteristics resulting in the most desirable spectroscopic and color-indicating properties among the dyes studied are *N*,*N*-diethylaniline substitution at the 4 position of the pyridine ring (which is essential for visible color indication) coupled with electron-donating substitution at the 2 and 6 positions of the pyridine ring (which is essential for high molar absorptivity and corresponding strong coloration of the red-shifted peak). Amongst all of these dyes, the one with the best potential as a general pH indicator is terpyridine dye F, as the red color indicating acidic conditions doesn't disappear in the presence of higher concentrations of acid, but instead changes slightly in its hue. Among the diethylamino substituted dyes with aryl D_1 and D_2 substitution, dyes B and D demonstrated the most desirable spectral characteristics (greatest absorptivities of red shifted peak upon protonation) and could potentially be applied as reliable color indicators of a relatively narrow pH range (approximately 2-3 units), as the color disappears at pH values both lower and higher than the equivalence point of the first protonation equilibrium. Finally, *tert*-butyl substituted dye H is also a strong candidate for a pH indicator, as it demonstrated a high molar absorptivity of the red shifted peak, (also presumably resulting from its electron donating substitution). Alkyl substituted dye H has the added benefit of simplified, easily interpreted spectral changes, as all

absorption in the base form peak region disappears at the equivalence point of the first protonation, and all absorption in both the base form peak region and singly protonated form (bathochromic) peak region disappears at the equivalence point of the second protonation.

In this study, structural features of 2,4,6-trisubstituted pyridines that result in desirable and undesirable spectroscopic and color-indicating responses for applications as pH indicators and ion probes have been determined and rationalized based on known spectroscopic phenomena. These findings should assist in the future design of donor-acceptor pyridine ion probes with optimal spectroscopic and color-indicating responses for applications as color indicators of ions. More studies need to be carried out to fully characterize the studied dyes in terms of their suitability as indicators. Particularly, correlated NMR-absorption studies using lower concentrations of acid in DMSO-*d*6 need to be carried out to determine the fate of the "disappearing" peak. Additionally, correlated NMR-absorbance studies should be carried out using deuterated acetonitrile as the solvent, which will facilitate the use of much lower acid concentrations to observe both the first and second protonation equilibria than those needed for DMSO (and the interfering peaks associated with the addition of acid will accordingly be lower). Additionally, given the greater base strength of the dyes in ACN and the resulting ability to observe the second protonation state in this solvent even when relatively low acid concentrations are present, deuterated ACN will be far more appropriate for NMR study of both equilibria. Further pK_a determinations will also be made for the dyes in solvent compositions containing varied percentages of EtOH so that dissociation constants in at least three different ethanol percentages are determined (in order to determine the aqueous pK_a via extrapolation to zero percent ethanol rather than assuming a relation between percent ethanol and p$_s K_a$). Dissociation

constants should also be determined for at least a few other dyes in this manner, as there are a number of promising candidates among the group studied that should be fully characterized. Finally, the best candidates among the dyes studied should also be characterized in terms of selectivity towards H^+ and other metal ions.

As mentioned in the introduction, while the studies discussed in part B concern a different family of compounds than those discussed in part A, both cyanine dyes and 2,4,6-trisubstituted pyridine derivatives share a number of similarities. The two groups of compounds have similar applications to industry based on their photophysical properties. Additionally, the red shifted peak observed upon protonation of the pyridine derivatives is analogous to the unusually long wavelength absorption demonstrated by the cyanine dyes; in both cases, the long wavelength absorption arises from extensive delocalization of a positive charge across a chromophore containing multiple auxochromic nitrogen atoms. Finally, in at least once study, these two families of compounds have been successfully combined to create pH-sensitive fluorescent probes suitable for *in vivo* pH measurements, with cyanine dye substitution of the pyridine moiety at the 4 position resulting in a large increase in its pK_a. Accordingly, the groups of compounds studied in parts A and B of this thesis are not only similar, but may potentially find future applications as fluorogenic bioanalytical pH and ion probes when linked together.

C. References

1 Peters, A. T.; Freeman, H. S. *Modern Colorants: Synthesis and Structure*; Springer Publishing Company: New York, 1995.

2 Watanabe, S.; Tani, T. Absorption spectra of J-aggregates of cyanine dyes adsorbed on AgBr. *J. Imag. Sci. Tech.* **1995**, *39*, 81-85.

3 Serak, S.; Kovalev, A.; Agashkov A. Space charge-induced reorientation in polymethyne dye-doped nematics under excitation with nanosecond laser pulses. *Opt. Commun.* **2000**, *181*, 391-399

4 Yoshida, T.; Zhang, J.; Komatsu, D.; Sawatani, S.; Minoura, H.; Pauporte´, T.; Lincot, D.; Oekermann, T.; Schlettwein, D.; Tada, H.; Wöhrle, D.; Funabiki, K.; Matsui, M.; Miura, H.; and Yanagi H. Electrodeposition of inorganic/organic hybrid thin films. *Adv. Funct. Mater.* **2009**, *19*, 17-43.

5 Qiao X.; Wang, L.; Maa, J.; Denga, Q.; Lianga, Z.; Zhanga, L.; Peng, X., Zhanga Y. High sensitivity analysis of water-soluble, cyanine dye labeled proteins by high-performance liquid chromatography with fluorescence detection. *Anal. Chim. Acta* **2009**, *640*, 114–120.

6 Williams, R. J.; Lipowska, M.; Patonay, G.; Strekowski, L. Comparison of covalent and noncovalent labeling with near-infrared dyes for the high-performance liquid chromatographic determination of human serum albumin. *Anal. Chem.* **1993**, *65*, 601-605.

7 Yarmoluk, S. M.; Losytskyy, M. Yu.; Yashchuk, V. M. Nonradiative deactivation of the electronic excitation energy in cyanine dyes: influence of binding to DNA. *J. Photochem. Photobiol., B.* **2002**, *67*, 57-63.

8 Colyer, C. Noncovalent labeling of proteins in capillary electrophoresis with laser-induced fluorescence detection. *Cell Biochem. Biophys.* **2000** *33*, 323-337.

9 Frangioni, J.V. In vivo near-infrared fluorescence imaging. *Curr. Opin. Chem. Biol.* **2003**, *7*, 626–634.

10 Murphy, S.; Schuster, G. B. Electronic Relaxation in a Series of Cyanine Dyes: Evidence for Electronic and Steric Control of the Rotational Rate. *J. Phys. Chem.* **1995**, *99*, 8516-8518.

11 Soper, S. A.; Mattingly, Q. L. Steady-State and Picosecond Laser Fluorescence Studies of Nonradiative Pathways in Tricarbocyanine Dyes: Implications to the Design of Near-IR Fluorochromes with High Fluorescence Efficiencies. *J. Am. Chem. Soc.* **1994**, *116*, 3744-3752.

12 Ranjit, S.; Gurunathan, K.; Levitus, M. Photophysics of Backbone Fluorescent DNA Modifications: Reducing Uncertainties in FRET. *J. Phys Chem. B* **2009**, *113*, 7861-7866.)

13 Cooper, M.; Ebner, A.; Briggs, M.; Burrows, M.; Gardner, N.; Richardson, R.; West, R. Cy3B: improving the performance of cyanine dyes. *J. Fluoresc.* **2004**, *14*, 145-150.

14 Tyutyulkov, N.; Fabian, J.; Mehlhorn, A.; Dietz, F.; Tadjer, A. *Polymethine Dyes*; St. Kliment Ohridski University Press: Sofia, 1991.

15 Gragg, J.; Henary, M. A Synthesis of Near-Infrared Heptamethine Cyanine Dyes. Thesis for the Masters Degree in the College of Arts and Sciences, Georgia State University, Atlanta, GA, 2010.

16 Haughland, R. P. *Handbook of Fluorescent Probes and Research Chemicals*, 9th ed.; Molecular Probes Inc: Eugene, 1996.

17 Berg, J. M; Tymockzko, J. L; Stryer. L. *Biochemistry*; W. H. Freeman and Company: New York, 2007.

18 Findik, S.; Arik, M.; Ceylan, M. A systematic study on the absorption and fluorescence properties of 2,4,6-triaryl and tripyridylpyridines. *Turk. J. Chem.* **2009**, *33*, 677-684.

19 Arny, H. V. *Principles of Pharmacy*. W.B. Saunders Co.: Philadelphia, 1947.

20 Basnet, A.; Thapa, P.; Karki, R.; Na, Y.; Jahng, Y.; Jeong, B. S.; Jeong, T. C.; Lee, C. S.; Lee, E. S. 2,4,6-Trisubstituted pyridines: Synthesis, topoisomerase I and II inhibitory activity, cytotoxicity, and structure-activity relationship. *Bioorg. Med. Chem*. **2007**, *15*(13), 4351-4359.

21 Hisamatsu, N.; Hiraishi, S. Thermal recording material providing yellow image. Japanese Patent 10250237, September 22, 1998.

22 Grasshoff, J. M.; Marshall, J. L.; Minns, R. A.; Ramos, S. M.; Stroud, S. G.; Telfer, S. J.; Yang, H.; Boggs, R. A.; Kolb, E. S. Process and composition for generating acid for imaging compositions. U.S. Patent 21856, November 26, 1997.

23 Angadiyavar, C. S.; Srinivasan, R. 2,4,6 Trisubstituted pyridine dye lasers. U.S. Patent 3986140, September 17, 1974.

24 Tang, B.; Yu, F.; Li, P.; Tong, L.; Duan, X.; Xie, T.; Wang, X. A Near-Infrared Neutral pH Fluorescent Probe for Monitoring Minor pH Changes: Imaging in Living HepG2 and HL-7702 Cells. *J. Am. Chem. Soc.* **2009**, *131*, 3016-3023.

25 Nakamoto, K. Ultraviolet spectra and structures of 2,2'-bipyridine and 2,2',2"-terpyridine in aqueous solution. *J. Phys. Chem.* **1960**, *64*(10), 1420-1425.

26 Garcia-Acosta, B.; Martinez-Manez, R. Sancenon, F.; Soto, J.; Rurack, K.; Spieles, M.; Garcia-Breijo; E.; Gil, L. Ditopic N-Crowned 4-(*p*-Aminophenyl)-2,6-diphenylpyridines: Implications of Macrocycle Topology on the Spectroscopic Properties, Cation Complexation, and Differential Anion Responses. *Inorg. Chem.* **2007**, *46*, 3123-3135.

27 Cantu, M. D.; Hillebrand, S.; Carrilho, E. Determination of the dissociation constants (pK_a) of secondary and tertiary amines in organic media by capillary electrophoresis and their role in the electrophoretic mobility order inversion. *J. Chromatogr. A.* **2005**, *1068*, 99-105.

28 *N,N-Dimethylformamide*; MSDS No. 9923813; Sciencelab.com, Inc.: Houston, TX, Nov 01, 2010. http://www.sciencelab.com/msds.php?msdsId=9923813 (accessed May 01, 2011).

29 Gutmann, V. Solvent effects on the reactivities of organometallic compounds. *Coord. Chem. Rev.* **1976**, *18*(2), 225-255.

30 Loudon, G. M. *Organic Chemistry*, 4th ed.; Oxford University Press: New York, 2005.

31 Sawyer, D. T.; Roberts, J. L. *Experimental Electrochemistry for Chemists*; John Wiley & Sons, Inc.: Hoboken, 1974.

32 Fritz, J. S. *Acid Base Titrations in Nonaqueous Solvents*; Allyn & Bacon Inc.: Boston, 1973.

33 Guthrie, J. P. Hydrolysis of esters of oxy acids: pKa values for strong acids. *Can. J. Chem.* **1978**, *56*, 2342-2354.

34 Reich, H. J. *Bordwell pKa Table: Acidities in DMSO*; Department of Chemistry, University of Wisconsin at Madison: Madison, WI, Feb 23, 2011. http://www.chem.wisc.edu/areas/reich/pkatable/index.htm (accessed Sep 30, 2011).

35 Eckert, F.; Leito, I.; Kaljurand, I.; Kütt, A.; Klamt, A.; Diedenhofen, M. Prediction of acidity in acetonitrile solution with COSMO-RS. *J. Comp. Chem.* **2009**, *30*(5), 799-810.

36 Kütt, A.; Movchun, V.; Rodima, T,; Dansauer, T.; Rusanov, E. B. ; Leito, I.; Kaljurand, I.; Koppel, J.; Pihl, V.; Koppel, I.; Ovsjannikov, G.; Toom, L.; Mishima, M.; Medebielle, M.; Lork, E.; Röschenthaler, G-V.; Koppel, I. A.; Kolomeitsev, A. A. Pentakis(trifluoromethyl)phenyl, a Sterically Crowded and Electron-withdrawing Group: Synthesis and Acidity of Pentakis(trifluoromethyl)benzene, -toluene, -phenol, and -aniline. *J. Org. Chem.* **2008**, *73*(7), 2607–2620.

37 Kütt, A.; Leito, I.; Kaljurand, I.; Sooväli, L.; Vlasov, V. M.; Yagupolskii, L. M.; Koppel, I. A. A Comprehensive Self-Consistent Spectrophotometric Acidity Scale of Neutral Brønsted Acids in Acetonitrile. *J. Org. Chem.* **2006** *71*(7), 2829–2838.

38 Kaljurand, I.; Kütt, A.; Sooväli, L.; Rodima, T.; Mäemets, V. Leito, I; Koppel, I. A. Extension of the Self-Consistent Spectrophotometric Basicity Scale in Acetonitrile to a Full Span of 28 pKa Units: Unification of Different Basicity Scales. *J. Org. Chem.* **2005**, *70*(3), 1019-1028.

39 Siow, K.; Ang, K. Thermodynamics of Ionization of 2,4-Dinitrophenol in Water-Dimethylsulfoxide Solvents. *J. Solution Chem.* **1989**, *18*(10), 937-947.

40 Avdeef, A.; Comer, J. A.; Thomson, S. J. pH-metric log P. 3. Glass Electrode Calibration in Methanol-Water, Applied to p*K*a Determination of Water-Insoluble Substances. *Anal. Chem.* **1993**, *65*, 42-49

41 Lee, C. K.; Jeoung, E. H., Lee, I. H. Effect of Mixtures of Water and Organic Solvents on the Acidities of 5-Membered Heteroaromatic Carboxylic Acids. *J. Heterocyclic Chem.* **2000**, *37*, 159-166.

42 Baumstark, A. L. *Chemistry 1211K Lab Manual: The Identification of an Organic Acid*, 3rd ed.; Georgia State University: Atlanta, 2004.

43 Scopes, R. K. *Protein Purification: Principles and Practice*, 2nd ed.; Springer-Verlag: New York, 1987.

44 Ruiz de Luzuriaga, A.; Garcia, I.; Mecerreyes, D.; Etxeberria, A.; Pomposo, J. A. Design and stabilization of block copolymer micelles via phenol-pyridine hydrogen-bonding interactions. Polymer **2010**, *51*(6), 1355-1362.

45 Xiang, M. L.; Jiang, M.; Zhang, Y. B.; Wu, C.; Feng, L. X. Intermacromolecular Complexation due to Specific Interactions 4. The Hydrogen-Bonding Complex of Vinylphenol-Containing Copolymer and Vinylpyridine-Containing Copolymer. *Macromolecules* **1997**, *30*, 2313–2319.

46 Nagakura, S.; Gouterman, M. Effect of Hydrogen Bonding on the Near Ultraviolet Absorption of Naphthol. *J. Chem. Phys.* **1957**, *26*(4), 881-886.

47 Brealey, G. J.; Kasha, M. The Role of Hydrogen Bonding in the n → p* Blue-shift Phenomenon. *J. Am. Chem. Soc.* **1954,** *77*, 4462-4468.

48 Knyazhansky, M. I.; Kharlanov, V. A.; Tymiansky, Y. R. Adiabatic structural relaxation in heterocyclic nitrogen-containing cations: The structure, absorption and fluorescence of the 2,4,6-triarylsubstituted pyridinium cations. *J. Photochem. Photobiol. A* **1998**, *118*, 151-156.

49 Joule, J. A.; Mills, K. *Heterocyclic Chemistry*; John Wiley & Sons Ltd.: West Sussex, 2010.

50 Larive, C. K. Bioanalytical Nuclear Magnetic Resonance Spectroscopy. *Anal. Bioanal. Chem*. **2004**, *378*, 1401-1402.

51 Lambert, J. B., Mazzola, E. P. *Nuclear Magnetic Resonance Spectroscopy: An Introduction to Principles, Applications, and Experimental Methods*; Pearson: Upper Saddle River, 2004.

52 Günther, H. *NMR Spectroscopy: Basic Principles, Concepts, and Applications*; John Wiley & Sons: New York, 1995.

53 Hendee, W. R.; Morgan, C. J. Magnetic resonance imaging. Part I--physical principles. *West. J. Med.* **1984**, *141*, 491-500.

54 Harris, D. *Quantitative Chemical Analysis*, 7th ed.; W.H. Freeman and Co.: New York, 2007.

55 Ingle, J. D. Jr. Theoretical and Experimental Investigation of Factors Affecting Precision in Molecular Absorption Spectrophotometry. *Anal. Chem*. **1975**, *47*, 1226.

56 Raghothama, S. NMR of Peptides. *J. Indian Inst. Sci.* **2010**, *90*(1), 145-161.

57 Kruus, P.; McGuire, M. J. Ion association in solutions of HCl in DMSO-water mixtures: ultrasonic absorption studies. *Can. J. Chem.* 1978, *56*, 1881-1888.

58 Huber, W. *Titrations in Nonaqueous Solvents*; Academic Press, Inc.: New York, 1967.

59 Holmes, D. *Determination of the 90° Pulse Width*. Max T. Rogers NMR Facility, Department of Chemistry, Michigan State University: East Lansing, MI, March 17 2004. http://www2.chemistry.msu.edu/facilities/nmr/handouts/90%20degree%20pulse.pdf (accessed September 20 2011).

60 Jacobsen, Neil E. *NMR Spectroscopy Explained: Simplified Theory, Applications and Examples for Organic Chemistry and Structural Biology*; John Wiley & Sons, Inc.: Hoboken, 2007.

61 Hannon, M. J.; Painting, C. L.; Plummer, E. A.; Childs, L. J.; Alcock, N. W. Competing Supramolecular Interactions Give a New Twist to Terpyridyl Chemistry: Anion- and Solvent-Induced Formation of Spiral Arrays in Silver(I) Complexes of a Simple Terpyridine. *Chem. Eur. J.* **2002**, *8*, 2225–2238.

62 McFadyen, W. D.; Wakelin, L. P. G.; Roos, I. A. G.; Hillcoat, B. L. Binuclear platinum (II)-terpyridine complexes. A new class of bifunctional DNA-intercalating agent. *Biochem. J.* **1986,** *238*(3), 757-763.